VYSOKÉ UČENÍ TECHNICKÉ V BRNĚ
BRNO UNIVERSITY OF TECHNOLOGY

FAKULTA CHEMICKÁ
FACULTY OF CHEMISTRY

ÚSTAV FYZIKÁLNÍ A SPOTŘEBNÍ CHEMIE
INSTITUTE OF PHYSICAL AND APPLIED CHEMISTRY

IZOLACE A STANOVENÍ STRUKTUR PROTEINŮ: HEXAMERIN POTEMNÍKA TRIBOLIUM CASTANEUM A TMPH FÁGA PHI812

ISOLATION AND DETERMINATION OF THE STRUCTURE OF HEXAMERIN OF TRIBOLIUM CASTANEUM AND TMPH PROTEIN OF PHI812 PHAGE.

DIPLOMOVÁ PRÁCE
MASTER'S THESIS

AUTOR PRÁCE — **Bc. Lucie Valentová**
AUTHOR

VEDOUCÍ PRÁCE — **Mgr. Pavel Plevka, Ph.D.**
SUPERVISOR

BRNO 2019

BRNO UNIVERSITY OF TECHNOLOGY
FACULTY OF CHEMISTRY

Master's Thesis Assignment

Number of thesis:	FCH-DIP1284/2018	Academic year: 2018/19
Institute:	Institute of Physical and Applied Chemistry	
Student:	**Bc. Lucie Valentová**	
Study programme:	Chemistry for Medical Applications	
Study field:	Chemistry for Medical Applications	
Head of thesis:	**Mgr. Pavel Plevka, Ph.D.**	

Title of Master's Thesis:

Isolation and determination of the structure of hexamerin of Tribolium castaneum and TmpH protein of phi812 phage.

Master's Thesis assignment:

1. Theoretical review focused on biological functions of bacteriophage phi812 Tail morphogenetic protein H (TmpH) and hexamerin.
2. Optimisation of methods for isolation of hexamerin from Tribolium castaneum pupae and bacterial expression and purification of protein TmpH.
3. Crystallization of isolated proteins.
4. Determination of Tribolium castaneum hexamerin structure using X-ray crystallography and cryo-EM.
5. Analysis and discussion of obtained results.

Deadline for Master's Thesis delivery: 10. 5. 2019

Master's Thesis is necessary to deliver to a secretary of institute in the number of copies defined by the dean. This assignment is part of Master's Thesis.

- - - - - - - - - - - - - - - -	- - - - - - - - - - - - - - - -	- - - - - - - - - - - - - - - -
Bc. Lucie Valentová	Mgr. Pavel Plevka, Ph.D.	prof. Ing. Miloslav Pekař, CSc.
Student	Head of thesis	Head of institute

In Brno, 31. 1. 2019

- - - - - - - - - - - - - - - -
prof. Ing. Martin Weiter, Ph.D.
Dean

ABSTRAKT

Tato práce se zabývá strukturní studií dvou proteinů: proteinu Tail morphogenetic protein H (TmpH) bakteriofága *Φ812*, který napadá Zlatého stafylokoka (*Staphylococcus aureus*) a hexamerinu z potemníka (*Tribolium castaneum*).

S. aureus je jedním z nejvíce rezistentních patogenů způsobující onemocnění s vysokou morbiditou a mortalitou. Bakteriofág *Φ812* je schopen infikovat a lyzovat 95 % kmenů *S. aureus* a má potenciální využití ve fágové terapii. Protein TmpH je součástí virionu tohoto fága. V rámci této práce bylo připraveno několik plazmidů nesoucích gen TmpH, které byly použity pro rekombinantní expresi proteinu v buňkách *E. coli* BL21(DE3). Protein byl vyčištěn afinitní a gelovou chromatografií. Pro čistý protein byly optimalizovány krystalizační podmínky.

Hexamerin je nejhojnějším proteinem larev a kukel hmyzu s dokonalou proměnou. V průběhu metamorfózy hexamerin slouží jako zdroj aminokyselin. V rámci této práce byl hexamerin izolován z kukel potemníka *T. castaneum*. Pro stanovení struktury hexamerinu byly použity dvě metody: rentgenová krystalografie a kryo-elektronová mikroskopie. Byly optimalizovány podmínky pro růst krystalů a vypěstovány krystaly vhodné pro sběr difrakčních dat. Nicméně struktura hexamerinu byla rychleji vyřešena kryo-elektronovou mikroskopií s rozlišením 3.2 Å. Znalost struktury hexamerinu umožní pochopení jeho funkce v regulaci vývoje hmyzu s dokonalou proměnou.

Klíčová slova: fágová terapie, *Staphyloccocus aureus*, fág *Φ812*, *Tribolium castaneum*, hexamerin, kryo-elektronová mikroskopie, rentgenová krystalografie

ABSTRACT

This thesis deals with structural studies of two proteins: Tail morphogenetic protein H (TmpH) from phage *Φ812,* which infects *Staphylococcus aureus*, and hexamerin from holometabolous beetle *Tribolium castaneum*.

S. aureus is one of the bacterial pathogens that are most often resistant to antibiotics and cause diseases with high morbidity and mortality. Bacteriophage *Φ812* infects and lyzes 95 % *S. aureus* strains and it is a potential agent for use in phage therapy. Protein TmpH is a part of the virion of this phage. As a part of the work on this thesis several plasmids carrying TmpH gene were prepared and used for recombinant protein expression using *E. coli* BL21(DE3). The produced protein was purified using affinity and size exclusion chromatography. Crystallization conditions for TmpH were optimized.

Hexamerin is the most abundant protein in larvae and pupae of *Holometabolous* insects. It serves as an amino acid source during the metamorphosis of pupae into adults. I developed the method for isolation of hexamerin from pupae of *T. castaneum.* Two methods were used to determine hexamerin structure: X-ray crystallography and cryo-electron microscopy. Conditions for hexamerin crystallization were optimized and crystals suitable for X-ray data collection were grown. Nevertheless, hexamerin structure was solved by cryo-electron microscopy at resolution of 3.2 Å. The structure of hexamerin may enable determination of its role in regulation of metamorphosis of holometabolous insects.

Keywords: phage therapy, *Staphyloccocus aureus*, phage *Φ812*, *Tribolium castaneum*, hexamerin, cryo-electron microscopy, X-ray crystallography.

VALENTOVÁ, Lucie. *Izolace a stanovení struktur proteinů: hexamerin potemníka Tribolium Castaneum a TmpH fága phi812*. Brno, 2019. Dostupné také z: https://www.vutbr.cz/studenti/zav-prace/detail/115833. Diplomová práce. Vysoké učení technické v Brně, Fakulta chemická, Ústav fyzikální a spotřební chemie. Vedoucí práce Mgr. Pavel Plevka, Ph.D.

ACKNOWLEDGEMENT

Here I would like to thank my supervisor Mgr. Pavel Plevka, Ph.D. for all his willingness, wise suggestions and especially for the opportunity to become a member of his research group. Next I would like to thank Ing. Tibor Füzik, Ph.D. for all his advices, huge patience, help and all the time he spent with teaching me everything I needed to know in the lab. I would also like to thank all members of Structural Virology for accepting me friendly in their group, for all their advice and sense of humor. Finally I would like to thank prof. RNDr. Ivana Márová, CSc. for encouragement and for her great personality.

DECLARATION

I declare that the diploma/bachelor thesis has been worked out by myself and that all the quotations from the literary sources are accurate and complete. The content of the diploma thesis is the property of the Faculty of Chemistry of Brno University of Technology and all commercial use is allowed only if approved by both the supervisor and the dean of the Faculty of Chemistry, BUT.

.....

student's signature

TABLE OF CONTENTS

1 INTRODUCTION

Structural biology provides an insight into the world of proteins and nucleic acids by visualizing their structures. It enables the study of the connection between the structure and function, interpretation of the molecular biology experiments, intelligent design of new drugs, and structure-based prediction of macromolecules behaviour [1]. Protein Data Bank nowadays contains information of more than 149 000 structures and thousands of new structures are being solved every year [2].

This thesis deals with structural studies of two proteins: Tail morphogenetic protein H (TmpH) from *Staphylococcus aureus* attacking bacteriophage *Φ812* and hexamerin from *Tribolium castaneum*. X-ray crystallography and cryo-electron microscopy were used to determine the structures.

Infections and illnesses caused by antibiotic-resistant *Staphylococcus aureus* range from skin infections to bacteraemia, pneumonia, and endocarditis. The bacterium is responsible for thousands of deaths per year [3]. World Health Organization placed this bacteria on the list of priority pathogens for which new treatments are urgently needed [4].

The development of new antibiotics is difficult and slow in comparison to the rate with which bacteria become resistant to antibiotics [5]. Recently bacteria resistant to carbapenem class of antibiotics, which were reserved as the last resort treatments, were found [6].

Bacteriophage *Φ812* is able to infect 95 % of *S. aureus* strains [7]. Phage therapy is widely discussed as an alternative to antibiotics. Bacteriophages are naturally occurring viruses that infect and kill bacteria [8]. Before it will be possible to use phages, phage derived enzymes, and bioengineered phages for medical treatments, a detailed knowledge of phage structure and its life cycle is needed [5].

The second protein studied in this thesis is hexamerin from *Tribolium castaneum*. *T. castaneum,* known as a red flour beetle, is a worldwide pest which causes damages of cereals, legumes, and dried stored products and has evolved resistance against a variety of insecticides [9].

Hexamerins of holometabolous insects serve as amino acid source during metamorphosis. Hexamerins can constitute up to 50 % of all proteins in haemolymph in late larval stages [10]. There is evidence that hexamerins are able to bind small organic compounds such as juvenile hormone which influences and controls the beetle life-cycle [11]. Knowledge of hexamerin structure and its relationship with juvenile hormone may further our understanding of the regulation of metamorphosis of *Tribolium castaneum* and may enable development of compounds for pest management.

2 THEORETICAL PART

2.1 Structural biology

The first devices which enabled the observation beyond the limitation of naked eye were the early microscopes made by Hooke [1] and Leeuwenhoek in 17th century [12]. Light microscopy reached its theoretical resolution limit at the end of the 19th century. To achieve higher resolution sources of illuminating radiation with shorter wavelengths than those of visible light were needed [1]. The discovery of X-rays in 1895 by Röntgen and electrons in 1897 by Thompson together with new findings and development in technology and molecular biology contributed to the establishment of a new scientific field – structural biology [1, 12].

Structural biology is a field of science that deals with determining the three dimensional structures of biological macromolecules (mostly proteins, nucleic acids, and their complexes) and uses these structures to interpret and predict functions and properties of these molecules [12]. Solved molecular structures are deposited in the Protein Data Bank (PDB). The number of solved structures gradually increased over the time and nowadays the PDB database contains atomic coordinates of more than 149 000 structures [2].

The three main methods for determination of structures of macromolecules are X-ray crystallography, electron microscopy (EM), and nuclear magnetic resonance (NMR) [1].

X-ray crystallography is based on the ability of crystals to strongly diffract X-ray beams. It was the first method used for determination of macromolecular structures [1]. The first diffraction patterns of protein crystals were observed in 1930s [13]. However, it took almost 30 years to find the way how to process diffraction data and to obtain the structure [14]. From its beginnings X-ray crystallography underwent major development (invention of synchrotron X-ray sources, sophisticated detectors, crystal samples cooled to very low temperatures to reduce the radiation damage, fast and user friendly data processing software) and it still remains the most widely used method for structure determination [12].

NMR measurement are performed with proteins in aqueous solution, thus no crystals are needed. Therefore NMR is a suitable technique for proteins that contain flexible regions and do not crystalize. This technique is limited by the size of the protein and cannot be used for determination of structures of macromolecules larger than about 50 kDa [1, 12]. Concentration of about 40 mg/ml for a 20 kDa proteins are recommended for NMR analysis, unfortunately, many proteins tend to precipitate at such concentration. However, NMR analysis is suitable for detecting weak interactions between proteins and their ligands. At the end of 2018 the PDB contained 12 534 structures solved by NMR [2].

The first electron microscope was constructed in 1930s by Ruska [15]. Another important milestone in the history of **electron microscopy** is the year 1975 when the first protein structure (the structure bacteriorhodopsin at the resolution of 7 Å) was solved by Henderson and Unwin by this technique [1, 16]. Nowadays electron microscopes are equipped with better electron sources with high acceleration voltages and direct electron detectors. Cryogenic temperatures are used to reduce the instability of the specimen molecules instead of heavy atoms staining [1, 16]. The number of structures solved by this technique grows exponentially every year. [1, 12, 16]

Other methods important for the development of structural biology are for example neutron crystallography that uses diffraction data of neutrons scattered by nuclei of atoms (whereas X-rays are scattered by electrons), spectroscopic methods that provide information about protein secondary structure (circular dichroism), local ligand geometry around a metal ion (electron spin resonance), and sub-nanometer surface topography (atomic force microscopy) [1, 17].

Structural biology is one of the pillars of the growth of molecular biology. Introduction of recombinant protein expression methods allow production of macromolecules for structural studies. [1, 18] Increasing computing power and information about already solved structures led in recent years to the development of *in silico* structure prediction methods [12].

From its origins in the last century structural biology has come a long way and today it enables studies of macromolecules and their interactions at atomic resolution. The key events that contributed to this field are shown in Figure 1 [1].

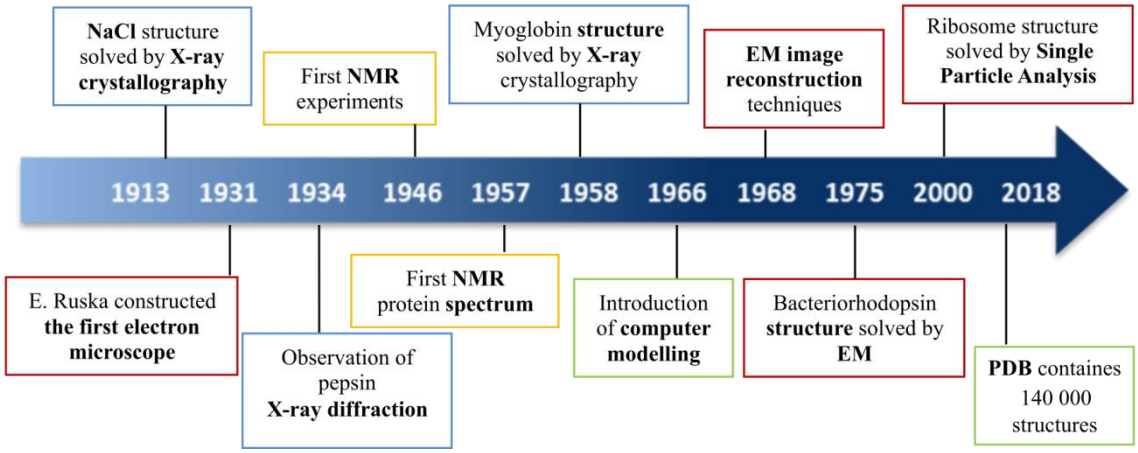

Figure 1: ***The milestones of structural biology****. Adapted from [1].*

2.1.1 Cryo-Electron Microscopy

Cryo-electron microscopy (cryo-EM) is based on imaging specimens under cryogenic conditions [16]. It is used for studying biological structures, tissues, and bacterial cells or protein molecules. Cryo-EM has three main branches: tomography, single particle electron microscopy, and electron crystallography [19].

2.1.1.1 The principle of cryo-electron microscope

The principle of cryo-EM is based on transmission electron microscopy. Electrons with high energy (in hundreds of kilo electron volts) are emitted from a source (superheated wire or field emission gun) and accelerated down the microscope column to the specimen [16]. Electrons scatter by interaction with specimen are focused by electromagnetic lenses and recorded on a detector. The inside of the microscope is maintained at high vacuum to prevent electron scattering by air molecules [19]. The specimen is maintained at the temperature of liquid nitrogen [20].

The electron beam is focused and directed on the specimen by a series of lenses and apertures. Condenser lenses and apertures are used to ensure the beam coherence, objective lens is used to focus the scattered electrons, and projector lenses produce magnified image on a detector (Figure 2). [16]

The short wavelength of electrons enables to achieve very high resolutions in the range of 1 – 2 Å [21]. Theoretical resolving power of cryo-EM (0.02 Å with electron accelerated to 300 keV) cannot be reached because of aberrations of electromagnetic lenses. [16]

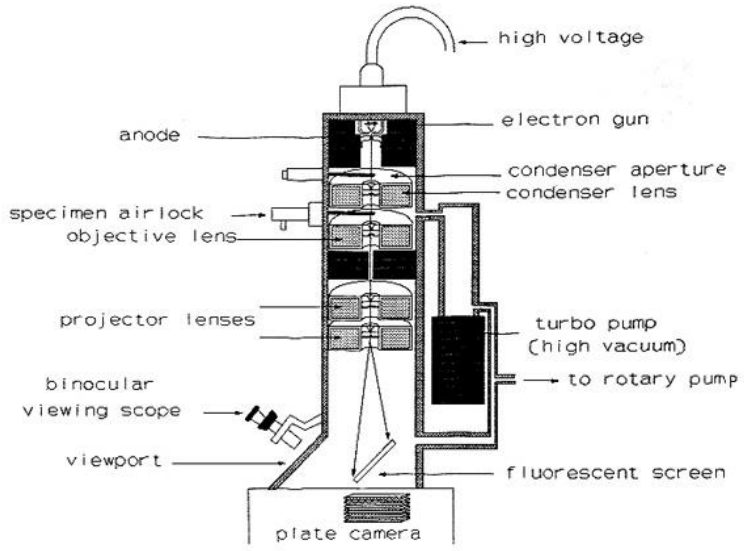

Figure 2: ***Scheme of transmission electron microscope****. Adapted from [16, 22].*

2.1.1.2 Sample preparation

Biological samples for electron microscopy must be stabilized to withstand the electron bombardment and vacuum in a microscope. Samples for cryo-electron microscopy are embedded in a layer of vitreous ice that closely approximates the original aqueous environment [16, 23]. Support grids for vitrified samples are usually made from copper covered by a layer of holey carbon, graphene or graphene oxide film [16].

Solution of a sample is deposited onto a cryo-EM grid and rapidly vitrified in liquid ethane, which leads to the formation of a layer of vitreous ice. The rapid cooling rate prevents the water molecules from crystalizing [24]. It was shown that plunge freezing is the best method for preserving the features of biological specimens [25].

In the method of negative staining the sample is mixed with a solution of heavy metal salt such as uranyl acetate or ammonium molybdate. The stain produces high contrast. However, only the surface of the molecule and channels and cavities accessible for the stain can be imaged, thus this method might be used only for the reconstructions of molecular shapes. [16, 23]

2.1.1.3 Single-particle analysis (SPA)

Because the images acquired using cryo-EM suffer from very low signal to noise ratio, many uniform particles need to be averaged to obtain interpretable results. Single particle analysis is the most used method for 3D reconstruction of electrostatic potential maps using large amount of 2D projections of the particle. Randomly placed particles in the ice give projections of random orientation of the particle. [21], [23]

During SPA reconstruction the orientation of the particle projections is estimated, and the following back projection of the images gives the reconstructed 3D model [19]. Because every dataset contains damaged particles and particles in alternative conformations, powerful 2D and 3D classification methods were introduced, which help to sort out set of homogenous particles used for final high-resolution reconstruction [16].

2.1.1.4 Tomography

Tomography is used for imaging of whole cells and cellular components. The specimen is tilted in the electron beam and at each tilt series of images are collected. The combination of these images is used to generate tomograms. The resolution of tomograms is around 50 Å. The specimen for tomography has to be thin enough to transmit the electron beam. Biological samples can be thinned by focused ion beam milling. [16, 19]

2.1.1.5 Electron crystallography

Electron crystallography is a method based on diffraction of electron beam in electron microscope by atoms in crystal lattice of the sample. The structure is determined by processing the images of electron diffraction pattern [26]. Electron crystallography is suitable for the structural studies of membrane proteins and proteins that do not form three dimensional crystals and whose structures cannot be determined by X-ray crystallography [27, 28].

2.1.2 X-ray crystallography

X-ray crystallography is the most widely used technique for molecular structure determination of biological macromolecules [29]. In its infancy (at the beginning of 20th century) X-ray crystallography was used to solve structures of inorganic compounds, salts, and minerals. After the discovery of proteins ability to crystalize and diffract X-ray beams in 1940s the protein crystallography gradually became powerful tool for structural analysis [18].

2.1.2.1 Principle of X-ray diffraction

Principle of X-ray crystallography is based on diffraction of the X-rays on crystal lattice. X-ray photons are scattered by electrons of atoms and the scattered rays interfere with each other. The interference might be either destructive or constructive. Constructive interference produces diffraction patterns and occurs if the Bragg's law is met (Figure 3, Equation 1). The condition described by Bragg's law:

$$2d \sin\theta = n\lambda \qquad (1)$$

d is an interplanar spacing, θ is an angle upon which X-rays impact on the plane, λ is X-ray wavelength and n is an integer. [30, 31]

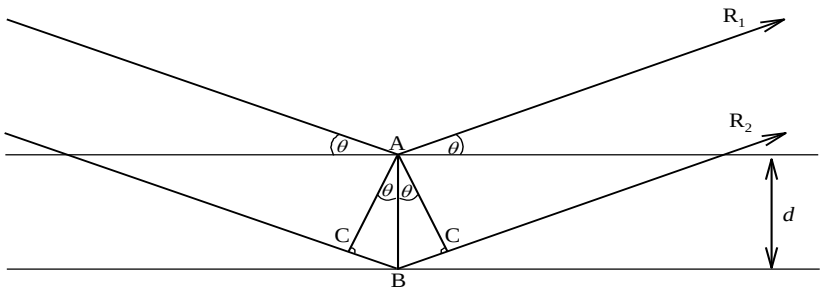

*Figure 3: **Scheme of Bragg's law**. Incoming rays R_1 and R_2 impact upon the angle θ and are reflected from the planes of crystal lattice with spacing d, adapted from [30].*

The sources of X-ray beams can be either electrons striking a copper anode or accelerating electrons in a synchrotron storage ring. A crystal is mounted on a goniometer head which enables its rotation [29]. Incoming X-ray beam is diffracted by the electrons in crystal lattice into many discrete beams that produce reflections, whose positions and intensities contain the information about the molecular structures of the crystallized macromolecules (Figure 4) [30]. From processed diffraction data the electron density map can be calculated and fitted with a chain of amino acid sequence [29].

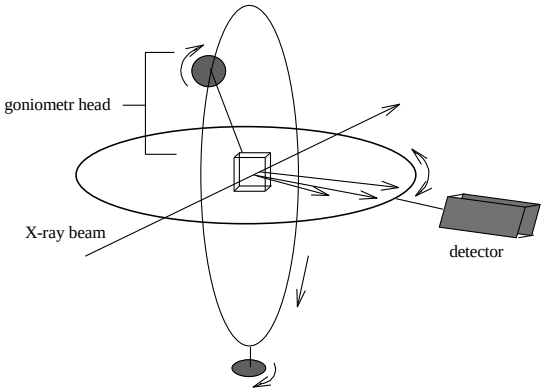

*Figure 4: **Scheme of X-ray data collection**. Based on [30].*

2.1.2.2 From crystal to structure

Crystals are composed from molecules ordered in identical orientations. Crystals can be divided into the unit cells. The unit cell is the smallest element from which the whole crystal can be built by transition in three dimensions [30].

Crystals are exposed to X-ray beam and diffraction patterns are measured. The pattern and its intensity carry the information about crystal symmetry, the unit cell dimensions, structure factor and amplitudes [30, 32].

The spot spacing in a diffraction pattern is determined by the dimension of the unit cell. The symmetry of the pattern carries information about the space group symmetry. There are 230 different space groups; however, proteins are composed solely of L-amino acids, therefore, they can crystallize only in 65 space groups [29].

For calculation of a map of electron density into which the structure of the studied macromolecule can be built, the information about the amplitude and phase angles of diffracted X-ray beam is necessary [29]. The phase angles cannot be measured directly (so called phase problem) and are obtained either by the molecular replacement or experimental phasing methods [29].

2.1.3 Protein crystallization

The ability of proteins to form crystals was discovered in 1840 [13]. After that crystallization served as protein purification approach and for demonstration of chemical purity. The interest in protein crystals increased with the invention of X-ray crystallography and beginnings of structural biology [18].

Protein crystals are usually small and fragile. Unlike inorganic crystals, protein crystals are held together by weak forces and the kinetics of their nucleation and growth is usually slower [18] . Protein crystals are usually not perfectly ordered and show certain amount of mosaicity. Crystals of the same protein grown in different crystallization conditions might differ in shape and form [30].

Protein crystals are grown by slow precipitation from their solutions called mother liquors [30]. The crystallization process has two steps: nucleation and growth (Figure 5). During nucleation originally disordered molecules become ordered, which leads to the formation of clusters that give rise to crystals [18]. Nucleation requires higher concentration of protein and precipitant than crystal growth [30].

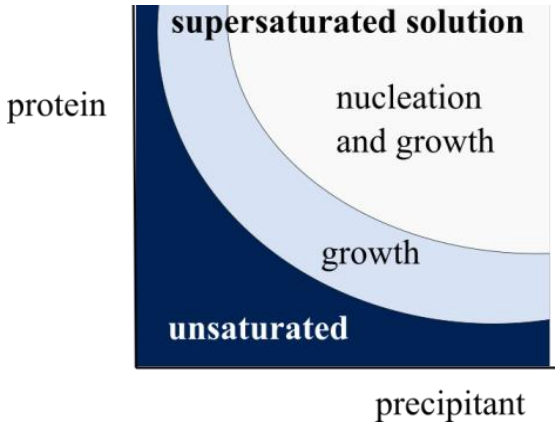

Figure 5: ***The phase diagram for the crystallization of macromolecules.*** *Crystals can grow only from supersaturated solution. Adapted from [18, 30].*

Protein crystallization is influenced by many factors: protein purity and concentration, concentration of precipitants, presence of ligands, buffer pH, temperature, and outer factors such as vibrations [30]. Crystallization process might result in several different solid forms of the protein: amorphous precipitates, phase separations, gels, or crystals [18].

Two most widely used techniques for protein crystallization are “Sitting drop” method and “Hanging drop” methods (Figure 6). Both methods are based on slow vapour diffusion between a drop with protein solution and mother liquor in the well. Slow evaporation of water from the drop leads to increasing of protein concentration until the supersaturation is reached and crystals start to form. [18, 33]

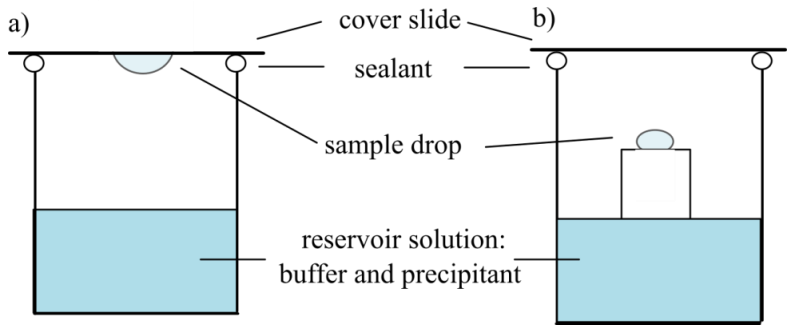

Figure 6: ***Protein crystallization using hanging and sitting drop setup.*** *a) Hanging drop method: droplet of crystal growing solution is mixed with protein on a slide that is inverted and sealed over a well with crystal growing solution. b) Sitting drop method: droplets of protein with crystallization solution are in a small well next to the crystal growing solution. Adapted from [30, 32].*

2.2 Phage therapy

The introduction of antibiotics in the 1940s caused a revolution in healthcare and improvement of the quality of human life [5]. Antibiotics found their place in medicine, agriculture, and holticulture and their global consumption is still rising [5, 34]. However every year thousands of people die because of infection with antibiotic-resistant bacteria [34]. Antibiotic-resistant bacteria were declared by WHO as a serious threat to global health in 2013 [35].

Bacteriophages are common in most environments. They are natural predators of bacteria and regulate their abundance and diversity [36]. Phage replication cycle depends on bacterial host. Two main types of phage replication are distinguished. Temperate phages attach to the receptor on bacterial cell surface and inject their genetic material into the host cells. Phage genome either persists extra chromosomally or becomes integrated into bacterial chromosome and replicates along with the host as a prophage (lysogen). Re-activation of temperate phages might be triggered by environmental factors that cause stress to bacterial host or the damage of the host DNA. [5]

Virulent (lytic) phages use bacterial replication system to produce next generation of phage progeny. In the end of the cycle the infected cell is lysed and mature phage particles are released [5, 37] Replication cycles of lysogenic and lytic phages are depicted in Figure 7.

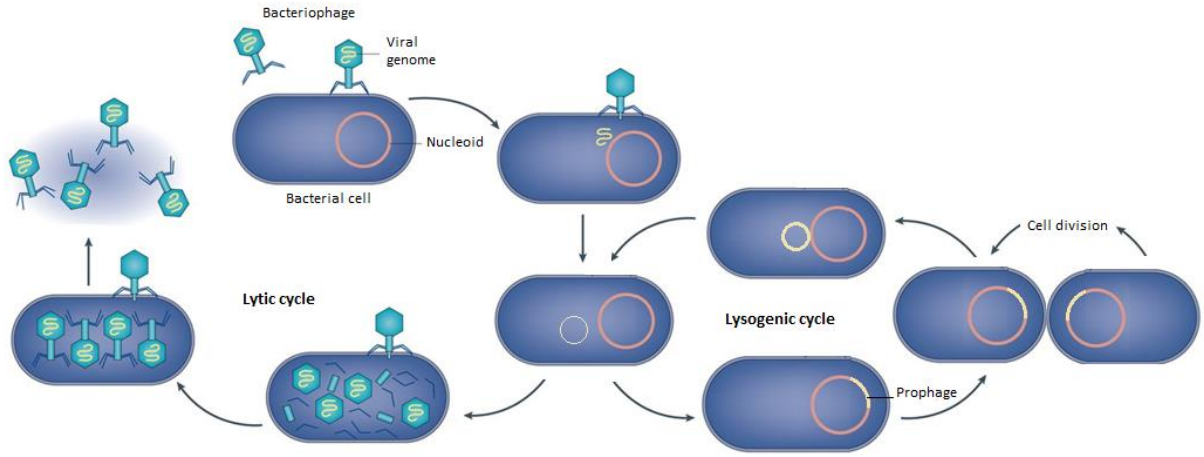

Figure 7: ***General scheme of lysogenic and lytic phage infection cycle*** *[38].*

Phage therapy is a possible alternative to antibiotics for treatment of bacterial diseases. Therapeutic potential of phages was recognized immediately after their discovery in 1917 [37].

However, the first studies and medical trials were limited by the technology available of the time and the results of these trials were not very successful. With the introduction of antibiotics the phage therapy was forgotten. Today phage therapy undergoes its renaissance [36].

Major advantages of phage therapy are its specificity (each phage can replicate only in certain bacterial species or strains), self-amplification (phages replicate in target bacterial cells) and biofilm degradation (unlike antibiotics phages can penetrate through bacterial biofilms and disperse it). Furthermore phages do not cause gastrointestinal side effects and can be used against multidrug resistant bacteria [5, 8].

As of 2019 there were two centres where phages therapy was applied to human patients: George Eliava Institute of Bacteriophages, Microbiology and Virology in Georgia and Phage Therapy Unit of the Medical Centre of the Institute of Immunology and Experimental Therapy PAS in Poland [39]. Stafal based on polyvalent staphylococcal phage is produced by Bohemia Pharmaceuticals [40].

Traditional phage therapy uses lytic phages which kill their bacterial hosts [5]. Recent approaches to phage therapy employ also lytic enzymes that might be also used as antimicrobial compounds [36].

2.2.1 Staphylococcus aureus attacking phage *Φ812*

Staphylococcus aureus is a gram positive pathogenic bacteria that causes bacteraemia, endocarditis, osteomyelitis and skin and tissue infections that might lead serious health complications or death [3]. WHO placed *S. aureus* on the priority pathogens list for which new treatment is urgently needed [4].

The first antibiotic-resistant strains of *S. aureus* occurred immediately after the introduction of the first antibiotics [37]. In 1960s methicillin resistant *S. aureus* strains (MRSA) were found. Their genome, transposons and plasmids carry genes for resistance against penicillin, trimethoprim, erythromycin, clindamycin, tetracycline and heavy metals. In 2002 *S. aureus* strain resistant to vancomycin, which was considered and used as the last resort therapy against *S. aureus*, was reported [3, 41]. Still, 95 % of *Staphyloccocus* strains are sensitive to the polyvalent phage *Φ812*, thus the phage has high potential to be used in phage therapy [7].

Twort-like phage *Φ812* belongs to the order *Caudovirales*, family *Myoviridae*. It is closely related to the phages *SK311*, *U16* and *Φ131*. Its genome consists of 146,5 kb linear double stranded DNA with G + C content 31,5 ± 0,2 mol % and T_m 82,2 ± 0,1 °C. [7, 39, 42]

Bacteriphage *Φ812* is composed from an icosaedral head (92 nm in diameter), tail (240 nm length and 18 nm width) baseplate and tail fibers (Figure 8) [43]. The attachment to the receptor located in the peptidoglycan-teichoic acid complex in the cell wall of *S. aureus* is mediated by the tail fibers [39, 43]. Then series of conformational changes causes detachment of the baseplate from the tip of the tail tube, the change of tail sheath proteins propagate along the tail, and as a result the baseplate is pulled toward the phage head and tail sheath contracts to 40 % of its original length [43]. Tail tube penetrates the cell wall to enable ejection of phage DNA to all cytoplasm. DNA release is regulated by the tail sheath contraction that enables the penetration of DNA into the neck and the conformational change of the tail tube that induces the genome ejection [43].

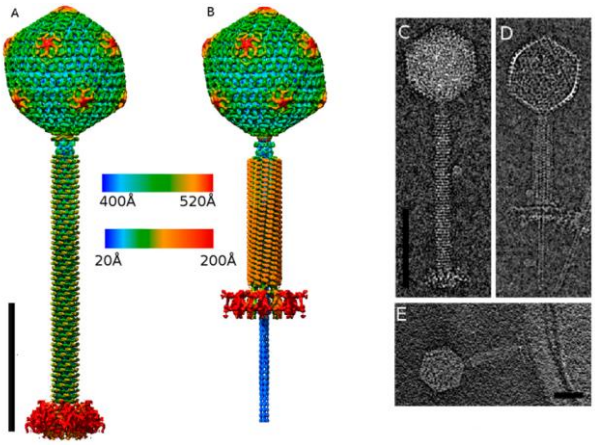

Figure 8: ***Cryo-electron microscopy of bacteriophage*** *Φ812. A) Three dimensional reconstruction of bacteriophage Φ812 in native conformation and B) after tail contraction. The heads are rainbow-colored according to the distance from the head center. The tails and baseplates are rainbow-colored according to the distance from the tail sixfold axis. C, D) Cryo-EM images of native and contracted phi812 virions, E) cryo-tomogram of phi812 virions attached to an S. aureus cell, scale bars 1,000 Å. Adapted from [43].*

2.2.1.1 Tail morphogenetic protein H

Tail morphogenetic protein H (TmpH) is a structural protein of phage *Φ812*. The gene of TmpH encodes 170 amino acids (Figure 9). TmpH is the product of gene *gp*156 located in the phage genome. There is homology between TmpH and protein 96 from bacteriophage K, putative major tail protein of bacteriophages SA5 and JA1, and protein 80 in phage G1, 71 in phage ISP and 142 in phage Sb-1. [44-46]

```
        10         20         30         40         50         60
LAKLNLYKGN ELLNSVEKTE GKSTITIENL DANTDYPKGT FKVSFSNDSG ESEKVDVPQF

        70         80         90        100        110        120
KTKAIKVISV TLDVDSLDLT VGDTHQLSTT ITPSEASNKN VSFESDKSGV ASVTSEGLIE

       130        140        150        160        170
AVSAGTANVT VTTEDGSHTD IVAVTVKEPI PEAPADVTVE PGENSADITV
```

Figure 9: ***Amino acid sequence of TmpH*** *[46].*

According to the information in NCBI GenBank database (GB: AZB49862.1) TmpH is part of *Φ812* phage tail and contains immunoglobulin-like domain at C-terminus [46]. The function of this protein is unclear but it was suggested that it might be a tail component responsible for the specific interaction of Twort-like phages with the host cell [45].

The Ig-like protein domains were identified in other phages from the family *Myoviridae.* It has been proposed that they provide survival advantage to phages by interacting weakly with carbohydrates on the bacterial cell surface. Thus, they allow the virus to stay attached to the cell while its tail fibres find their receptors. [45, 47]

2.3 Pest management

The second protein studied in this thesis is hexamerin from *Tribolium castaneum*. *T. castaneum* is a worldwide pest resistant against a variety of insecticides [9].

The intensive applications of broad-spectrum insecticides and fumigants lead to a number of adverse effects such as water and soil contamination, development of resistance among the target pests, toxicity to non-target organisms and human health risks [48, 49]. Frequently discussed alternatives to synthetic chemical insecticides are plant-derived compounds called bioinsectides (for example extracts of *Carica papaya, Ricinus communis*) [48], methods of biological control (that uses natural enemy species or parasitoids) [50] and using of insecticides based on insects hormones [49].

In insects there are two important hormones that control their life cycle: the juvenile hormone (JH) and ecdosyne. Both influence the timing and nature of molting in all members of the *Insecta* family (Figure 10) and the hormone-based insecticides either mimic or inhibit their activity. [49, 51, 52]

The most efficient hormone-mimicking insecticides: tebufenozide, methoxyfenozide, and chromafenozide are non-steroidal agonists of ecdosyne. They bind to ecdosyne receptor and trigger pre-mature molting process, that is never finished [53]. These insecticides show low toxicity for mammals and do not have any negative impact on the environment [49].

Juvenile hormone plays several roles: it modulates the function of ecdosyne and maintains the insect in larval state, stimulates vitellogenesis, regulates cast differentiation, polyphenism and reproductive diapause [54]. Many JH analogues were designed, synthesized, and analysed for insecticidal activity. Some of them are already commercially available (methoprene, hydroprene, fenoxycarb); these insecticides are suitable for control of insects in adult stage [49].

For control of immature larval pests the use of compounds that inhibit the JH biosynthesis and cause precocious induction of metamorphosis would be suitable, however these insecticides are not yet commercially available [54]. Insect protein hexamerin serves as a JH binding protein and there is an evidence that it effects the levels of JH [10].

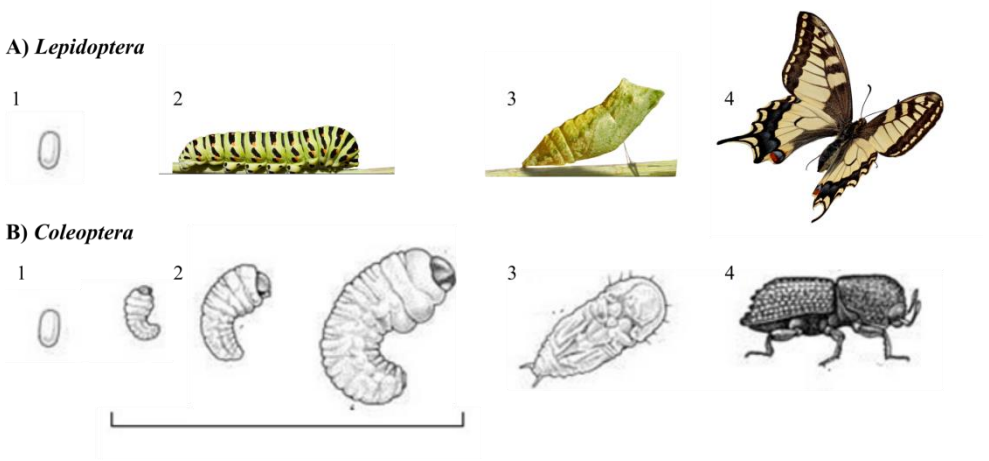

Figure 10: ***The process of metamorphosis in holometabolous insect.*** *The development comprises of several sages: 1. egg, 2. larva, the number of larval instars is species dependent, 3. pupa, 4. adult. Metamorphosis is regulated hormonally: in larva both ecdysone and JH are secreted, high titers of JH maintain the insect in larval stage; (JH causes repression of metamorphic gene expression). After the final larval molt, JH titer decreases and ecdysone triggers metamorphosis that results in the pupal transformation. Adapted from [49, 52, 55].*

2.3.1 Tribolium castaneum

Red flour beetle *Tribolium castaneum* is a widespread pest which damages cereals, grain, and dried stored products [9]. It is classified into the genus *Tribolium*, family *Tenebrionidae*, order *Coleoptera* (NCBI: txid7070) [56, 57]. *Tribolium castaneum* genome consists of ten pairs of chromosomes with the size of 160 Mb and almost 16 000 of genes [9, 58]. For its economic importance and the ease with which it can be reared in a laboratory it constitutes a common invertebrate model organism for various genetic and molecular studies [9, 59].

T. castaneum displays a typical holometabolous life cycle with 5 – 9 larval instars. Duration of embryonic and larval development and the length of metamorphosis are in the range of 31 – 148 days and depend on the growth conditions [9]. The lifespan of an adult insect is around 3 years. The beetle is highly prolific. It starts to reproduce at 1 month of age and females produce on average 200 – 500 eggs in their life-span [58]. Stages of *Tribolium castaneum* development are shown in Figure 11.

Laboratory beetles are usually raised on a mixture of wheat flour and dried brewer's yeast. They do not require water supply, but humidity below 40% reduces their fecundity. Its optimal habitat temperature is 30 °C [56], lower temperatures lead to prolongation of generation time, for long-term maintenance of stocks 23°C is recommended [9].

Figure 11: ***Stages of Tribolium castaneum development****. A) larvae, B) pupae, C) adult beetle. Adapted from [60].*

T. castaneum has propensity to develop resistance against a variety of insecticides and thus the studies of its lifecycle and behaviour and looking for new alternatives of classical synthetic insecticides are important [61].

2.3.1.1 Tribolium castaneum hexamerin

Hexamerins are the most abundant proteins in larval stages of holometabolous insects [62]. Hexamerins accumulate in the haemolymph of larvae and constitute up to 50 % of all proteins. [10] They evolved from crustacean hemocyanins, but lost the ability to bind copper ions and to transport oxygen [62]. Hexamerins serve as amino acid source during the non-feeding period, when pupae undergo the metamorphosis into the adult stage [10].

Hexamerins from different species have different sequence of amino acids. As the name indicates they usually consist of six homologous subunits with molecular weight around 80 kDa. Hexamerins of some species are enriched in aromatic amino acids (up to 26 % Phe and Tyr) or methionine (up to 10 %). [10]

The nomenclature of hexamerins is not well defined. Most of them have been identified in larval stages and were named larval serum proteins [63], larval haemolymph proteins [64], storage proteins [65] or they got species names like calliphorin, manducin or lucin [10]. Because of the high content of aromatic amino acids some of them were termed arylphorins [10]. Therefore in 1991 Telfer proposed that all related hexameric insects storage proteins should be called "hexamerins" [66].

Hexamerins are massively accumulated during larval stage while later in the adult stage of development disappear [10]. It was experimentally proven that radioactively labelled hexamerin amino acid become part of adult tissues [67]. Nowadays there is also evidence that hexamerins have other specific functions and are required in some particular other roles, such as cuticule formation and humoral immune defence [10].

Hexamerins bind small organic compounds such as riboflavin or biliverdin and serve as specific transporters of these molecules. With considerably high affinity $K_D \sim 10^{-9}$ they bind to juvenile hormone (JH) [10, 68]. It was found that JH bounds to the first domain of hexamerin [10].

Up to date there are 10 records for *Tribolium castaneum* hexamerin in UniProt database (Table 1). They are mostly named larval serum proteins and all have around 700 amino acids. Similarity scores between these sequences range from 27 to 99 % sequence identity. The structure of *Tribolium castaneum* hexamerin is unknown and it is one of the goals of this thesis to determine it.

Table 1: ***Summary of Tribolium castaneum hexamerin records in UniProt database****.*

Protein name	**Database ID**	**Size [amino acids]**	**Size [kDa]**
Pro-phenol oxidase subunit 2	Q49I38_TRICA	683	79.370
Phenoloxidase subunit A3-like Protein	Q49I39_TRICA	682	79.101
Phenoloxidase subunit A3-like Protein	D2A424_TRICA	683	79.339
Phenoloxidase subunit A3-like Protein	A0A139WGK2_TRICA	912	105.881
Larval serum protein 1 gamma chain-like protein	D6WUQ9_TRICA	698	84.554
Larval serum protein 2-like Protein	D6WUR0_TRICA	701	84.601
Larval serum protein 2-like Protein	D6WUR1_TRICA	695	83.049
Larval serum protein 2-like Protein	D6WUQ8_TRICA	748	91.020
Larval serum protein 2-like Protein	D6WXB6_TRICA	703	83.586
Larval serum protein 2-like Protein	D6WUQ7_TRICA	748	90.989

3 AIMS OF THE THESIS

1. Theoretical review focused on biological functions of bacteriophage *Φ812* Tail morphogenetic protein H (TmpH) and hexamerin.
2. Optimisation of methods for isolation of hexamerin from *Tribolium castaneum* pupae.
3. Optimisation of methods for bacterial expression and purification of protein TmpH.
4. Crystallization of isolated *Tribolium castaneum* hexamerin and TmpH.
5. Determination of *Tribolium castaneum* hexamerin structure using X-ray crystallography and cryo-EM.
6. Analysis and discussion of obtained results.

4 MATERIALS AND METHODS

4.1 Materials

4.1.1 List of chemicals

Acetic acid, 99.8 %	PENTA	Methanol	SIGMA
Acetone	PENTA	Midori Green DNA stain	Elisabeth Pharmacon
Acrylamide/bis-acrylamide	SIGMA	Nickel sulphate heptahydrate	SIGMA
Agarose	SIGMA	Nonidet-(TM) P 40	SIGMA
Ammonium acetate	MERCI	Octyl-thio-glukoside	GOLDBIO
Ammonium citrate dibasic	SIGMA	PMSF	SIGMA
Ammonium chloride, > 99,5%	SIGMA	Polyethylen glycol 10 000	SIGMA
Ammonium hydroxide solution	SIGMA	Polyethylen glycol 1000	SIGMA
Ammonium sulfate, p. a.	PENTA	Polyethylen glycol 1500	SIGMA
Ampicilin	CARL ROTH	Polyethylen glycol 20 000	SIGMA
Barium chloride	MERCI	Polyethylen glycol 200	SIGMA
BIS-TRIS	SIGMA	Polyethylen glycol 2000	SIGMA
Briliant Blue G-250	SIGMA	Polyethylen glycol 300	SIGMA
Calcium acetate hydrate	SIGMA	Polyethylen glycol 3350	SIGMA
Calcium chloride dihydrate	SIGMA	Polyethylen glycol 400	SIGMA
Citric acid monohydrate	PENTA	Polyethylen glycol 4000	SIGMA
Chloramphenicol	CARL ROTH	Polyethylen glycol 4600	SIGMA
Chloroform	SIGMA	Polyethylen glycol 550	SIGMA
Cobalt (II) chloride hexahydrate	SIGMA	Polyethylen glycol 600	SIGMA
DMSO	SIGMA	Polyethylen glycol 6000	SIGMA
DTT, dithiothreitol	SIGMA	Polyethylen glycol 8000	SIGMA
EDTA	SIGMA	Potassium acetate	SIGMA
Ethanol, 99.8 %	PENTA	Potassium hydroxide	MERCI
Ethylenglycol	PENTA	Potassium chloride	SIGMA
Glucose	PENTA	2-propanol	PENTA
Glycerol	PENTA	Propylenglycol	PENTA
Guanidine hydrochloride	SIGMA	Sodium acetate	SIGMA
Yeast extract	PENTA	Sodium chloride	SIGMA
HEPES	SIGMA	Sodium citrate tribasic dihydrate	SIGMA
HEPES sodium salt	SIGMA	Sodium dodecyl sulphate	SIGMA
Imidazole	SIGMA	Sodium hydroxide	SIGMA
IPTG	SIGMA	Sodium sulfate	SIGMA
Instant Blue gel stain	SIGMA	TAE Buffer (50 × concentrate)	Electran-Vitrum
Kanamycin	CARL ROTH	TCEP-HCl	GOLDBIO
LB agar	SIGMA	TEMED	SIGMA
LB Broth	SIGMA	TRIS	GE
LB medium in tablets	SIGMA	Tween 20	SIGMA
Lithium sulfate monohydrate	SIGMA	Urea	SIGMA
Lysozyme from chicken egg	SIGMA	Water for PCR	SIGMA
Magnesium acetate	SIGMA	Zinc chloride	SIGMA
Magnesium chloride hexahydrate	PENTA	Zinc sulfate heptahydrate	SIGMA
Magnesium sulfate anhydrous	SIGMA	Zinc acetate	SIGMA

4.1.2 List of enzymes

BseR-I	New England BioLabs
Lysozyme	SIGMA
Nde-I	New England BioLabs
Phusion HF DNA Polymerase	New England BioLabs
T4 DNA polymerase	New England BioLabs
Turbo Nuclease	Abnova

4.1.3 Standards for agarose gel electrophoresis and polyacrylamide gel electrophoresis in the presence of sodium dodecyl sulphate (SDS-PAGE)

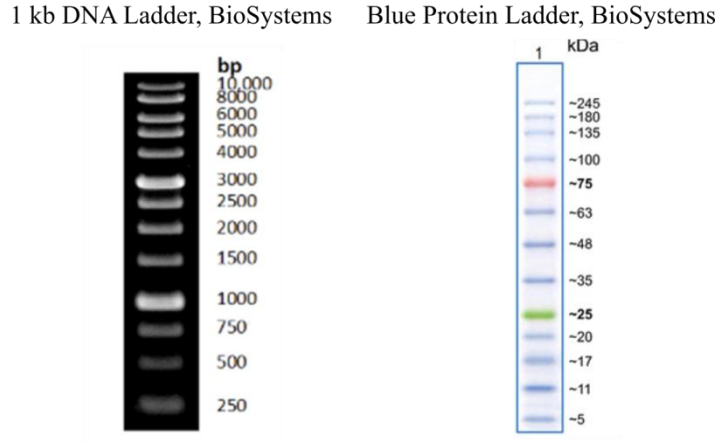

Figure 12: ***A) DNA molecular weight marker, B) SDS-PAGE Molecular weight standard.***

4.1.4 List of buffers

Table 2: ***Chemical composition of buffers used for purification. (****A: affinity chromatography on prepacked columns, B: buffers for chromatography of hydrophobic interactions, C: for affinity chromatography on NiNTA resin, D: buffer for size exclusion chromatography, H and Q buffers for hexamerin isolation).*

lysis buffer A	50 mM Tris pH 8, 150 mM NaCl, 1 % octylthioglucoside, 1 mg/ml lysozyme, 2 µl Turbo Nuclease®
loading buffer A	50 mM Tris pH 8, 150 mM NaCl, 25 mM Imidazole
elution buffer A	50 mM Tris pH 8, 150 mM NaCl, 350 mM Imidazole
loading buffer B	50 mM Tris pH 8, 50 mM NaCl, 1M $(NH_4)_2SO_4$
elution buffer B	50 mM Tris pH 8, 50 mM NaCl
equilibration buffer C	50 mM Tris pH 8, 250 mM NaCl, 25 mM Imidazole
wash buffer C	50 mM Tris pH 8, 250 mM NaCl
elution buffer C	100 mM Tris pH 8, 250 mM NaCl, 300 mM Imidazole
superdex buffer D	50 mM Tris pH 8, 150 mM NaCl
lysis buffer H	60 mM HEPES pH 7.5, 100 mM KCl, 10 mM $MgCl_2$, 4 mM DTT, 1% NP-40
final buffer H	30 mM HEPES pH 7.5, 150 mM KCl, 5 mM $MgCl_2$ and 2 mM DTT
wash buffer Q	30 mM HEPES pH 7.5
elution buffer Q	30 mM HEPES pH 7.5, 1 M KCl
final buffer Q	30 mM HEPES pH 7.5, 100 mM KCl

4.1.5 List of primers

Table 3: ***Table of used primers in 5'– 3' direction****.*

TmpH_pET22T	
forward	AGATTGGTGGCATGGCTAAGTTAAATTTATACAAAGG
reverse	GAGGAGAGTTAAGACTTACACAGTAATATCTGCGCTATTTTCACC
TmpH_pET22b	
forward	AAGGAGATATACATATGGCTAAGTTAAATTTATACAAAGG
reverse	AGCAGGTATTTCATACTATACAGTAATATCTGCGC

4.1.6 List of equipment

3D Rotatory Mixer, MiuLab
ÄKTA Prime FPLC system, GE Healthcare Life Sciences
ÄKTA Pure FPLC system, GE Healthcare Life Sciences
Apparatus for Electrophoresis, Labnet
Autoclave EL D-line 2840 TUTTNAUER, Breda
Biovanguard Class II Safety Cabinet, Telstar
BOSCH PBD 40
Centrifuge 4-16 KS, SIGMA
Centrifuge 5424 R, Eppendorf
Centrifuge 5424, Eppendorf
Centrifuge Z 32HK, HERMLE Labortechnik GmbH
Delta Max Core, Beckham Coulter
Digital Hot Plate Stirrer MS7-H550-Pro, SCILOGEX
Dry Bath Incubator DKT200, MiuLab
Electronic Analytical Balance Mark M21-44i, BEL Engineering
Electronic Balance Mark ES 2201, BEL Engineering
Electronic Balance Mark KERN EMB 600-2, P-Lab
GeneQ Thermocycler type E, BIOER
Laboratory Shaker PRO 30 Reciprocal, Labnet
Magnetic Stirrer NMS-3 000, BIOSAN
Microcentrifuge MiniStar, VWR
Microcentrifuge Microspin 12, BIOSAN
Mini Incubator I5110A-230V, Labnet
Mixing Block MB-102, BIOER
UV/VIS spectrophotometer Nanodrop 2000c, Thermo Fisher Scientific
Optical microscope Leica S8AF
PBD 40 stand drill, BOSCH
pH meter PL-700 PVS, Gondo
Photometer Dilu IMPLEN OD600, IMPLEN GmbH
Plasma cleaner, Quorum Technologies
Power Supply ENDURO 300V, Labnet
Incubator shaker INNOVA 44, New Brunswick Scientific
Sonicator Q700, QSONICA
Transmission electron microscope Titan Krios, Thermo Fisher Scientific
Transmission electron microscope Talos Arctica, Thermo Fisher Scientific
Transmission electron microscope Tecnai G2 F20, Thermo Fisher Scientific
UV transilluminator UVITEC, Cambridge
Ultrasonic Cleaner SONICA, SOLTEC
Vitrification robot Mark IV, Thermo Fisher Scientific
Vortex Gene-2-T, P-Lab
Vortex V-1 Plus, BIOSAN
standard laboratory glass and equipment

4.2 Methods

4.2.1 Molecular cloning

4.2.1.1 Restriction digest of plasmid DNA

Restriction digest of plasmid DNA was done in PCR tubes in total reaction volume of 10 µl for 2 hours at 37 °C. The reaction mixture contained chemicals listed in Table 4. The sample for negative control contained 1 µl of ddH_2O instead of the restriction enzyme. The results of the reaction were verified by agarose gel electrophoresis.

Table 4: ***Restriction digest mixture composition****. Reagents are in order in which they were added to the mixture.*

ddH_2O	up to 10 µl
buffer Cut Smart 10x	1/10 of total volume
plasmid	1 µg
restriction enzyme	10 units (generally 1 µl)

4.2.1.2 Agarose gel electrophoresis

The gel for agarose gel electrophoresis was prepared by mixing warm 1% agarose solution in TAE buffer (0.5 g in 50 ml TAE per gel) with 2.5 µl of Midori Green. The wells for sample application were prepared by inserting a comb before the gel was left to cool. In general, a sample for electrophoresis consisted from 3 µl of TAE buffer, 1 µl of Gel Loading Dye, Purple (6×) (New England, BioLabs) and 2 µl of DNA sample. For the estimation of molecular weight 1 kb DNA Ladder was used as molecular weight marker (Figure 12). Electrophoresis was run for approximately 30 minutes under constant voltage of 160 V. The stained DNA was visualised under UV light.

4.2.1.3 Polymerase chain reaction

PCR was used to amplify the DNA sequence containing the gene of TmpH. Primers were designed using AmplifX software. Proof-reading Phusion High-Fidelity DNA Polymerase possesses 5′→ 3′ polymerase activity, 3′→ 5′ exonuclease activity and generates blunt-ended products. It was chosen because of its high accuracy and speed. The composition of reaction mixture is listed in Table 5. Total reaction volume was 25 µl.

Table 5: ***The composition of PCR reaction mixture****. Reagents are in order in which they were added.*

ddH2O	up to 25 µl	17 µl
Phusion Buffer HF	5×	5 µl
$MgCl_2$	50 mM	0.5 µl
dNTPs	10 mM (each)	0.5 µl
forward primer	100 µM	0.25 µl
reverse primer	100 µM	0.25 µl
DNA template	10 ng/µl	1.0 µl
Phusion® HF DNA Polymerase	100 U/µl	0.5 µl

PCR was performed in thermocycler using the following program:

- heated lid: 105 °C, preheated lid
- initial denaturation: 98 °C, 1 min
- 10 cycles: 10 s, 98 °C 15 s, 60 °C 10 s, 72 °C
- 10 cycles: 10 s, 98 °C 15 s, 55 °C 10 s, 72 °C
- 15 cycles: 10 s, 98 °C 15 s, 50 °C 10 s, 72 °C
- final extension: 72 °C, 5 min
- final hold: 10 °C

4.2.1.4 Ligation independent cloning

Insert (gene of TmpH amplified by PCR) as well as a vector (plasmid linearized by restriction digest) were purified using Monarch Nucleic Acid Purificatoin Kit (New England, BioLabs) according to the manufacturer protocol.

Sticky ends modifications of the insert and vector were done by treating them with T4 DNA polymerase in a reaction mixture of composition showed in Table 6.

Table 6: ***Reaction mixture for sticky ends modification of insert and vector****. Reagents are in order in which they were added to the mixture.*

		insert	vector
ddH2O	up to 20 µl	15.1 µl	15.1 µl
NEB2 buffer	1/10 volume	2 µl	2 µl
dGTP	100 mM	0.5 µl	-
dCTP	100 mM	-	0.5 µl
DTT	100 mM	1 µl	1 µl
PCR product	~ 100 µg/ml	1 µl	-
linearized plasmid	~ 1000 µg/ml	-	1 µl
T4 DNA polymerase	3 U/µl	0.4 µl	0.4 µl

Reaction mixture was incubated in thermocycler using the following program:

- heated lid: 105 °C, preheated lid off
- initial denaturation off
- 30 min, 22 °C
- 20 min, 72 °C
- final hold: 4 °C

Finally, an insert and vector were mixed and incubated for 15 minutes at room temperature. Sticky ends annealed by hydrogen bonds and a new construct was formed. NEB® Turbo competent cells were transformed by the newly formed construct. As a negative control 1 µl of ddH_2O was added instead of the insert into the annealing reaction mixture (Table 7).

Table 7: ***Annealing reaction mixture composition****.*

vector	1 µl
insert	2 µl
EDTA 25 mM	1 µl

4.2.1.5 T4 DNA Polymerase mediated cloning

Monarch Nucleic Acid Purificatoin Kit was used to purify the insert (gene of TmpH amplified by PCR) and vector (plasmid linearized by restriction digest). Reaction mixture of total volume 10 µl (Table 8) was pipetted into PCR tube and incubated for 2.5 min at room temperature and 15 min on ice. Prepared construct was used for the transformation of NEB® Turbo competent cells. Negative control was done by adding 1 µl of ddH_2O instead of the insert.

Table 8: ***The composition of reaction mixture for T4 mediated cloning****.*

vector	6.0 µl
insert	2.0 µl
NEB 2 buffer	1.0 µl
T4 DNA Polymerase	0.4 µl
ddH_2O	0.6 µl

4.2.1.6 Transformation of chemically competent cells

Competent cells of *Escherichia coli* NEB® Turbo stored at -80 °C were thawn on ice. Prepared DNA construct was added to the thawn competent cells and the cells were incubated 20 minutes on ice, to let the plasmid DNA bind to the cell surface [69]. Then the mixture was incubated for 1 minute at 42 °C (heat shock) and then for 2 minutes on ice. Super optimal broth with catabolite repression medium (SOC) (400 µl) was added and the whole mixture was incubated at 37 °C. After 1 hour, the cell suspension was centrifuged (3 000 g, 3 min) and the resulting supernatant was gently discarded. The pellet was resuspended in the remaining liquid and spread over lysogeny broth agar (LB) plates with appropriate antibiotic. The plates were incubated over night at 37 °C.

4.2.1.7 Colony PCR

The screening of colonies for the presence of desired plasmid was done by Colony PCR. From each plate of transformed cells at least 5 colonies were picked and used for inoculation of 4 ml lysogeny broth (LB) media with proper selection antibiotic. After 3 hours of incubation at 37 °C 0.5 µl of culture from each tube was pipetted into a PCR tube and mixed with Colony PCR Master Mix (Table 9).

Table 9: ***Colony PCR Master Mix composition****. Final volume of one reaction is 12.5 µl.*

	per reaction [µl]
ddH_2O	9.10
Elizyme Buffer (5× conc.)	2.50
dNTPs (10 mM each)	0.25
F primer (100 µM)	0.06
R primer (100 µM)	0.06
Elizyme Tac. polymerase (5 U/µl)	0.06
template (cell suspension)	0.50

Colony PCR reaction was run in the thermocycler using the following program:

- initial denaturation: 4 min, 95 °C
- 30 × cycle: Denaturation 15 s, 95 °C
  Annealing 15 s, 55 °C
  Extension 15 s, 72 °C
- final extension: 4 min, 72 °C
- final hold: 4 °C

Agarose gel electrophoresis was used to verify the presence of the transformed plasmid. Cultures containing transformed cells with construct of interest were used for glycerol stock preparation and as an inoculum for larger amount of LB media (120 ml) which was incubated overnight (37 °C, 250 rpm). Plasmid was isolated and purified from the overnight grown cultures by kit GenElute™ HP Plasmid Midiprep Kit (Sigma-Aldrich). The correctness of the insert was verified by DNA sequencing.

4.2.1.8 Glycerol stock preparation

E. coli cells containing the plasmid of interest were preserved for future use by freezing in glycerol broth [70]. To 1 ml of overnight grown cell culture 0.5 ml of sterile glycerol was added, the mixture was vortexed for 1 min and then immediately stored at -80 °C.

4.2.2 Production of proteins in *E. coli*

For the recombinant protein production, the *E. coli* strain BL21(DE3) was used. Conditions 37 °C and 250 rpm were chosen as a starting point for protein expression optimization. The expression of the gene under the T7 promoter was triggered either by adding of isopropyl β-D-1-thiogalactopyranoside (IPTG) to the culture at exponential phase of growth or by lactose when using auto-induction media. The expression lasted 5 hours and was monitored by taking 1 ml samples of cell culture every hour. The yields of the protein were analysed by SDS-PAGE electrophoresis.

4.2.2.1 Protein production induced by IPTG

Isopropyl β-D-1-thiogalactopyranoside is a non-hydrolyzable analogue of lactose that could serve as a *lac* operon inducer [71]. The protein expression was performed at 37 °C and 250 rpm in 500 ml of LB media with appropriate antibiotic inoculated using 500 µl of overnight culture (0.1% inoculum). The cells were cultivated until the optical density of the cell culture reached OD_{600} = 0.4 – 0.6, then 0.4 mM IPTG (final concentration) was added. After 5 hours the cells were harvested by centrifugation at 5 000 g for 10 min, supernatant was discarded and the pellets were stored at -20 °C.

4.2.2.2 Protein production in auto-induction media

Medium ZYP-5052 (Table 10; 500 ml) [72] containing proper antibiotic was inoculated with 500 µl of overnight culture (cells grown in LB medium) and cultivated at 37 °C, 250 rpm. After 24 hours the optical density OD_{600} was measured each 30 minutes until it stopped increasing. Then the cells were harvested by centrifugation at 5 000 g, 10 min and the pellets were stored at -20 °C.

Table 10: ***ZYP-5052 medium components according to*** *[72]. For 1 l of media: 928 ml ZY, 50 ml 20 × P, 20 ml 50 × 5052 and 2 ml 500 × $MgSO_4$ should be mixed.*

stock solution		per 1L media
ZY	1% tryptone	10 g/l
	0.5% yeast extract	5 g/l
20 × P	1.0 M $Na_2HPO_4 \cdot 7H_2O$	268 g/l
	1.0 M KH_2PO_4	136 g/l
	0.5 M $(NH_4)_2SO_4$	66 g/l
50 × 5052	25 % glycerol	250 g/l
	2.5 % glucose	25 g/l
	10 % α-lactose	100 g/l
500 × $MgSO_4$	1 M $MgSO_4 \cdot 7H_2O$	24.65 g/100 ml

4.2.2.3 Cell lysis

During the expression tests 1 ml samples were taken every hour. They were centrifuged at 20 000 g, supernatant discarded and the pellet resuspended in lysis buffer A. The amount of lysis buffer used was dependent on the density of the culture (Table 11). The samples were mixed for 15 minutes on rotary mixer. Then, 10 µl of lysate was taken, representing the total amount of proteins in the lysate, and the samples were centrifuged at 20 000 g, 5 min. Supernatant (10 µl) was taken for further analysis, representing the soluble fraction of proteins in the lysate. To analyse the yield and solubility of the expressed protein the lysates were analysed on 15% SDS-PAGE.

Table 11: ***The amount of lysis buffer added according to the time after the induction with IPTG in which the sample was taken****.*

time [h]	lysis buffer [µl]
0	50
1	70
2	90

time [h]	lysis buffer [µl]
3	110
4	130
5	150

4.2.2.4 SDS-PAGE

Visualization and analysis of protein samples was done using SDS-PAGE. Protein loading buffer (PLB 5× concentrated) (2.5 µl) was added to 10 µl of sample. The mixture was incubated at 95 °C for 3 minutes and then loaded into the wells in polyacrylamide gel. The electrophoresis was run in SDS buffer under 180 V until the samples got concentrated by the stacking gel and then with using constant voltage of 250 V for approximately 30 minutes. Gel visualization was done by staining either by Blue Silver [73] or by Instant Blue™ Protein Stain. For protein molecular weight determination Blue Protein Ladder standard was used (Figure 12).

4.2.3 Protein purification

4.2.3.1 Affinity chromatography on prepacked HisTrap™ columns

Immobilized metal ion affinity chromatography (IMAC) is based on reversible interaction between transition metal ion (Co^{2+} Ni^{2+}, Cu^{2+}, Zn^{2+}) immobilized on a matrix and protein affinity tag [85].

Harvested cells were lysed for 30 min on rotary mixer in 20 ml of lysis buffer A and then centrifuged at 20 000 g for 10 min. Imidazole with the final concentration of 25 mM was added to the supernatant and the solution was loaded onto 5 ml HisTrap™ column. Flow rate was set to 5 ml/min. Wash was performed with 5 column volumes of buffer A. Elution was triggered with 350 mM imidazole in elution buffer A.

4.2.3.2 Affinity chromatography on NiNTA resin

The column was filled with NiNTA resin (3 ml bed volume) and equilibrated with 10 ml of equilibration buffer C. Equilibrated resin was mixed with 20 ml of the cell lysate in lysis buffer A with concentration of NaCl increased to 250 mM. The mixture was incubated for 60 minutes on rotary mixer at 4 °C. Flow through fraction was drained by gravity flow. Wash was done with 10 bed volumes of wash buffer C. Protein was eluted with elution buffer C (3 ml fractions).

4.2.3.3 Size exclusion chromatography (SEC)

Elution fractions containing TmpH were concentrated and loaded on Superdex column for size exclusion chromatography. Purification with size exclusion chromatography is based on the effect of inverse sieving [79]. SEC was used to increase protein purity and change the buffer composition (to remove the imidazole and to decrease the concentration of NaCl).

4.2.3.4 Removal of N-terminal tag using Ulp1-ac protease

Cleavage of the N-terminal tag (His-tag Smt3 fusion) was done by Ulp1-ac protease. Fractions that contained desired protein were mixed with 15 mM TCEP (tris(2-carboxyethyl)phosphine, which serves as reducing agent) and 1 mM PMSF (phenylmethylsulfonyl fluoride, serine protease inhibitor). The cleavage was done overnight at room temperature on rotary mixer. Control samples without Ulp1-ac protease were prepared in the same way and incubated at -20 °C, the second at room temperature.

4.2.3.5 Precipitation with ammonium sulphate

Ammonium sulphate solution saturated at 0 °C was prepared by dissolving 191.7 g of $(NH_4)_2SO_4$ in 250 ml dH_2O at 25 °C and cooling it down to 0 °C. Precipitation was done by adding ammonium sulphate to the final concentration of 2.2 M [74] into 20 ml of cell lysate (one cell pellet harvested by centrifugation at 5 000 g from 0.5 l of cell culture lysed in lysis buffer A). This solution was incubated 10 min on ice with 30 s vortexing cycles performed every 2 minutes. Then the solution was centrifuged at 20 000 g for 5 minutes and the supernatant was discarded. The pellet was resuspended in 15 ml of loading buffer B. This sample was used for separation using chromatography of hydrophobic interactions. Whole purification process was done on ice or at 4 °C.

4.2.3.6 Chromatography of hydrophobic interaction (HIC)

HIC is based on reversible adsorption of biomolecules to hydrophobic surface in chromatographic column [82]. Sample precipitated by ammonium sulphate and dissolved in loading buffer B was loaded on the HiTrap Phenyl HP 1 ml column (GE Healthcare) equilibrated with loading buffer B. Gradient elution was done by decreasing the concentration of salt with elution buffer B. Samples for SDS-PAGE analysis were desalted by methanol – chloroform protein precipitation.

4.2.3.7 Quantitative protein precipitation for SDS-PAGE analysis

A Salt containing protein sample (100 µl) was mixed with 400 µl of methanol and vortexed. Then 100 µl of chloroform were added and the sample was vortexed again. After addition of 300 µl ddH_2O and vortexing, the sample was centrifuged at 14 000 g for 2 minutes. The top aqueous layer of the supernatant was pippeted off and 400 µl of methanol were added into the tube. After vortexing the solution was centrifuged at 14 000 g for 3 minutes. The supernatant containing methanol was pippeted away and the pellet was dried in a dry bath incubator. The dried pellet was resuspended in 10 µl of elution buffer B and used for SDS-PAGE analysis.

4.2.4 DLS analysis

DLS measurements were performed on Delta Max Core instrument. Each measurement was done with 20 acquisitions with acquisition time 5 s. Laser power was set depending on the protein concentration and size (for TmpH of concentration 1 mg/ml it was set up to 30 %, for protein hexamerin of concentration of 10 mg/ml 5% laser power was sufficient). Results of the experiment (correlation curves and histograms) were calculated using Delta Max software.

4.2.5 Preparation of protein crystallization screens

Crystallization screens were prepared in Biomolecular Interactions and Crystallization Core Facility at CEITEC MUNI. Sitting drop vapour method was used for the screening. In each well from 96 well plate three different ratios of protein:precipitant were mixed (200 + 100) nl, (100 + 100) nl and (100 + 200) nl. The plates were stored at 20 °C in crystallization hotel (Rigaku Minstrel HT-UV) and automatically photodocumented at visible and UV light.

The list of used crystallization screens for TmpH crystallization is following:

- Classics Suite, manufacturer Qlagen-Nextal
- Classics II Suite, manufacturer Qlagen-Nextal
- PEGs Suite, manufacturer Qlagen-Nextal
- PEGs II Suite, manufacturer Qlagen-Nextal
- MIDAS, manufacturer Molecular Dimensions
- MORPHEUS, manufacturer Molecular Dimensions

The list of used crystallization screens for hexamerin crystallization is following:

- Classics Suite, manufacturer Qlagen-Nextal
- Classics II Suite, manufacturer Qlagen-Nextal
- PEGs Suite, manufacturer Qlagen-Nextal
- PEGs II Suite, manufacturer Qlagen-Nextal

4.2.6 2D optimization of protein crystallization conditions by hanging drop method

To optimize the crystallization conditions the hanging drop method was used. For the most promissing conditions from sitting drop screening the 2D screens on 24 wells plates were prepared. For each well two drops with protein:precipitant ratios of 1:1 and 1:2 were mixed. The total volume of each drop was 1 µl and the total volume of the well reservoir was 500 µl. The crystallization drops were inspected under the light microscope.

Figure 13 shows experimental setup of 2D screens crystallization optimization of TpmH. The concentration of protein was changed in one direction and the concentration of precipitant in the other. The used concentrations of TmpH were 18 mg/ml, 15 mg/ml and 12 mg/ml. The original chemical composition of each condition is listed in Table 12, the compound whose concentration was changed is written in bold. The crystallization plates were stored at 20 °C.

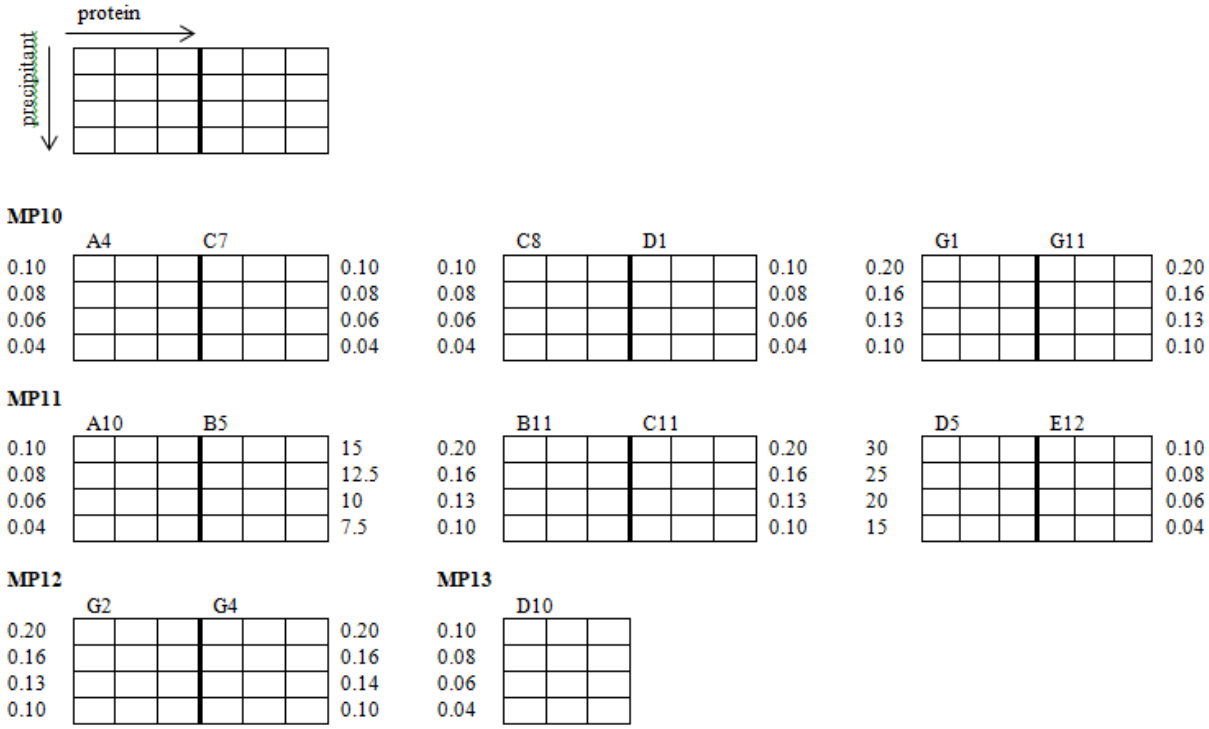

Figure 13: ***The experimental setup of 2D screens for TmpH crystallization optimization****. The concentration of TmpH is varied in x-axis (18 mg/ml, 15 mg/ml, 12.5 mg/ml) and the concentration of precipitant is changed in y-axis (numbers written along the side in mol/dm^3). Each plate is marked by number of condition and screen from which it was derived.*

Table 12: ***Chemical composition of promising conditions for TmpH crystallization****. The first column contains name of the screen and its label in CrystalTrack system, the second column contains condition specification, chemical composition is written in the third column. The compound written in bold was chosen as a precipitant whose concentration was changed in 2D screen.*

screen	condition	orginal composition
MP10 PEGs Suite 11 mg/ml	A4	25 % v/v PME 550, 0.1 M **sodium acetate pH 4.6**
	C7	25 % w/v PEG 3 000, 0.1 M **MES pH 6.5**
	C8	25 % w/v PEG 4 000, 0.1 M **MES pH 6.**5
	D1	25 % w/v PEG 3 000, 0.1 M **HEPES pH 7.5**
	G1	20 % w/v PEG 3 350, 0.2 M **magnesium chloride**
	G11	20 % w/v PEG 3 350, 0.2 M **ammonium sulphate**
MP11	A10	30 % w/v PEG 400, 0.1 M MES pH 6.5, 0.1 M **magnesium chloride**

PEGs II Suite 11 mg/ml	B5 B11 C11 D5 E12	15 % w/v **PEG 1 500** 20 % w/v PEG 3 000, 0.1 M HEPES pH 7.5, 0.2 M **sodium acetate** 20 % w/v PEG 4 000, 0.1 m Tris pH 8.5, 0.2 M **lithium sulphate** 30 % w/v **PEG 4 000** 20 % w/v PEG 4 000, 5 % w/v 2-propanol, 0.1 M **tri-sodium citrate**
MP12 Classics 8.5 mg/ml	G2 G4	28 % v/v PEG 400, 0.1 M HEPES pH 7.5, 0.2 M **calcium chloride** 30 % v/v PEG 400, 0.1 M HEPES pH 7.5, 0.1 M **magnesium chloride**
MP13 Classics II 8.5 mg/ml	D10	20 % w/v PEG monomethylether 5 000, **bis-tris pH 6.5**

Figure 14 shows experimental setup of 2D screens for optimization of hexamerin crystallization. The original chemical compositions of these conditions are listed in Table 13. The actual concentration of selected precipitant in each well is written on the side. The used hexamerin concentrations were: 15 mg/ml, 12.5 mg/ml and 10 mg/ml. The crystallization plates were stored at 20 °C.

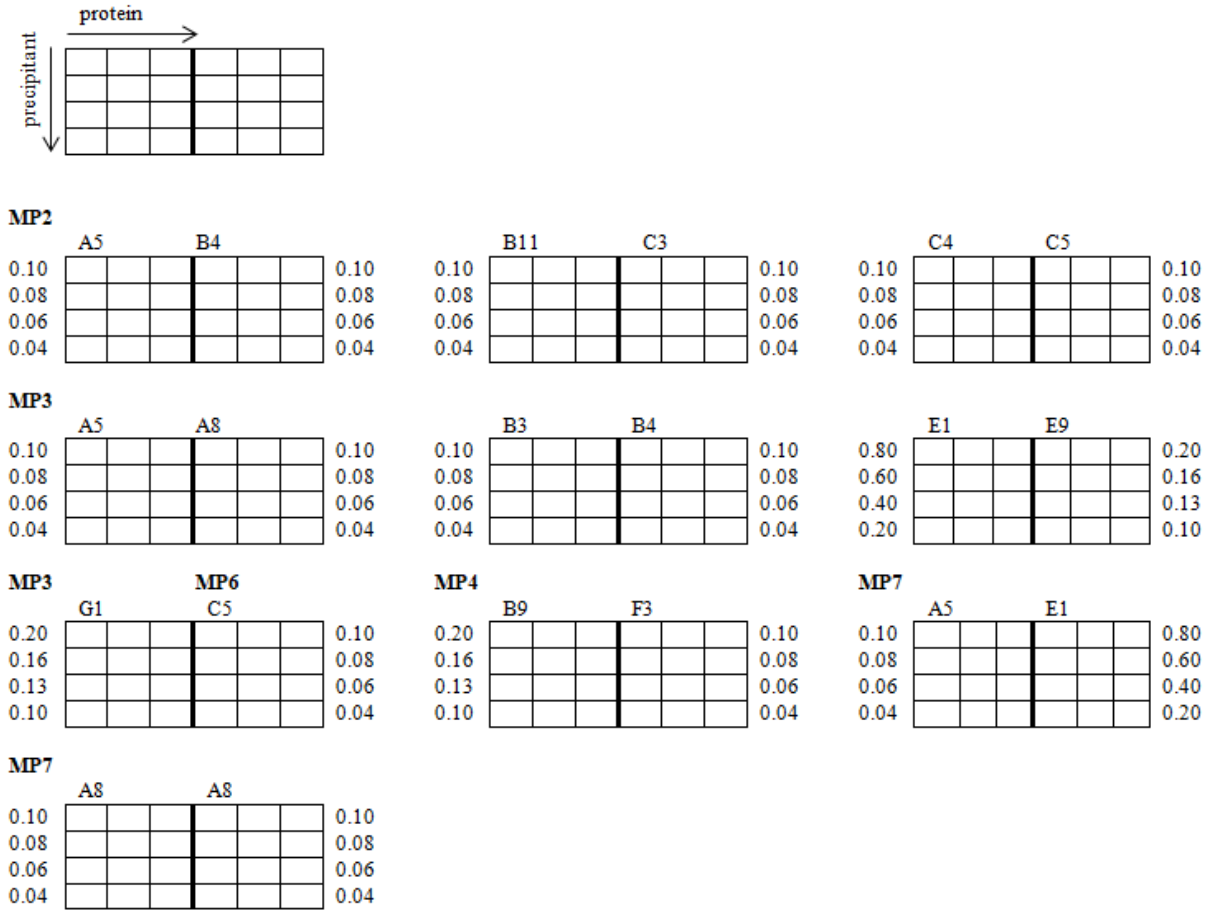

Figure 14: ***The experimental alignment of 2D screens for hexamerin crystallization optimization.*** *2D screens were set on crystallization plates with 24 wells, the concentration of protein hexamerin was varied in x-axis (15 mg/ml, 12.5 mg/ml, 10 mg/ml) and the concentration of precipitant changed in y-axis (concentration of precipitant is written in mol/dm^3 along the side). Each plate is labeled by number of condition and screen from which it was derived.*

Table 13: ***Promising conditions from the crystallization screens and their composition****. Name of the screen, its label in system and used hexamerin concentration are in the first column, the second column contains condition specification and in the third column its chemical composition is written. The compound in bold text was chosen as a precipitant which concentration was changed in 2D hanging drop optimization screens.*

screen	condition	composition
MP2 PEGs Suite 12.5 mg/ml	A5	25 % w/v PEG 1 000, 0.1 M **sodium acetate** pH 4.6
	B4	25 % v/v PEG monomethylether 550, 0.1 M **HEPES** pH 7.5
	B11	25 % w/v PEG 1 000, 0.1 M **trishydrochloride** pH 8.5
	C3	25 % w/v PEG 6 000, 0.1 **sodium acetate** pH 4.6
	C4	25 % w/v PEG 8 000, 0.1 M **sodium acetate** pH 4.6
	C5	20 % w/v PEG 10 000, 0.1 M **sodium acetate** pH 4.6
MP3 PEGs II Suite 12.5 mg/ml	A5	0.1 M **$MgCl_2$**, 25 % w/v PEG 400, 0.1 M sodium acetate pH 4.6
	A8	0.1 M **$CaCl_2$**, 30 % w/v PEG 400
	B3	25 % w/v PEG 1 000, 0.1 M **HEPES** pH 7.5
	B4	30 % w/v PEG 1 000, 0.1 M **Tris** pH 8.5
	E1	0.8 M **LiCl**, 8 % w/v PEG 4 000, 0.1 M Tris pH 8.5
	E9	0.2 M **ammonium sulfate**, 16 % w/v PEG 4 000, 0.1 M HEPES pH 7.5
	G1	0.2 M **lithium sulfate**, 25 % w/v PEG monomethylether 5 000, 0.1 M Tris pH 8.5
MP4 Classics Suite 25 mg/ml	B9	0.2 M $NH_4H_2PO_4$, 0.1 M tris pH 8.5, 50 % v/v 2-methyl-2,4-pentanediol
	F3	8 % w/v PEG 8 000, 0.1 M **trishydrochloride** pH 8.5
MP6 PEGs Suite 25mg/ml	C5	20 % w/v PEG 10 000, 0.1 M **sodium acetate** pH 4.6
MP7 PEGs II Suite 25 mg/ml	A5	0.1 M **$MgCl_2$**, 25 % w/v PEG 400, 0.1 M sodium acetate pH 4.6
	A8	0.1 M **$CaCl_2$**, 30 % w/v PEG 400, 0.1 M **sodium acetate** pH 4.6
	E1	0.8 M **LiCl**, 8 % w/v PEG 4 000, 0.1 M Tris pH 8.5

4.2.7 Isolation and purification of hexamerin

T. castaneum pupae (5 g) were pre-homogenized in 20 ml of lysis buffer H by PBD 40 stand drill equipped with Teflon pestle. The homogenate was poured into glass Dounce homogenizer and further homogenized using pestle A followed by pestle B at least 20 times. The last remaining aggregates were disrupted by sonication (10 s cycles with amplitude 70, Sonicator Q700). To get rid of cell debris and lipids, the lysate was centrifuged for 10 minutes at 20 000 g at 4° C. At the top of the supernatant floated a layer of lipidic compounds, whereas the pellet contained cell debris. The clear middle supernatant was carefully pipetted into a clean tube. SDS-PAGE electrophoresis was used to analyse the samples from supernatant and resuspended pellet. In case, when significant amount of hexamerin remained in the pellet, the sonication step was repeated. The concentration of the prepared protein fraction was spectrophotometrically estimated using NanoDrop.

4.2.8 Hexamerin purification on MonoQ® 5/50 column

In the first step PEG 20 000 was added to final concentration 8 % w/v to 7.5 ml of protein extract isolated from *T. castaneum*. The solution was gently mixed and incubated on the ice for 10 minutes. Then it was centrifuged at 17 500 g for 10 min. The resulting supernatant containing PEG was removed. To get rid of residual PEG solution the centrifugation was repeated at 14 500 g for 1 minute. The pellet was resuspended in 5 ml of final buffer H and spinned at 20 000 g for 10 minutes. Supernatant containing hexamerin was saved.

To get rid of nucleic acids the supernatant was treated with Turbonuclease (0.2 µl per 1 ml of sample), 15 min on rotary mixer at room temperature and then centrifuged at 20 000 g for 10 minutes. The

resulting supernatant was loaded onto MonoQ Column 5/50 (GE Healthcare). After loading, the column was washed with wash buffer Q, then gradient elution with elution buffer Q was performed. Fractions with hexamerin were loaded on PD-10 Desalting column to reduce the salt concentration to that of final buffer Q.

4.2.9 Preparation of negatively stained sample for transmission electron microscopy

Carbon-coated grids were glow discharged in argon:oxygen 3:1 atmosphere for 30 s from both sides. Hexamerin sample (6 µl) at the concentration of 0.01 mg/ml was pipetted on the grid. After one minute of incubation, the excess liquid was blotted away with Whatman filter paper. Then two wash steps with ddH_2O were applied. The sample was stained using a 3 µl drop of 2% uranyl acetate for approximately 1 min. The excess liquid was blotted away from the grid leaving a thin film of stain. Finally the grid with the stained sample was air dried.

4.2.10 Preparation of vitrified sample for cryo-electron microscopy

Quantifoil^{TM} grids (1.2/1.3, mesh 300) were glow-discharged in argon:oxygen 3:1 atmosphere plasma for 30 s from each side. The solution with hexamerin was briefly sonicated just before grids preparation to disrupt aggregated hexamerin particles. Hexamerin solution (4 µl of 0.7 mg/ml) was applied on a grid. Grids were blotted (blotting force -2, blotting time 3 s, 100% humidity) and plunged frozen in liquid ethane using Vitrobot Mark IV. The prepared samples were stored in liquid nitrogen.

4.2.11 Preparation of vitrified sample for cryo-electron microscopy on graphene grids

Graphene coated grids were glow discharged in argon:oxygen 3:1 atmosphere plasma for 30 s. To enhance the graphene hydrophility the grids were dipped in 50 mM 1-pyrenecarboxylic acid in DMSO for 1 min [75] and then washed in ethanol and isopropanol. Hexamerin (4 µl) of concentration 0.05 mg/ml was applied on the grid and the grid was blotted and plunged frozen in liquid ethane using Vitrobot Mark IV (blotting time 5 s, blotting force -2).

4.2.12 Cryo-electron microscopy of *Tribolium* hexamerin

Data collection was performed on Titan Krios electron microscope operated at 300 kV equipped with K2 Summit detector operating in electron counting mode. Objective aperture of 100 µm and energy filter in zero-loss mode with 20 eV slit were used. The microscope optics was aligned before data acquisition and automatic data collection was done using EPU software. Total 1 s exposure was fractionated into 50 fractions and the final movie was saved as Mrc stack. Defocus applied during data acquisition varied between -1.2 µm – -4µm. The total dose applied on sample was 50 $e^-/Å^2$.

4.2.13 Cryo-EM data processing and molecular building

The acquired movies were aligned and summed using Motioncor2 producing dose-weighted micrographs. Particles were picked automatically using crYOLO neural network based automatic boxer [76]. Hand selected hexamerin particles (~5000) served as initial dataset to train the neural network.

The extracted particles were subjected to multiple rounds of 2D classification, to remove bad particles included by the autopicking process. The initial 3D refinement was followed by 3D classification, where the orientations and the shifts were used from the initial refinement process and the particles were classified into 3 classes. Particles from 3D class presenting the finest features were selected for the next round of 3D refinement. Subsequent steps of 3D refinement, CTF refinement and particle polishing lead to the final map with the resolution of 3.2 Å. “Gold standard” approach was used during the refinement process. All the classification and refinement steps were done using RELION3 software [77].

Manual model building was done in *Coot* and the built structure was refined using REFMAC5 [78, 79]. Online tool MolProbity was used for structure validation [80].

5 RESULTS AND DISCUSSION

5.1 Tail morphogenetic protein H

Physical properties of protein TmpH were calculated using ExPASy Protparam tool [81]. Molecular weight of the protein is 17 830.62 Da, its theoretical pI is 4.34 and the extinction coefficient measured at 280 nm in water is 2 980 $M^{-1}cm^{-1}$.

The biological role of protein TmpH is not clear. According to the literature it is a part of tail of *Φ812* involved in phage attachment to cell. From personal conversation with my colleague Mgr. Zuzana Cielniková Ph.D, who is studying the whole phage *Φ812* by cryo-EM, protein TmpH is probably part of the phage head. Further verification of this claim will be necessary.

5.1.1 TmpH in vector pET22T

5.1.1.1 Construction of TmpH_pET22T expression vector

The gene of TmpH in plasmid pET28b was provided by Mgr. David Buchta. This vector includes non-cleavable His-tag on C-terminus of the protein which makes it sub-optimal for structural studies. Therefore, the TmpH gene was cloned into plasmid pET22T.

The plasmid pET22T (5.4 kb, low copy) contains N-terminal His_6-tag fused with Smt3 domain, that is recognized and cleaved by Ulp1-ac protease. The construction of TmpH_pET22T was done using ligation independent cloning. TmpH gene for the insertion was amplified using PCR and the vector pET22T was linearized using BseR-I (Figure 15). Primers designed in Amplifix software are listed in Table 3.

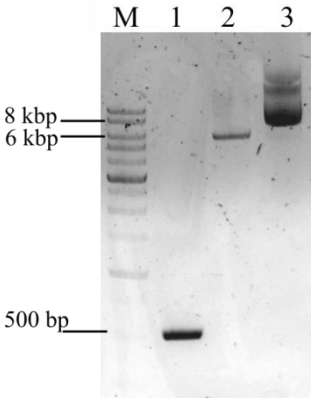

Figure 15: ***Agarose gel electrophoresis analysis of PCR product and linearized vector****. M: DNA Ladder, 1: amplified gene of TmpH (513 bp), 2: pET22T linearized by BseRI (expected size 5.4 kbp), 3: pET22T uncleaved control.*

NEB ® Turbo competent cells were transformed with construct TmpH_pET22T. The success of the transformation was confirmed by colony PCR and the correctness of the sequence was verified by sequencing. Expression of TmpH using TmpH_pET22T in *E. coli* BL21(DE3) was tested. Expression tests were done at 37 °C, 250 rpm, 5 hours in LB media induced by IPTG and auto-induction media ZYP-5052 (Figure 16). Because of the high level of expression and solubility of the produced TmpH, it was not necessary to further optimize the expression conditions.

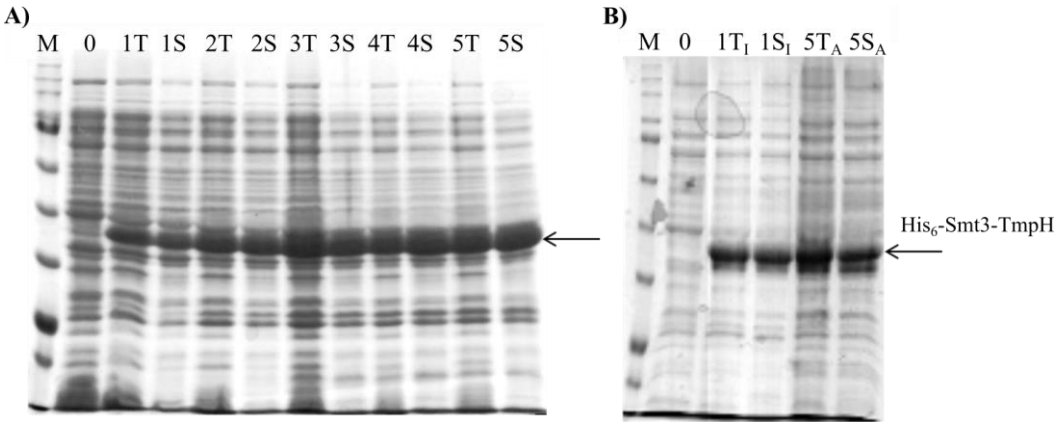

Figure 16: ***Blue silver stained SDS-PAGE 15% gel of BL21(DE3) lysates after test expression****. A) Gel from expression induced by IPTG, numbers above lanes denote hours after induction, M: marker, T: total fraction, S: soluble fraction.B) Gel from expression in auto-induction media, M: marker, 0h: non induced media, $5T_I + 5S_I$ total and soluble fractions from IPTG induced media after 5 hours of expression, $5T_A + 5S_A$ soluble fractions from auto-induction media after 5 hours of expression. Arrows show the expected size of His$_6$-Smt3-TmpH.*

5.1.1.2 Purification of His$_6$-Smt3-TmpH

The protein purification was done out from 0.5 l of cell culture via IMAC on HisTrap™ HP column (GE Healthcare). The gel from SDS-PAGE analysis of the fractions from the affinity chromatography is shown in Figure 17.

Elution fractions containing TmpH were mixed and the His$_6$-Smt3 tag was cleaved by Ulp1-ac protease. Most of the protein of interest did not bind to the HisTrap™ HP column, and could be found mainly in flow through (Figure 17), which indicates that the tag is not accessible to the Ni^{2+} ions on the column. The flow through fraction was treated with Ulp1-ac protease as well to find out if the His$_6$-Smt3 tag that was inaccessible to the Ni^{2+} ions would be recognized by the protease.

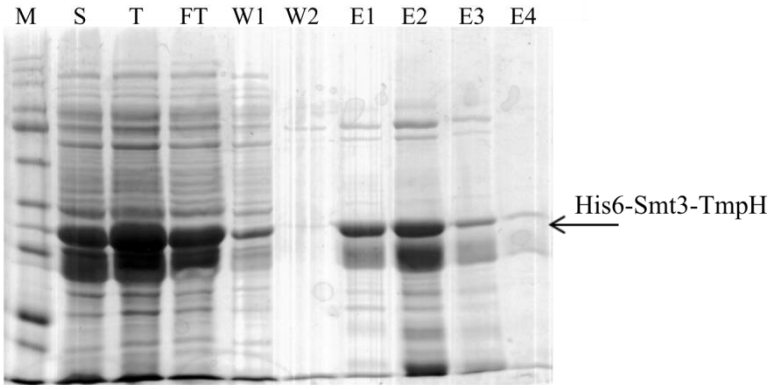

Figure 17: ***SDS-PAGE (15%) analysis of TmpH purification on HisTrap™ column****. M: Blue Protein marker, T: cell lysate, S: cell lysate - soluble fraction loaded on HisTrap™ column, FT: flow through, W: wash fractions, E: elution fractions.*

The results from SDS-PAGE analysis (Figure 18) showed that the sample from elution fractions contains three components corresponding to the cleaved His$_6$-Smt3 tag, to protein TmpH without tag, and to protein TmpH with uncleaved tag. In the sample from flow through fraction the tag was not cleaved at all, it was not accessible either for IMAC purification or Ulp1-ac protease.

From this it was concluded that the His_6-Smt3 tag is in most cases probably buried in folded protein and inaccessible for the Ulp1-ac and IMAC purification. Only a low percentage of the total amount of the protein is folded with accessible tag, which leads to the poor yield of purification process. Moreover protein TmpH with His_6-Smt3 tag cannot be used for structural studies, the size of the His_6-Smt3 tag (approximately 12 kDa) is as big as 2/3 of the protein itself and it would significantly influence the crystallization and TmpH structure. From these reasons it was decided to clone the gene of TmpH into plasmid pET22b and to try to purify the protein without any tag.

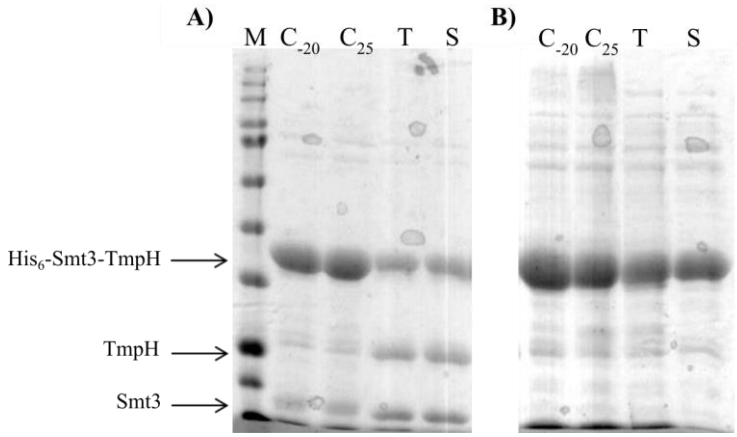

Figure 18: ***SDS-PAGE analysis of Ulp1-ac cleaved protein.*** *Panel A) sample from elution fractions, panel B) sample from flow through, M: blue protein marker, S: soluble fraction, T: total fraction, C_{-20} control stored at -20 °C, C_{25} control stored at 25 °C. The 15% gels were stained by Blue silver stain.*

5.1.2 TmpH in vector pET22b

5.1.2.1 Construction of TmpH_pET22b expression vector

Gene of TmpH was cloned into plasmid pET22b (5.5 kbp) via T4 mediated cloning. The plasmid was linearized using restriction endonucleas Nde-I. The insert sequence of TmpH was amplified using PCR. Used primers are listed in Table 3.

Transformation of NEB®Turbo cells with construct TmpH_pET22b was successful and was confirmed by colony PCR (Figure 19). Gel from SDS-PAGE analysis of expression test is in Figure 20. TmpH was expressed as a soluble protein. From the results of the expression test the time of 3 hours was chosen as the most suitable for achieving high yield of the protein.

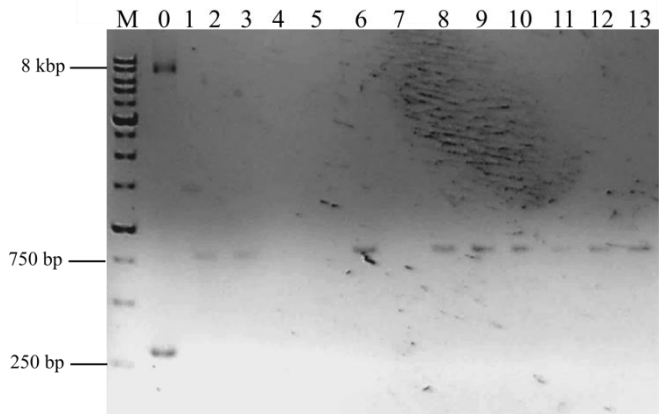

Figure 19: ***Agarose gel electrophoresis of products of colony PCR****. PCR was performed using pET22b as a template as negative control. PCR products of expected size identified the colonies carrying the plasmid of interest (lanes 2, 3, 6, 8 – 13), M: marker.*

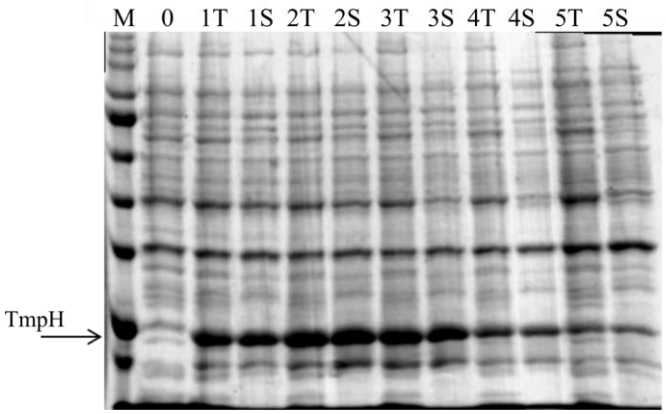

Figure 20: ***SDS-PAGE analysis of E. coli BL21(DE3) cell lysates****. Expression of TmpH in cells was induced by addition of IPTG (0.4 mM final concentration) during exponential phase of growth. Samples were taken every hour post induction. 0: non-induced cells; 1 – 5: samples taken 1 – 5 hours post induction; T: total lysate of the cells; S: fraction with soluble proteins. Gel (15%) is stained by Blue silver. Arrow shows the expected size of TmpH.*

5.1.2.2 Purification of TmpH

TmpH expressed in E. coli BL21(DE3) using the vector TmpH_pet22b, lacked any tag that may be used for affinity chromatography. Therefore, the purification procedure consisted of protein precipitation using ammonium sulphate followed by hydrophobic interactions chromatography on HiTrap® Phenyl HP 1 ml column (GE Healthcare).

Formerly used lysis buffer A contains detergent (octylthioglucoside) that might cause low effectivity of HIC purification. Therefore, the composition of lysis buffer was changed and the detergent was replaced by 1 mM EDTA and sonication step was added to the lysis procedure.

Figure 21Figure 21 shows SDS-PAGE analysis of purification of TmpH on HiTrap® Phenyl HP 1 ml column. The protein did not bind to the column very firmly and the biggest part of TmpH was in the flow through. The purification was repeated with HiTrap® Butyl HP 1 ml column (GE Healthcare) with similar results (data not shown).

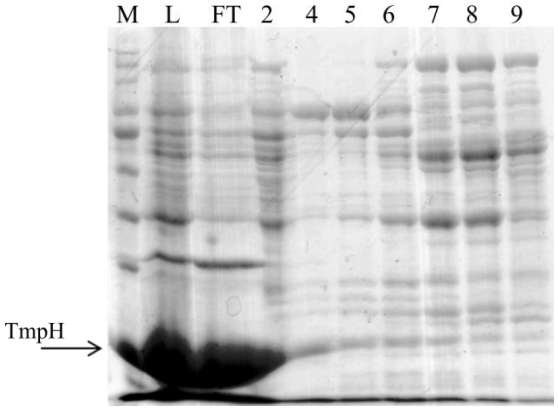

Figure 21: ***SDS-PAGE analysis of HIC purification of TmpH on HiTrap® Phenyl column.*** *Before loading on the gel samples were desalted by methanol – chloroform precipitation. M: marker, L: load, FT: flow through, 2 – 9 elution fractions. Gel (15%) is stained stained by Blue Silver.*

5.1.3 TmpH in vector pET28b

The production of pure TmpH protein without any tag or extra amino acid residues on the C/N-terminus, was not successful. Therefore, we continued with purification of C-terminally His_6 tagged TmpH. Construct TmpH_pET28b was provided by Mgr. David Buchta. Gene of TmpH was inserted into the plasmid using *Nco*-I, *BamH*-I restriction sites [82].

NEB®Turbo competent cells and BL21(DE3) cells were successfully transformed with plasmid TmpH_pET28b. The expression tests were performed at 37 °C and 250 rpm, expression was induced by 0.4 mM IPTG (final concentration) (Figure 22). TmpH was present in the soluble fraction of cell lysate.

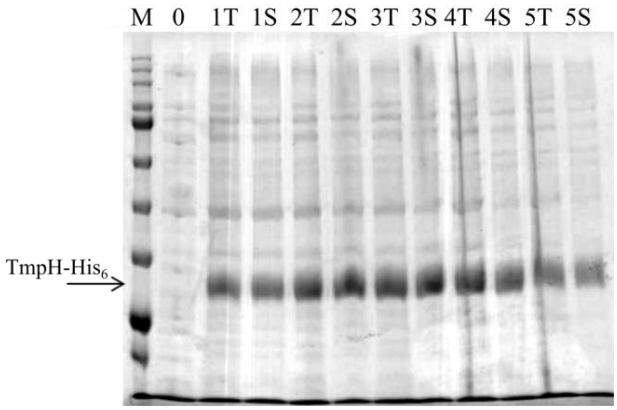

Figure 22: ***Blue silver stained SDS-PAGE 15% gel of BL21(DE3) lysates after expression test.*** *M: marker, T: total fraction, S: soluble fraction, 0: non induced media, number 1 – 5 denote hours after induction. Arrow shows the expected size of TmpH-His_6.*

5.1.3.1 Purification of TmpH-His_6

Purification procedure was done using affinity chromatography on NiNTA resin (Figure 23). Although most of the protein was in the flow through fraction, the amount is lower than in previous IMAC purification of TmpH with His_6 tag on C-terminus. To be sure that the presence of desired protein TmpH-His_6 in flow through is not caused by simply overloading the column, different amount of load and resin bed volumes were tried with similar results (data not shown).

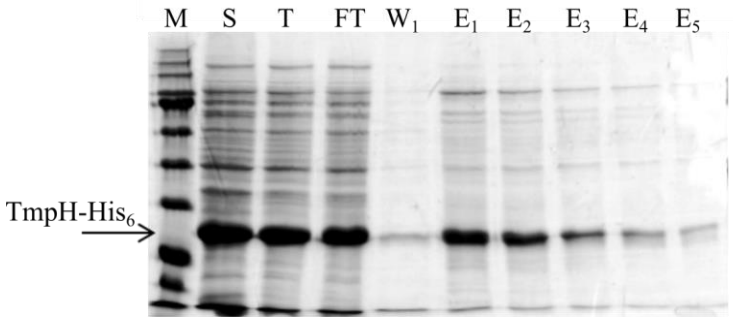

Figure 23: ***Instant blue stained PAGE-SDS 15% gel from TmpH purification on NiNTA resin.*** *M: marker, T: total fraction, S: soluble fraction in this case equal to load, FT: flow through, E: elution fraction. Arrow shows expected size of TmpH-His_6.*

Joined elution fractions from purification on NiNTA resin containing the protein TmpH-His_6, were loaded on Superdex column 75 pg 16/600 (GE Healthcare). Chromatogram and gel from SDS-PAGE analysis are shown in Figure 24 and Figure 25. Protein TmpH contains only 4 Phenylalanines and 2 Tyrosines and no Tryptophanes, therefore the signal from the UV detector is very low [83]. Retention time of the peak suggests that TmpH exists in solution as pentamer.

Size-exclusion purified TmpH-His_6 was concentrated and used for crystallization screening, Dynamic Light Scattering (DLS) analysis (to investigate if the protein is indeed a pentamer) and Mass Spec analysis to confirm its identity as TmpH.

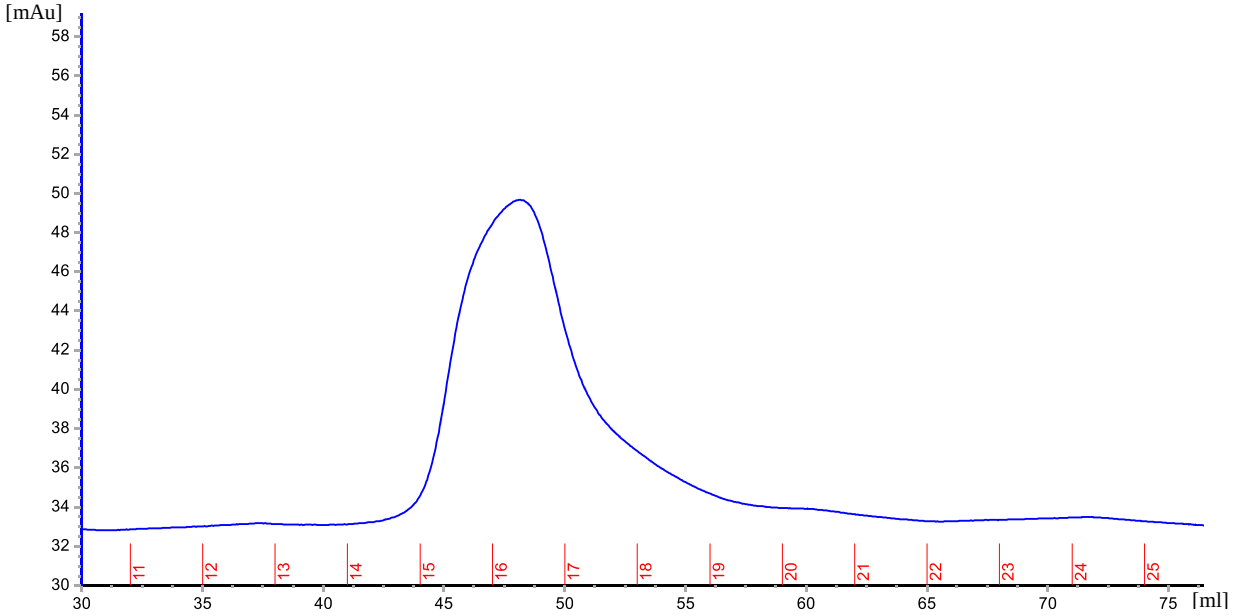

Figure 24: ***Chromatogram from TmpH-His_6 purification by SEC on Superdex 75 pg 16/600 column****. Blue line represents the signal from UV detector (280 nm) red number corresponds to the fractions. Retention time of eluted peak suggests that TmpH-His_6 is in solution as a pentamer.*

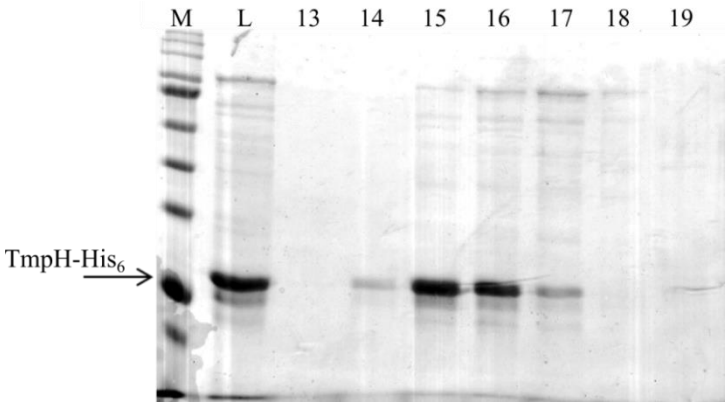

Figure 25: ***SDS-PAGE analysis of TmpH-His_6 purification on Superdex 75 pg 16/600 column****. M: marker, L: load, 13 – 19 elution fractions. Gel (15%) is stained by Instant Blue stain. Arrow shows the expected size of TmpH-His_6.*

5.1.4 DLS analysis of TmpH

According to the elution time of TmpH-His_6 in SEC, the protein forms pentamers. To independently determine the oligomeric state of the protein DLS analysis on Delta Max Core was performed. The size distribution of particles (Figure 26) indicated that the sample contained homogenic set of particles of even size that corresponded to the pentameric state of the protein (5 × 17.830 kDa = 89.150 kDa).

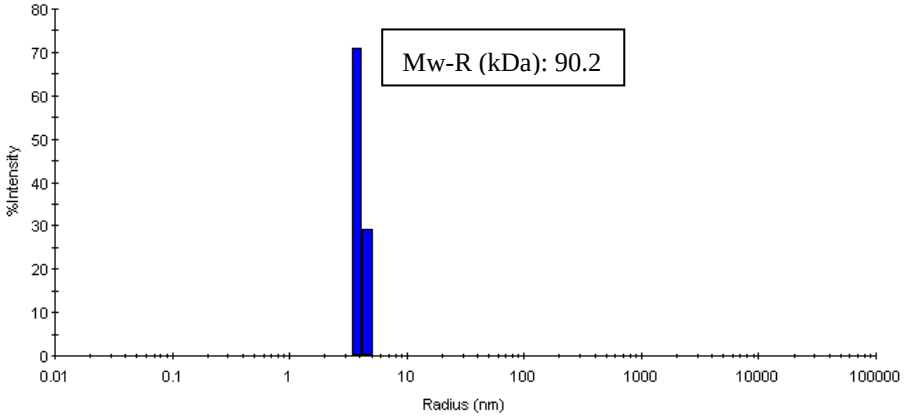

Figure 26: ***Histogram of particle size distribution measured by DLS analysis.*** *Purified sample of TmpH-His_6 was measured at concentration 1 mg/ml in buffer 150 mM NaCl, 50 mM Tris pH 8. Hydrodynamic radius of particles predicts pentameric oligomeric state of the protein.*

5.1.5 Mass spectroscopy analysis of TmpH-His_6

Mass spectroscopy analysis was performed by the Proteomic Core Facility at CEITEC MUNI (in-gel digestion using trypsin at 40 °C, 2 h, MALDI MS/MS). Results confirmed that the sample of the purified protein contained mostly TmpH-His_6 (Figure 27).

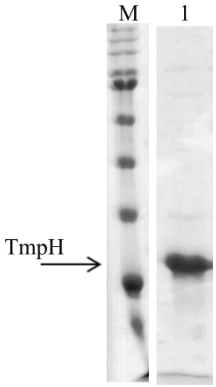

Figure 27: ***Final purity of TmpH-His_6 analyzed by SDS-PAGE****. Instant Blue stained SDS-PAGE 15% gel from which a band was sent to Mass spec analysis, M: marker, 1: sample of TmpH, concentration 4 mg/ml, 10 µl loaded. Final purity of TmpH was more than 90 %.*

5.1.6 Crystallization screening

The purification procedure was repeated several times to get enough material for the crystallization screening. (Multiple purifications were chosen instead of one big, because of the low efficiency of the IMAC purification step). The appropriate protein concentration for crystallization was determined using pre-crystallization test from PCT^{TM} Hampton Research.

Crystallization screens (six different screening 96 well plates) were prepared in Biomolecular Interaction and Crystallization Core Facility at CEITEC MUNI. Crystallization plates were inspected under normal light, because the protein TmpH does not provide strong fluorescence signal after UV excitation (only 4 Phenylalanines, 2 Tyrosines and no Tryptophane). Inspection was done via online service Rigaku CrystalTrack.

After 3 weeks of crystallization, many crystallization conditions gave results where small crystals of various forms and were observable. Photos of several drops in which some form of the crystals occurred and their chemical composition are shown in Figure 28 and in Table 12.

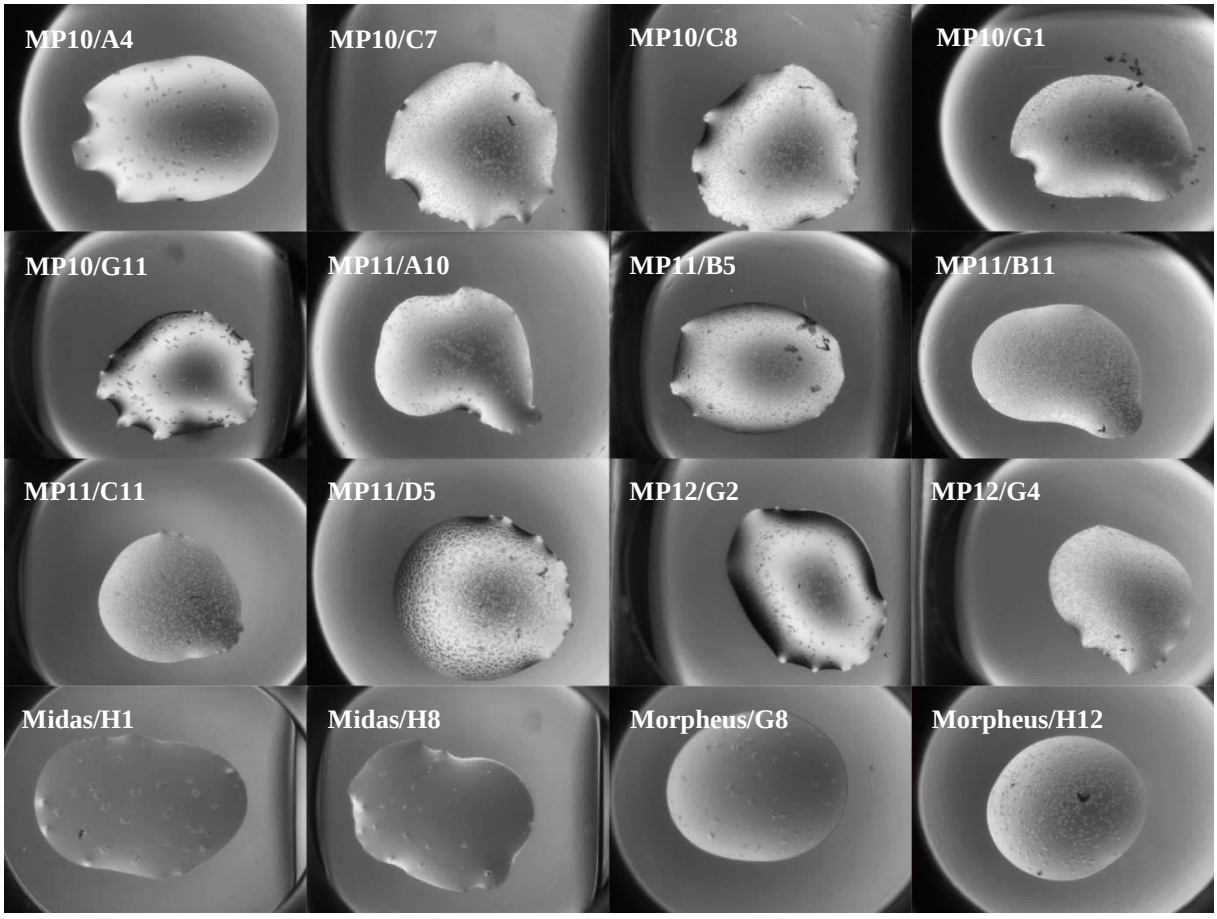

Figure 28: ***Photos of drops with protein crystals of TmpH-His$_6$.*** *Crystallization conditions are noted in the top left corner of the image, the composition of these conditions is listed in Table 12.*

Hanging drop crystallization setups were prepared based on selected crystallization conditions, to produce bigger crystals for diffractometric measurements. Although microprecipitation of the protein in the drops occurred (Figure 29), the reproduction of the crystallization from the screen was not successful and further 2D optimization of the conditions will be necessary.

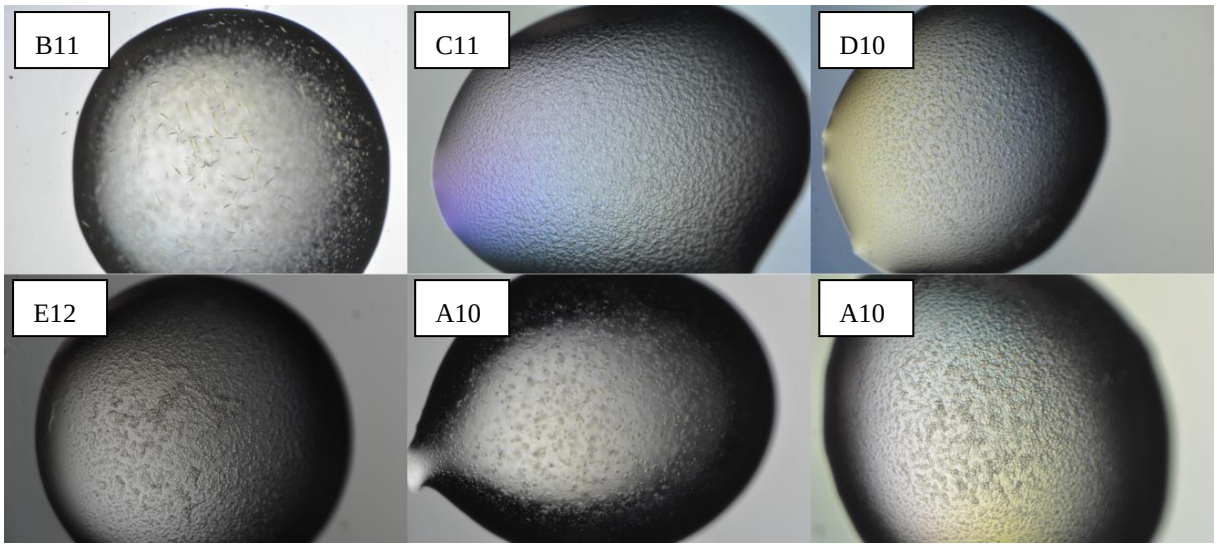

Figure 29: ***Results of TmpH crystallization in hanging drops****. After two month of storage no big crystals occurred, the majority of drops contained microprecipitate. B11: 20 % w/v PEG 3 000, 0.1 M HEPES pH 7.5, 0.13 M sodium acetate, 18 mg/ml TmpH; C11: 20 % w/v PEG 4 000, 0.1 M Tris pH 8.5, 0.2 M lithium sulphate, 18 mg/ml TmpH; D10: 20 % w/v PEG monomethylether 5 000, 0.08 bis-tris pH 6.5, 12 mg/ml TmpH; E12: 20 % w/v PEG 4 000, 5 % w/v 2-propanol, 0.06 M tri-sodium citrate, 15 mg/ml TmpH; A10: 30 % w/v PEG 400, 0.1 M MES pH 6.5, 0.1 M magnesium chloride, 18 mg/ml TmpH; A10: 30 % w/v PEG 400, 0.1 M MES pH 6.5, 0.1 M magnesium chloride, 15 mg/ml TmpH.*

5.1.7 Structure prediction of TmpH

Problems with the crystallization of TmpH might be caused by high degree of disorder of the amino acid chain or the protein may be composed of several domains and it could be easier to crystalize them separately. For these reasons we decided to use Raptor X prediction server to calculate the structure of TmpH. Template based tertiary structure prediction was used [84]. Sugar binding proteins 4uidA (domains 4 and 5) and 4uicA (31 - 844) from *Geobacillus stearothermophilus* were used as templates for the prediction.

P-value equal to $7.61 \cdot 10^{-6}$ serving for the evaluation of the model relative quality is smaller than 10^{-4} which is a good indicator for mainly β-proteins [84]. And the real molecule of TmpH is therefore with high likelihood similar to this model. The predicted structure (Figure 30) covers the whole TmpH sequence (117 amino acids). According to the model the protein TmpH is probably composed of two β-sheets domains connected by a flexible linker of 6 amino acids. Secondary structure of 49 % of the protein was predicted as β-sheet. The remaining part of the protein was predicted as loops, which might cause troubles during the crystallization.

The predicted structure of TmpH will be used after successful crystallization and measurement of diffraction data as a model for molecular replacement.

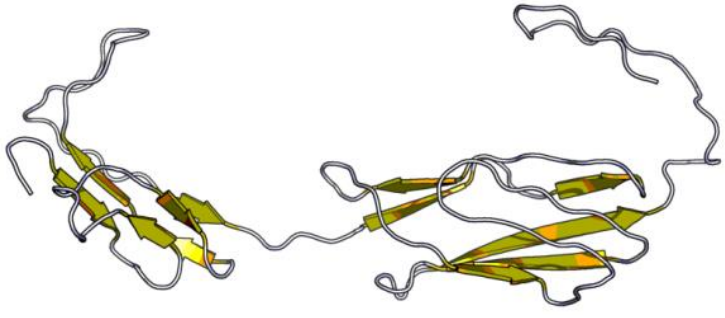

Figure 30: ***Raptor X predicted structure of TmpH.*** *Protein TmpH is probably composed of two domains connected with flexible linker of 6 amino acids.*

5.1.8 TEM analysis of TmpH

In order to find out if it were possible to solve the structure of TmpH by cryo-EM, several vitrified samples of TmpH-His_6 deposited on holey carbon coated grids were prepared. The grids with TmpH were frozen by plunge freezing in liquid ethane. The screening of prepared grids using TEM Thalos Arctica revealed that the protein is too small for a cryo-EM analysis (Figure 31). Therefore, X-ray crystallography seems to be the most suitable method for TmpH structure determination.

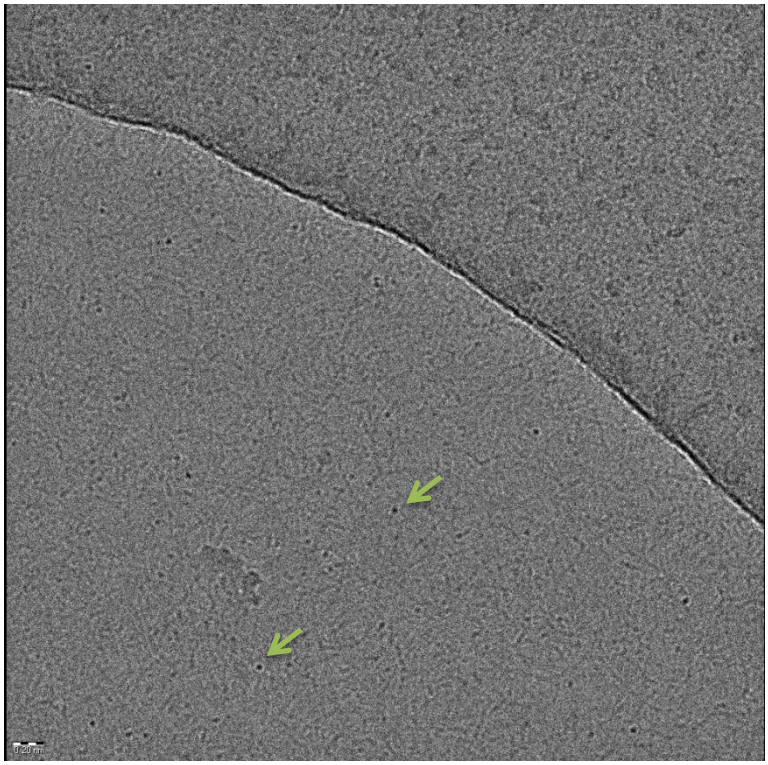

*Figure 31: **Cryo-EM of TmpH**. Samples of TmpH (at concentration 0.02 mg/ml) were vitrified and inspected using transmission electron microscope Thalos Arctica. The most abundant features denoted by green arrow might correspond to the TmpH protein, however they are too small for further microscopy analysis. Scale bar 20 nm.*

5.2 Structure of hexamerin of *T. castaneum*

5.2.1 Hexamerin isolation

Hexamerin was isolated from *T. castaneum* pupae (Figure 32). *T. castaneum* larvae feed on flour and live freely [9] (in comparison with bees larvae that are kept in combs and fed by workers [85]). Therefore, the beetle larvae and pupae have firm exoskeletons, which have to be disrupted in the purification process.

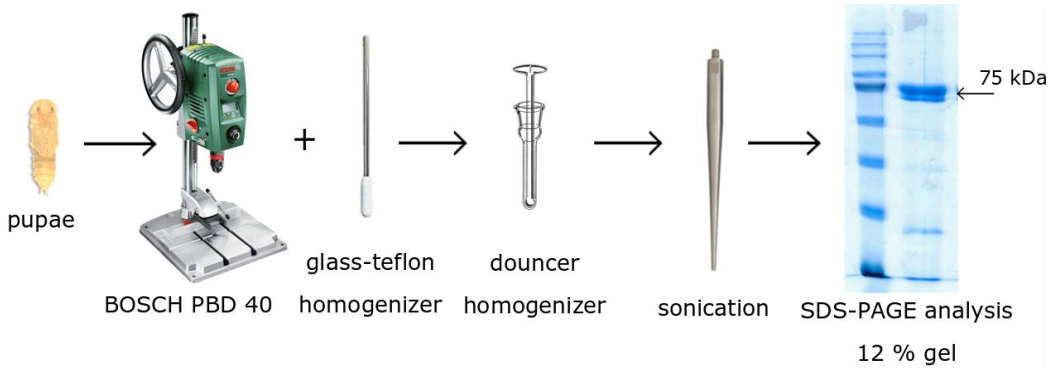

Figure 32: ***Scheme of hexamerin isolation procedure****.*

The protein extraction steps from the pupae led to clear protein solution with concentration of 27 mg/ml. The major component of this solution was hexamerin (Figure 33). In a diluted sample two distinct bands were observed, which were identified by mass spectroscopy (MALDI MS/MS, in-gel digestion using trypsin, 40 °C, 2 h, Proteomics Core Facility CEITEC MUNI) as two isoforms of hexamerin: Hexamerin 2 isoform x1 (NCBI ref. seq.: XP_008197347.1) and Hexamerin 4 isoform x1 (NCBI ref. seq.: XP_008197349.1). The sequence similarity of these isoforms is 70 %.

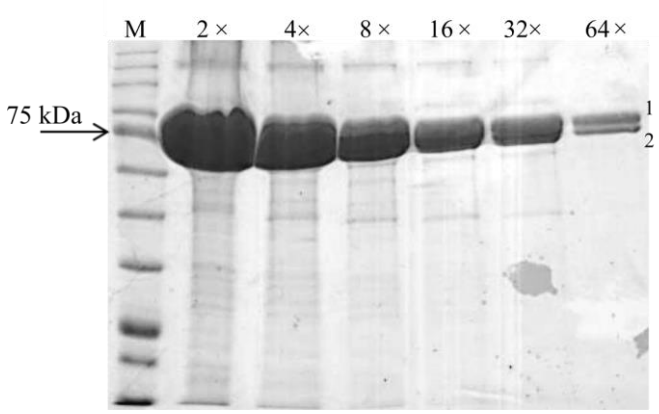

Figure 33: ***SDS-PAGE analysis of protein extract prom Tribolium castaneum pupae****. Sample (10 µl) was loaded on 12% gel. Used dilution factors are shown above the lanes. In the sample with dilution 64× there are two bands labelled with numbers 1 and 2. Two isoforms of hexamerin were detected by mass spectroscopy in bands 1 (Hexamerin 2 isoform x1) and 2 (Hexamerin 4 isoform x1). Gel was stained by Blue Silver stain.*

5.2.2 Hexamerin crystallization screening

The pre-crystallization test (PCT™ Hampton Research) was used to determine the appropriate hexamerin concentration for crystallization screening. The concentrations of 25 mg/ml and 12.5 mg/ml were used for chosen screens (4.2.5). The screening for suitable crystallization conditions was performed at Biomolecular Interactions and Crystallization Core Facility at CEITEC MUNI.

The first crystals appeared after 13 days of crystallization. The size and quality of the crystals was suitable for diffraction analysis at a synchrotron. Multiple (48) crystals were analysed at Synchrotron SOLEIL, beamline Proxima I. Diffractions of many of them contained ice rings caused by improper cryoprotection of the crystals. The best diffractions were obtained from crystal grown in condition A8.3 PEGs II Suite shown in Figure 34.

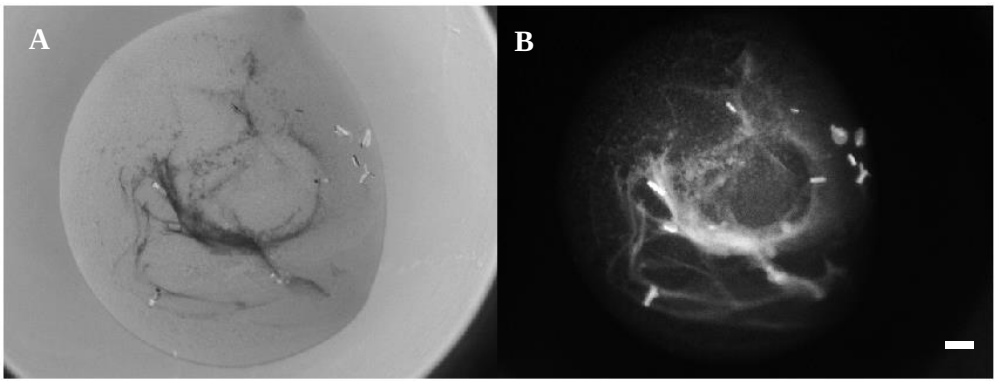

Figure 34: ***Images of crystals in condition A8.3 PEGs II Suite.*** *A) Bright field and B) UV images of hexamerin crystals. Crystallization conditions: hexamerin concentration 12.5 mg/ml, 0.1 M $CaCl_2$, 30 % w/v PEG 400, 0.1 M sodium acetate pH 4.6, scale bar corresponds to 0.100 mm.*

Diffractions from this crystal extended to the resolution of 3.7 Å and the whole data set was collected. Unfortunately, obtained diffraction pattern was of poor quality and the data cannot be processed Figure 35.

From crystallization screens 19 conditions were selected as suitable for further testing. Chemical composition of these conditions and pictures of crystals grown in these conditions are listed in Table 13 and shown in Figure 36, respectively. For all of these conditions optimization screens were set up.

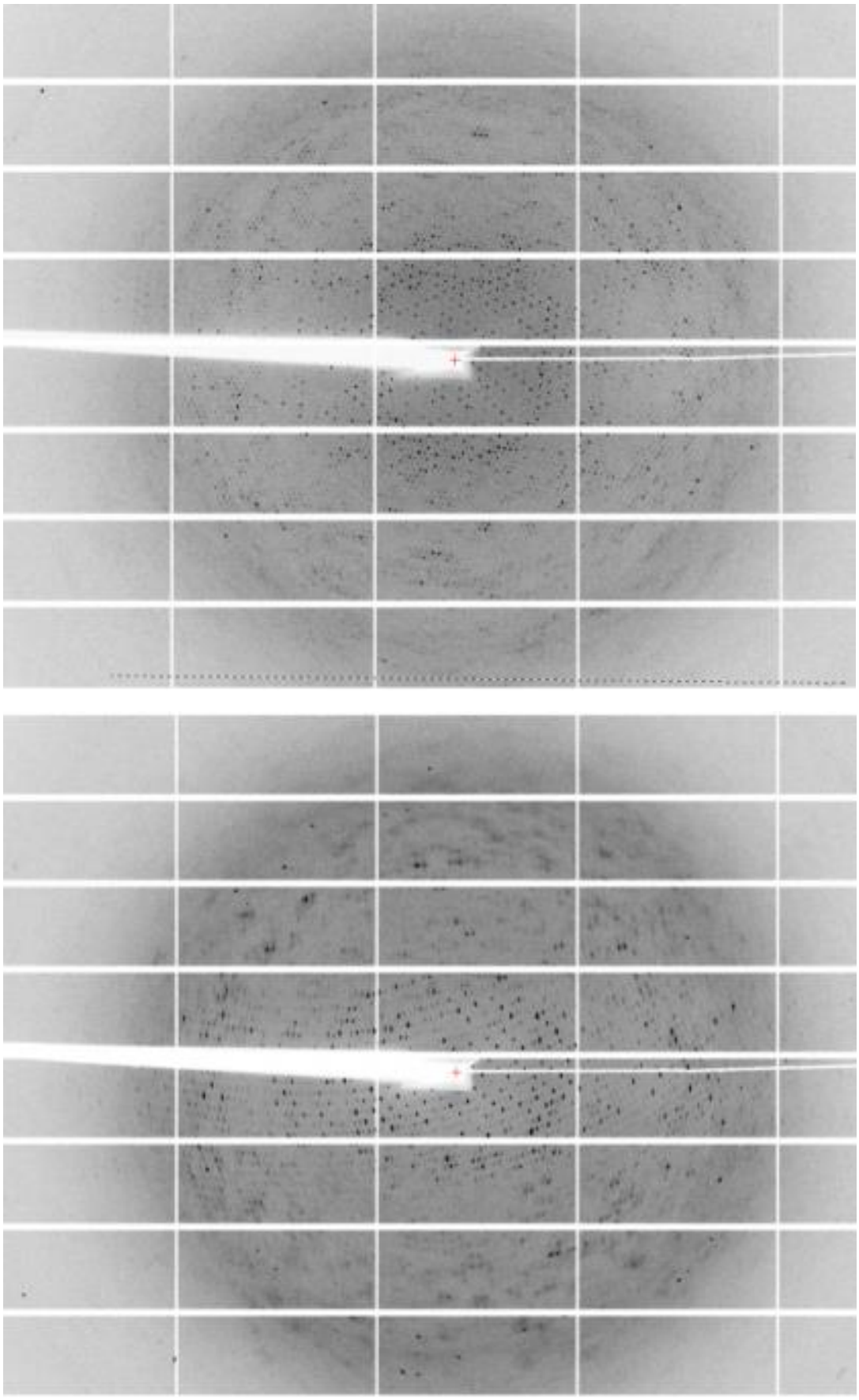

Figure 35: ***Diffraction patterns of hexamerin crystal X-ray scattering.*** *Hexamerin crystals were grown in condition A8. Diffraction measurements were done at Beamline Proxima I, SOLEIL Synchrotron, France.*

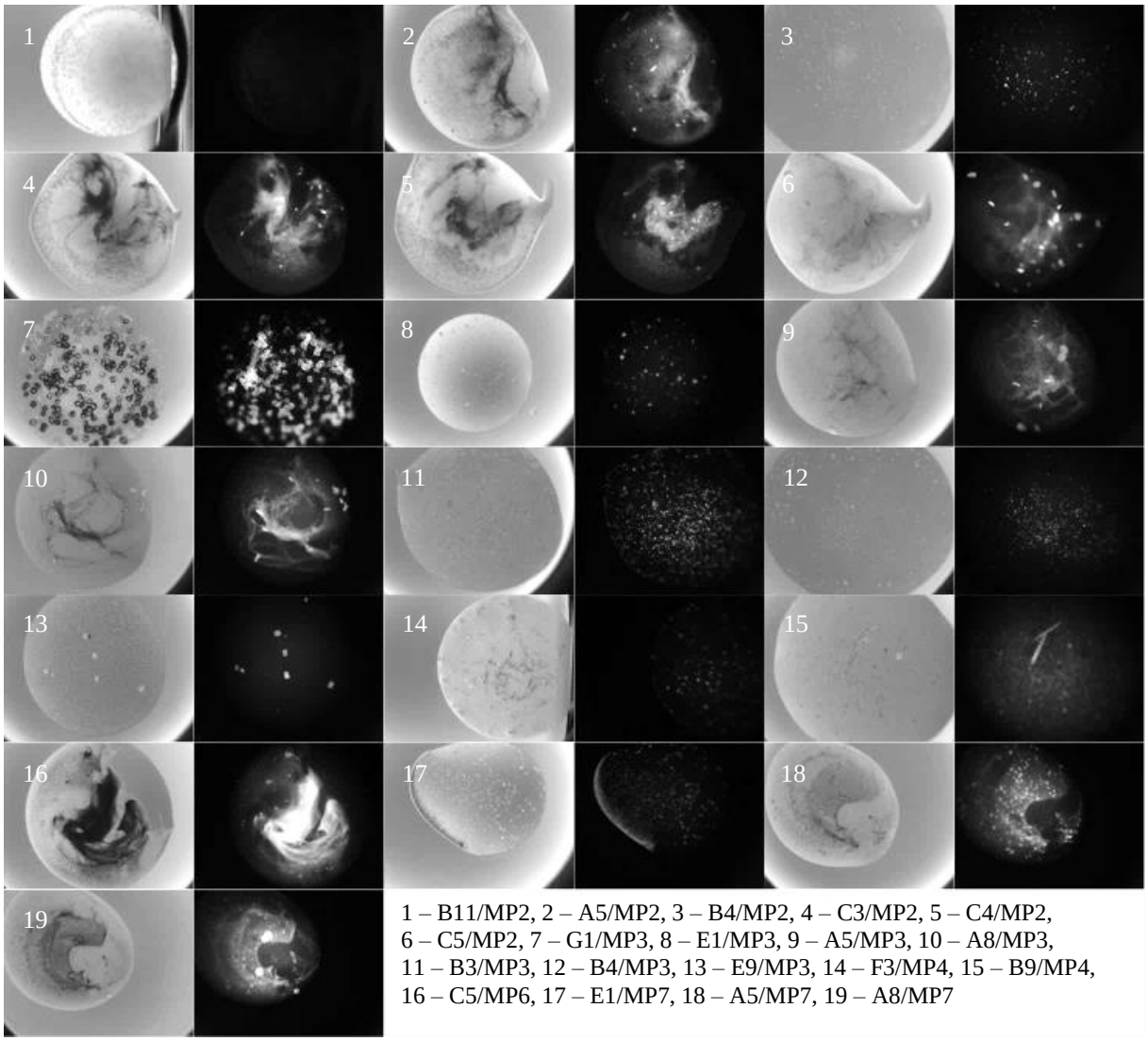

Figure 36: ***Photos of crystallization drops in selected conditions for hexamerin crystal growing.*** *Each drop is documented under normal and UV light. The details of the conditions are described in Material and Methods section 4.2.6.*

5.2.3 Optimization of hexamerin crystallization conditions

To obtain bigger crystals with less mosaicity, crystallization condition were optimized. Optimization 2D screens were set up using hanging drop method. Crystals grown in different conditions varied in shapes and sizes; some of them polarized visible light. Compact crystals with sharp edges as well as those reminding butterfly wings and needles were obtained. Some of the most notable results of the crystallization are shown in (Figure 37). Plates with optimization of conditions E9 and G1 from PEG II Suite contained crystals in almost all drops (Figure 38 and Figure 39). In these conditions the influence of protein-precipitant ratio on crystallization could be observed. All photos were taken after 27 days of crystal growth at 20 °C.

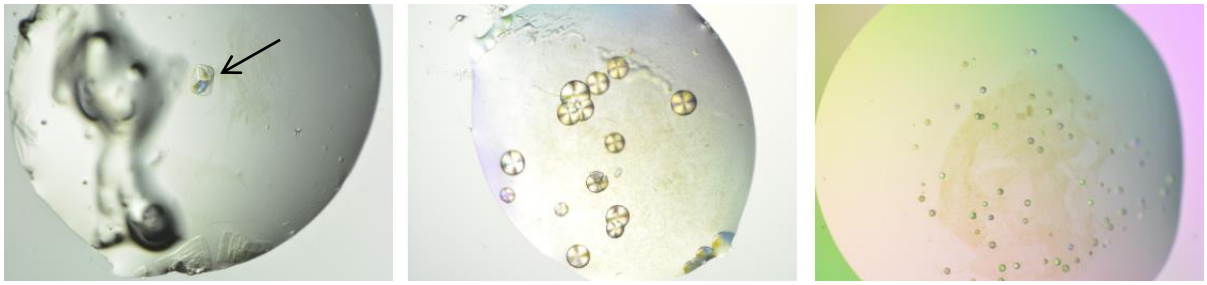

Figure 37: ***Different shapes of hexamerin crystals****. From left to right: 1) butterfly wing like crystal (arrow) in condition 30 % w/v PEG 400, 0.1 M $CaCl_2$, 0.1 M sodium acetate pH 4.6, 6 mg/ml hexamerin;2) diamond like spherolites in 20 % w/v PEG 400, 0.1 M $CaCl_2$, 0.1 M sodium acetate pH 4.6, 6 mg/ml hexamerin; 3) glass balls in 25 % w/v PEG 400, 0.1 M $MgCl_2$, 0.1 M sodium acetate pH 4.6, 15 mg/ml hexamerin.*

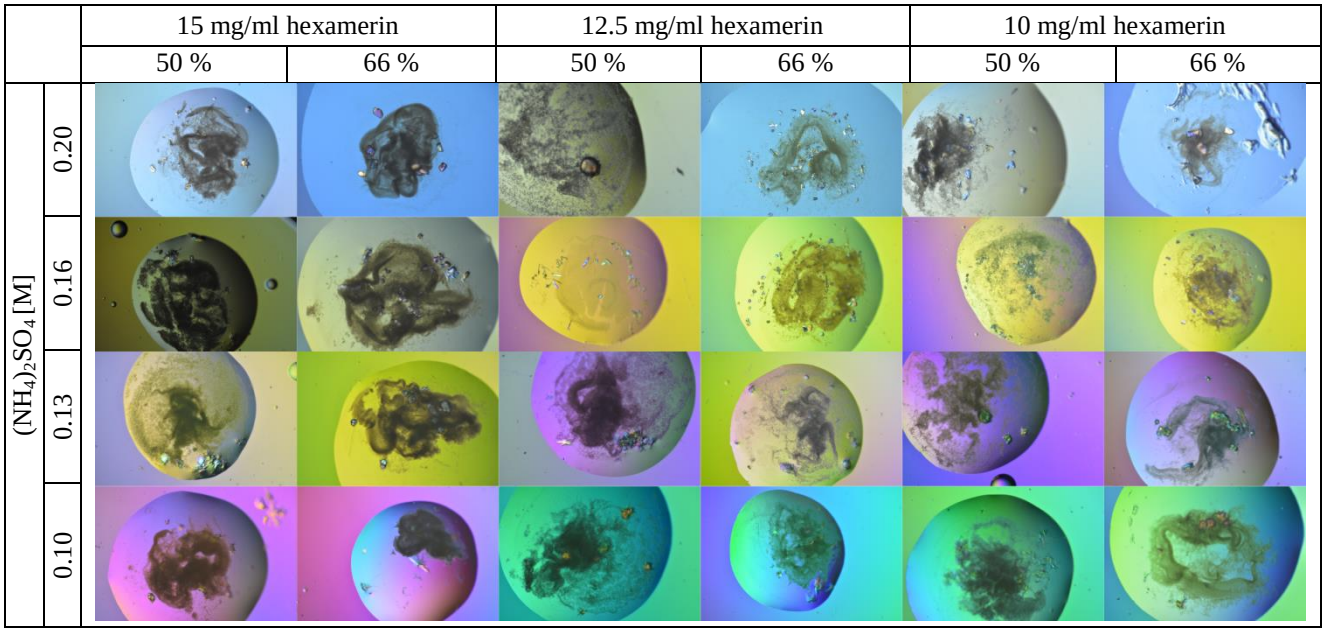

Figure 38: ***2D optimization of crystallization condition E9 from PEGs II Suite****. 16 % w/v PEG 4 000, 0.1 M HEPES pH 7.5 and ammonium sulfate (original concentration 0.2 M). For each concentration of protein there are two drops one with 50 % (v/v) of hexamerin and one with 66 % (v/v) of the protein. The crystals in various forms and shapes could be seen. The volume of each drop is 1 µl.*

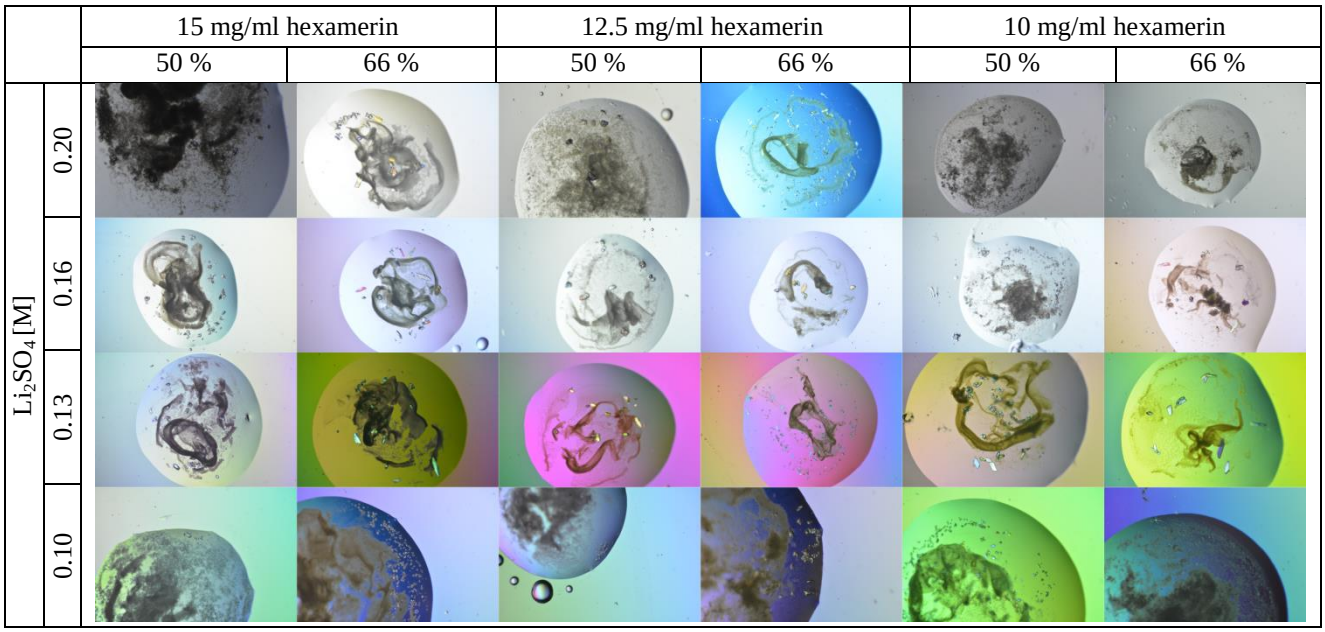

Figure 39: ***2D optimization of crystallization condition G1 from PEGs II Suite****. 25 % w/v PEG monomethylether 5 000, 0.1 M Tris pH 8.5 and lithium sulfate (original concentration 0.2 M). For each concentration of protein there are two drops one with 50 % (v/v) of hexamerin and one with 66 % (v/v) of the protein. The volume of each drop is 1 µl.*

5.2.4 Electron microscopy of negatively stained hexamerin

Grids with negatively stained hexamerin samples were examined in transmission electron microscope Tecnai G2 TF20 operated at 200 kV and equipped with a 4k CCD camera Eagle II (Thermo Fisher Scientific). Hexamerin particles were observed in two orientations: flower-like top orientation and side orientation (Figure 40). The top orientation was preferred and hexamerin particles had tendency to form chains and to stick to each other, forming 2D aggregates.

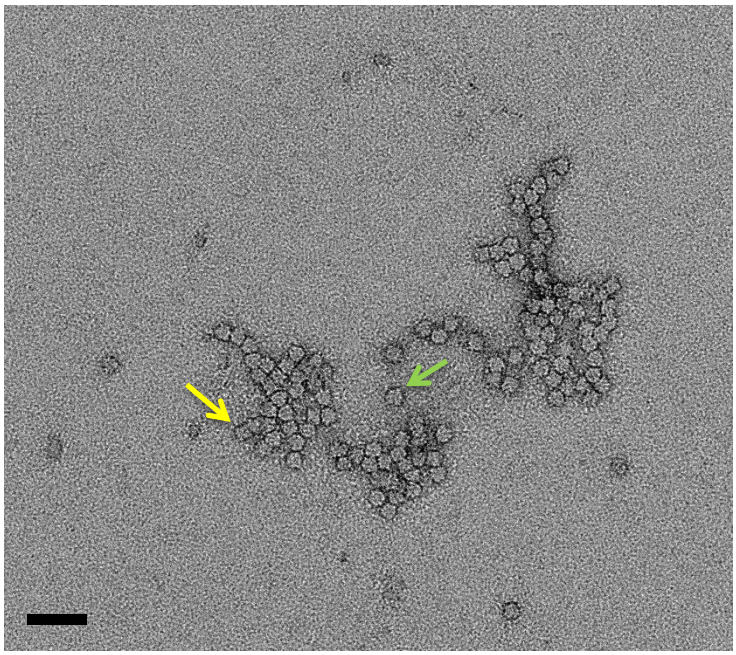

Figure 40: ***Negatively stained sample of hexamerin from T. castaneum****. Hexamerin of concentration 0.01 mg/ml stained with 2% uranyl acetate, magnification 62k, top orientation (green arrow), side orientation (yellow arrow), scale bar corresponds to 50 nm, TEM Tecnai G2 F20.*

5.2.5 Cryo-electron microscopy of *Tribolium castaneum* hexamerin

Grids for cryo-electron microscopy were screened on TEM Tecnai TF20. Selected grids with best sample distribution were loaded into Titan Krios microscope for data collection. In total 1514 micrographs were collected (Figure 41). From these 115 952 particles were picked by autoboxing and several rounds of 2D classification were performed (Figure 42). After 2D classifications 47 594 particles were selected and 3D classification was performed resulting in 9 292 best particles, that formed a homogenous dataset.

The final reconstruction was performed according to the "gold standard" and the resolution estimated by Fourier shell correlation ($FSC_{0.143}$) of two halves was 3.2 Å (Figure 43). The quality of D3 symmetrized electro-static potential map (Figure 44) was good enough for building of molecular structure of *T. castaneum* hexamerin, that consists from 6 identical hexamerin protomers.

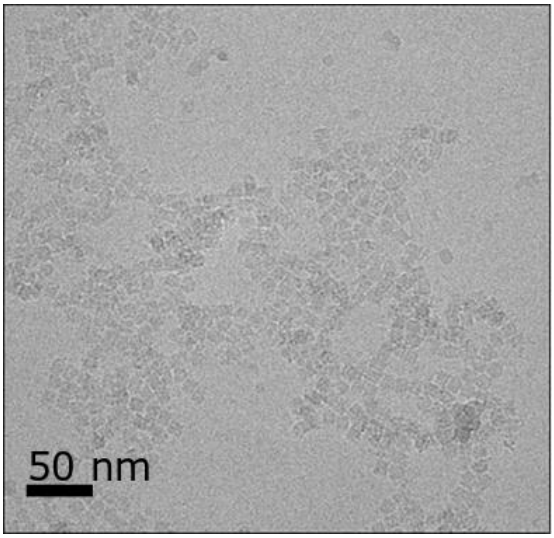

Figure 41: ***Cryo-EM micrograph of hexamerin from T. castaneum.*** *Hexamerin molecules form 2D aggregates in vitreous ice.*

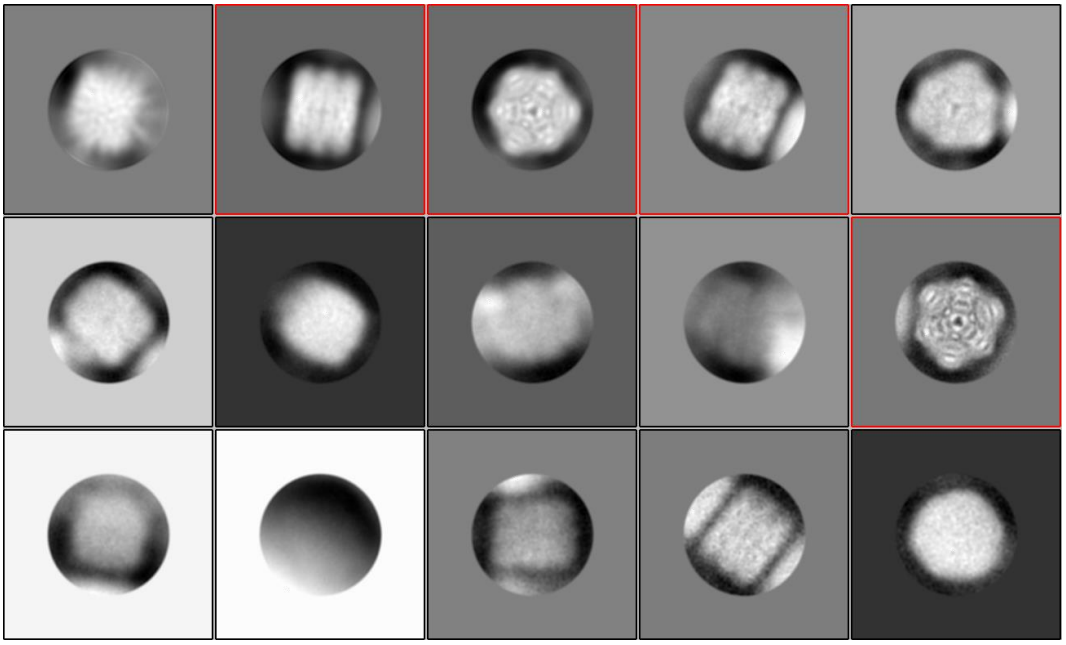

Figure 42: ***Class averages (2D) of automatically picked hexamerin particles by crYOLO****. RELION was used for 2D classification of the initial dataset. Class averages of 15 most populated clasess out of 100 are shown. Particles from classes highlighted by red frame were select selected for further processing.*

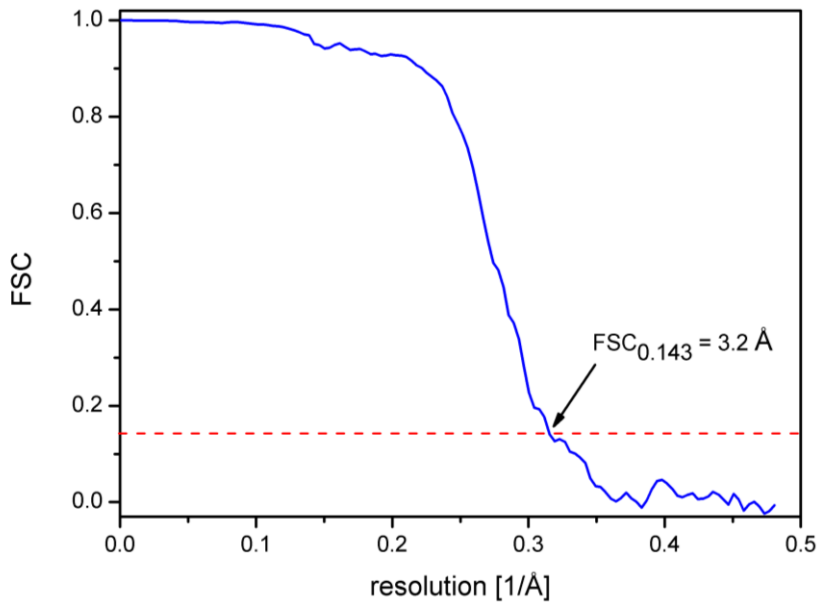

Figure 43: ***Fourier shell correlation curve of reconstructed half datasets of the final refinement****. Reconstruction was done according to "gold standard", where the particles were divided into two random datasets and reconstructed independently. Final resolution of the maps was estimated according to FSC143 criterion.*

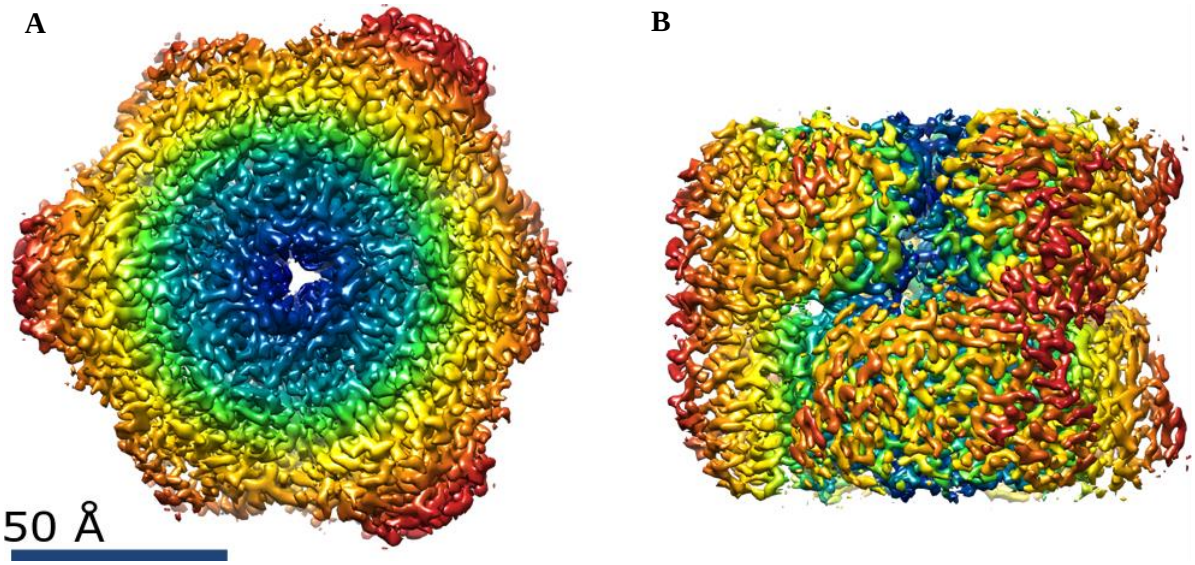

Figure 44: ***Rainbow colored 3D reconstructed electro-static potential maps.*** *A) top view and B) side view, crated in UCSF Chimera [86].*

5.2.6 Structure building of *T. castaneum* hexamerin

Building of molecular structure of *T. castaneum* hexamerin was done in software *Coot* [78]. The structure of *Apis melifera* hexamerin 70b (solved by X-ray crystallography to resolution of 2.0 Å in our laboratory) and predicted structure of *T. castaneum* hexamerin were used as starting models. For the prediction of *T. castaneum* hexamerin structure RaptorX web server was used [84]. Hexamerin from *Bombix mori* (PDB ID 3WJM) served as a template for the prediction [87]. *T. castaneum* hexamerin structure was refined in the programs REFMAC5 [79] and PHENIX [88]. Model geometry validation was performed using the MolProbity online tool [80].

According to the results of mass spec analysis and features of the electro-static potential maps, the sequence Hexamerin 4 isoform x1, was chosen for building (Figure 45). The structure of the hexamerin protomer (Figure 46) covers 607 out of the total 698 amino acids (87 %).

MRFIVVAILG CCALALAFPE PNKQFLERQR DILRLFRHIN QPSYYKDHQE IAQSFHLHDH
YDHYTKPEIA KHYHQIYEYG LLPRGEVFSV FYEEHLQQAI ALYKLFYYAK DYDTFYRTAV
WARQHVNEGV FLYSFSVAIV HREDTYGIVL PPIYEIYPHY FYNNEVIQEA YRYKQQYYNQ
EHGYTINANY SGFYLNLHPE QSLSYFTEDV GVNSFYYYYN IYYPHWLGGE DFDFAHDRRG
EQYYYVYQQI LARYYLERLS NDFGEIPFFN YEVPFENGYY PLLQYPNGLF FPQRPNYAKL
YEYFYNYGQK YGNNRYAYSY TFVQDYERRI RDAIDRGYVF SHDGQRINLF SEDGVNILGN
LIESNPDSPD RHFYGALHVY ARHLLGYSSQ PLDKYHVAPS ALQHYETSLR DPAFYQFYKR
IVLYFQKYKS YLPSYTEHDL HFQGVEVKSV EFDRLVTYFD HFYTDISNAV YVTPQEYDSE
KVQVRVRQYR LNHKPFTYRV HVSSDKEQQA VVRIYLGPKY DEYGRYINIS HNRLNFVEVD
HFKYQLKVGE NVIERNSHQN YFYQNDRTSY RQLYKQVLGA LNGNGEFNVN ANEAYFGFPR
RFLLPKGNYG GQEFQFFVIV SPYVPYKYHQ EGYDASKYYY PRVGSGAHHI DNYAFGYPFD
RPIHYDQIFH NVPNAYFYTT KIYHRHADDI NASTSAHQ

Figure 45: ***Sequence of Tribolium castaneum hexamerin 4 isoform x1 used for structure building****. Amino acids that are missing in the cryo-EM structure are highlighted in blue.*

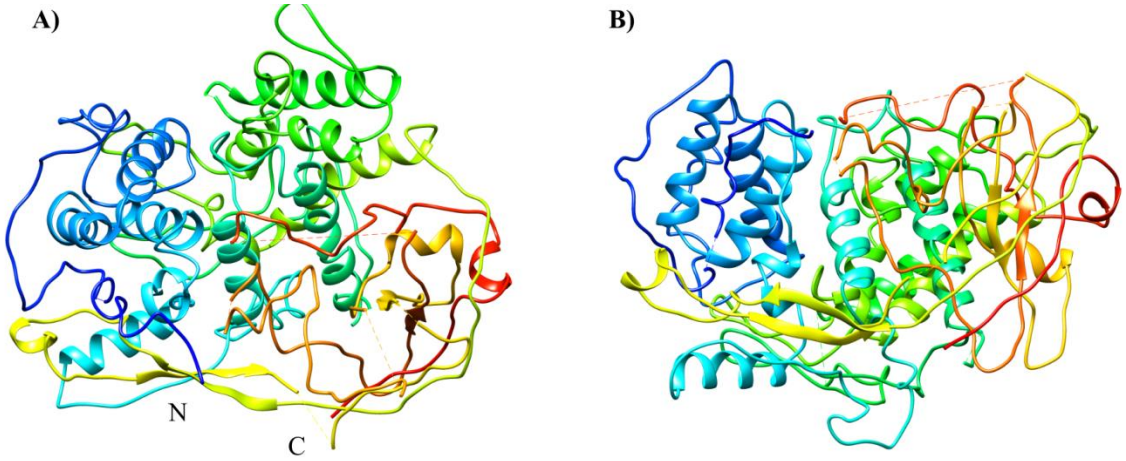

Figure 46: ***Hexamerin protomer in rainbow color****. A) Top view and B) side view, missing parts of the sequence are in dashed line, created in UCSF Chimera [86].*

Biological assembly of T. castaneum hexamerin consists of six hexamerin protomers organized with D3 symmetry. The complete structure is shown in Figure 47. Figure 48 and Figure 49 show the overall statistics of the quality of the built structure [80] and Ramachandran diagram [78].

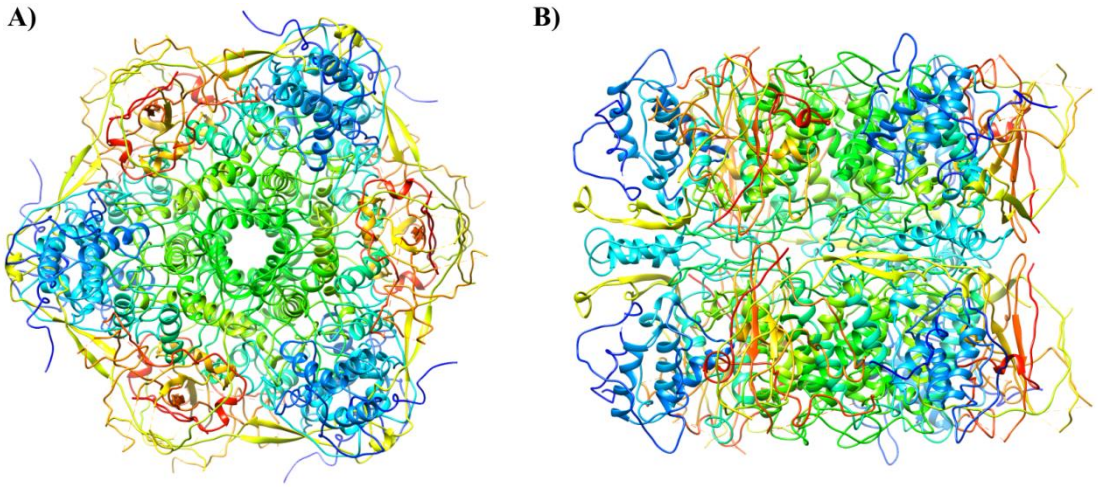

Figure 47: ***Rainbow colored structure of Tribolium castaneum hexamerin****. A) Top view, B) side view, created in UCSF Chimera [86].*

Clashscore, all atoms:	6.26	
Clashscore is the number of serious steric overlaps (> 0.4 Å) per 1000 atoms.		
Poor rotamers	4	0.73%
Favored rotamers	524	95.97%
Ramachandran outliers	6	1.03%
Ramachandran favored	463	79.42%
MolProbity score^	2.09	
Cβ deviations >0.25Å	0	0.00%
Bad bonds:	0 / 5432	0.00%
Bad angles:	16 / 7376	0.22%
Cis Prolines:	0 / 29	0.00%
Twisted Peptides:	6 / 592	1.01%

Figure 48: ***Overall statistics of built hexamerin model generated in MolProbity*** *[80].*

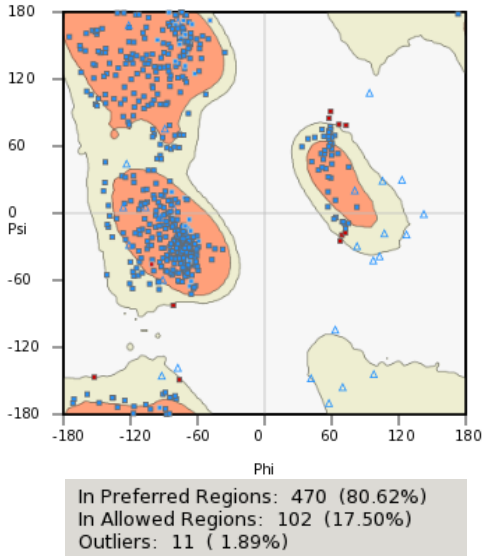

Figure 49: ***Ramachandran diagram of refined hexamerin protomer structure****. Model was refined in programs Refmac [89] and Phenix [88], diagram was generated in Coot [78].*

5.2.7 Comparison to other hexamerins

Figure 50 shows structural differences among hexamerins from three different organisms: *Bombix mori* [87], *Apis melifera* (provided by my colleague Mgr. Maria Gondová) and *T. castaneum*. Whereas the similarity of the *Bombix mori* and *Apis melifera* hexamerin sequence to *Tribolium castaneum* hexamerin is 37 % and 40 % respectively, their three-dimensional structures are very similar.

All three hexamerins are composed of six hexamerin subunits, with central part formed by helices. They differ in the arrangement of β-sheets at the edges. In the structures of hexamerins from *Bombix mori* and *Apis melifera* (both solved by X-ray crystallography) the glycosylation at the edge of each subunit is visible. The structure of *Apis melifera* hexamerin contains molecule of putative juvenile hormone.

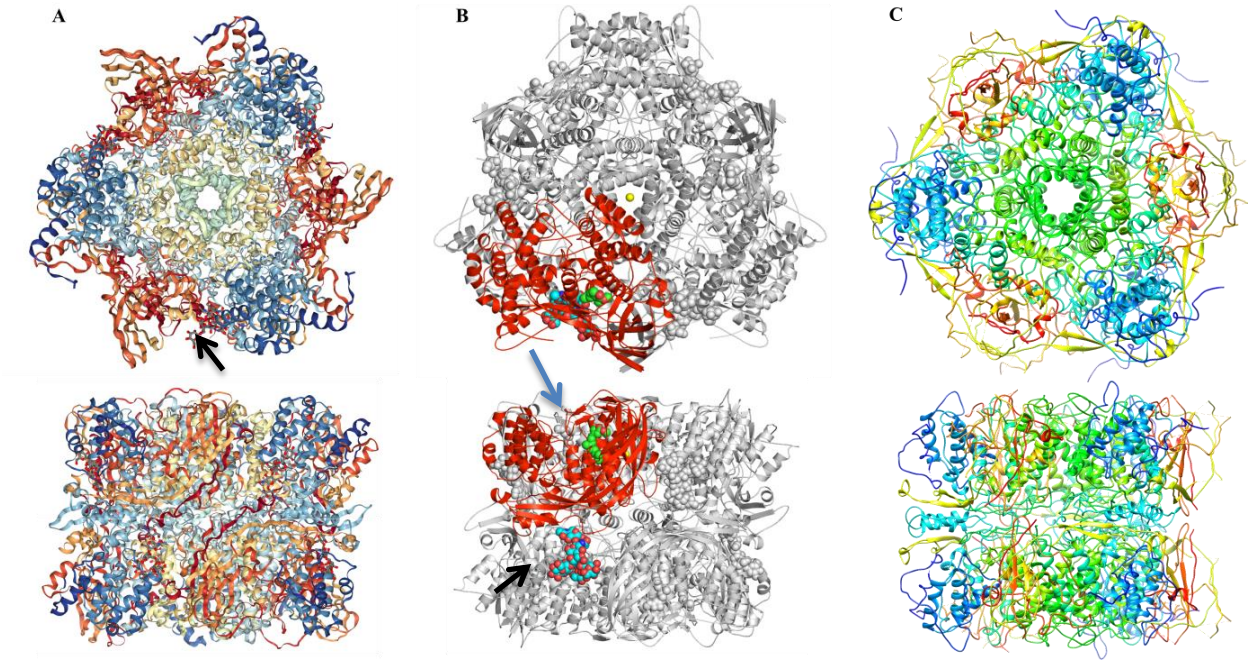

Figure 50: ***Structural comparison of hexamerins from different insect species****. Top views (above) and side views (below) of A) Hexamerin from Bombix mori [87], B) hexamerin from Apis melifera (picture provided by Mgr. Maria Gondová), C) hexamerin from Tribolium castaneum. Glycosylation marked with black arrow, position of juvenile hormone by blue arrow.*

5.2.7.1 Presence of juvenile hormone in hexamerin of T. castaneum

According to the literature, hexamerin serves as juvenile hormone binding protein [10, 11]. Hexamerin is depleted during metamorphosis and juvenile hormone is gradually released. From the information about other known hexamerin structures it was expected that electron density corresponding to juvenile hormone will be identified in the maps of *T. castaneum* hexamerin.

The structure of *T. castaneum* hexamerin was compared to that of *Apis melifera* hexamerin 70b with incorporated juvenile hormone and the position of the cavity in which juvenile hormone might be placed in *T. castaneum* hexamerin was identified (Figure 51). Amino acid residues that surround the cavity are mostly hydrophobic (tyrosines, phenyalanines, leucinse, valins). Small cloud of electron density probably corresponding to the juvenile hormone was identified in the electron density maps of *T. castaneum* hexamerin.

The position of the cavity is close to the edge of the cryo-EM map, where the map quality is worse than in the middle. The reason for this might be that the particles in micrographs (see Figure 41) interact with each other and form chains and therefore the amount of information about their edges is lower than about the middle of the particles.

For this reason it is necessary to find cryo-EM sample conditions in which the particles will be separated.

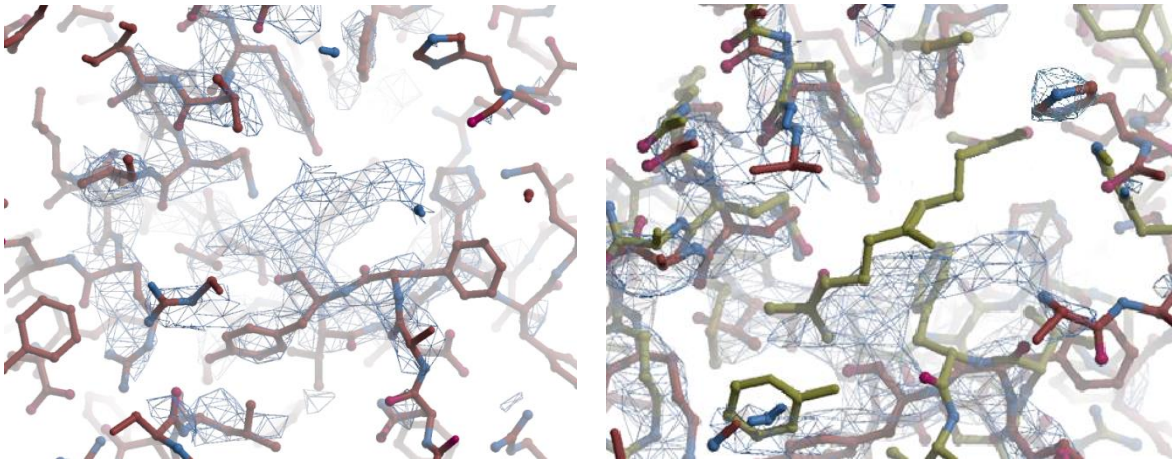

Figure 51: ***Possible cavity for juvenile hormone****. On the left: Tribolium castaneum electron density map fitted with red chain of hexamerin amino acids, in the middle there is an extra density probably of juvenile hormone. On the right: T. castaneum hexamerin electron density map (blue) with red structure of Tribolium hexamerin and yellow structure of Apis melifera hexamerin with a molecule of juvenile hormone.*

5.2.7.2 Putative glycosylation of hexamerin of T. castaenum

Typical sign of hexamerins among different insect species is the presence of N-glycosylations. These glycosylations might play a role in the protein folding and stability [87, 90] and were found in all four types of hexamerin from *Apis melifera* [62], in *Antheraea pernyi* arylphorin [90], in *Musca domestica* hexamerin [91] and in *Bombix mori* hexamerin [87]. In all cases the glycosylation is on asparagine at the edge of each of the six hexamerin subunits. For the same reason from which it was not possible to determine with certainty the electron density of the juvenile hormone it is also not possible to observe the glycosylation of *T. castaneum* hexamerin. Therefore, new data collection with sample of higher quality will be necessary.

5.2.8 DLS analysis of *T. castaneum* hexamerin

Tendency of *T. castaneum* hexamerin to form aggregates was verified by DLS analysis using Delta Max Core. The hexamerin sample contained two populations (Figure 52). The first one (645.3 kDa) corresponds to a hexamer of subunits ($6 \times$ 84.2 kDa Da = 505 kDa), the second represents large aggregates.

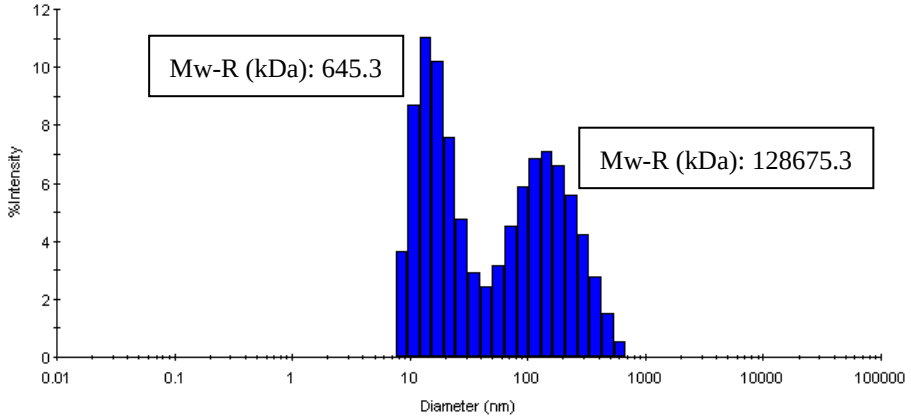

Figure 52: ***Histogram of particle size distribution measured by DLS analysis.*** *Sample of hexamerin was measured at concentration 10 mg/ml in buffer H. Hexamerin sample contain two populations of particles, one roughly corresponds to one hexamerin composed of 6 hexamerin subunits, the second represents hexamerin aggregates.*

5.2.9 Purification of hexamerin using ion exchange chromatography

Possible reasons why hexamerins might form chains and aggregates observed on micrographs and confirmed by DLS analysis could be the presence of nucleic acids, other contaminants or detergent NP-40. To prepare a grid with discrete hexamerin particles the isolate of hexamerin sample was purified by three additional purification steps: 1) precipitation with PEG 20 000 (removal of the detergent, Figure 53), 2) treatment with TurboNuclease (removal of the nucleic acids), and 3) ion exchange chromatography (IONEX, Figure 53).

Ion exchange chromatography was done on MonoQ column in buffer with pH 7.5. Hexamerin's pI is 6.39. In the buffer with pH above the hexamerin pI the hexamerin should be negatively charged and it should bind to the positively charged anion exchanger. However, hexamerin bound only weakly (Figure 53, Figure 54) and most of it washed out of the column during the wash step. Fractions containing hexamerin were desalted, concentrated and used for cryo-electron microscopy and DLS measurements.

As it could be seen on the SDS-PAGE gel from IONEX purification, additional purification steps lead to a sample of hexamerin which is clearer, but it does not help to prevent hexamerin to form aggregates as much as expected (Figure 55).

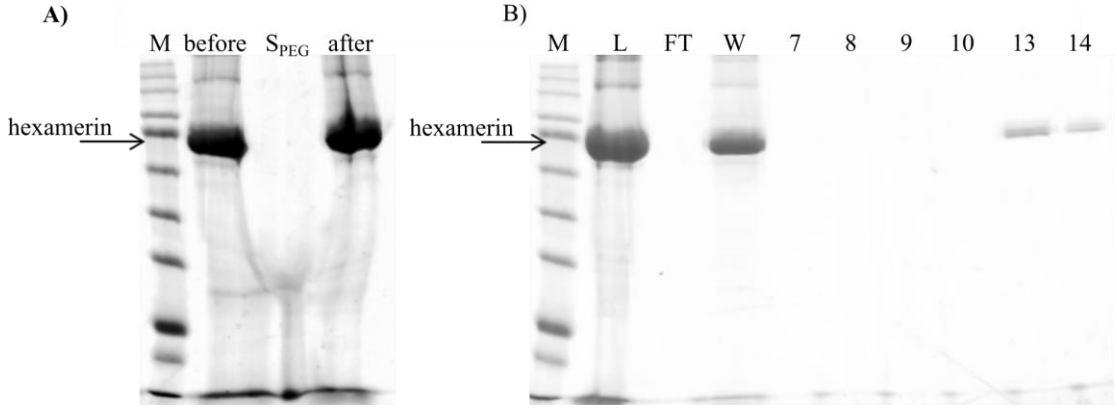

*Figure 53****: SDS-PAGE analysis of hexamerin purification by PEG precipitation and IONEX on MonoQ column****. A) Gel from precipitation with PEG 20 000, M: marker, before: original sample, S_{PEG}: supernatant with PEG, after: sample of hexamerin after PEG precipitation in buffer without detergent. B) Gel from Ion exchange chromatography on MonoQ column, L: load, FT: flow through, W: wash, E: elution fractions. Gels (12%) were stained by Instant Blue stain.*

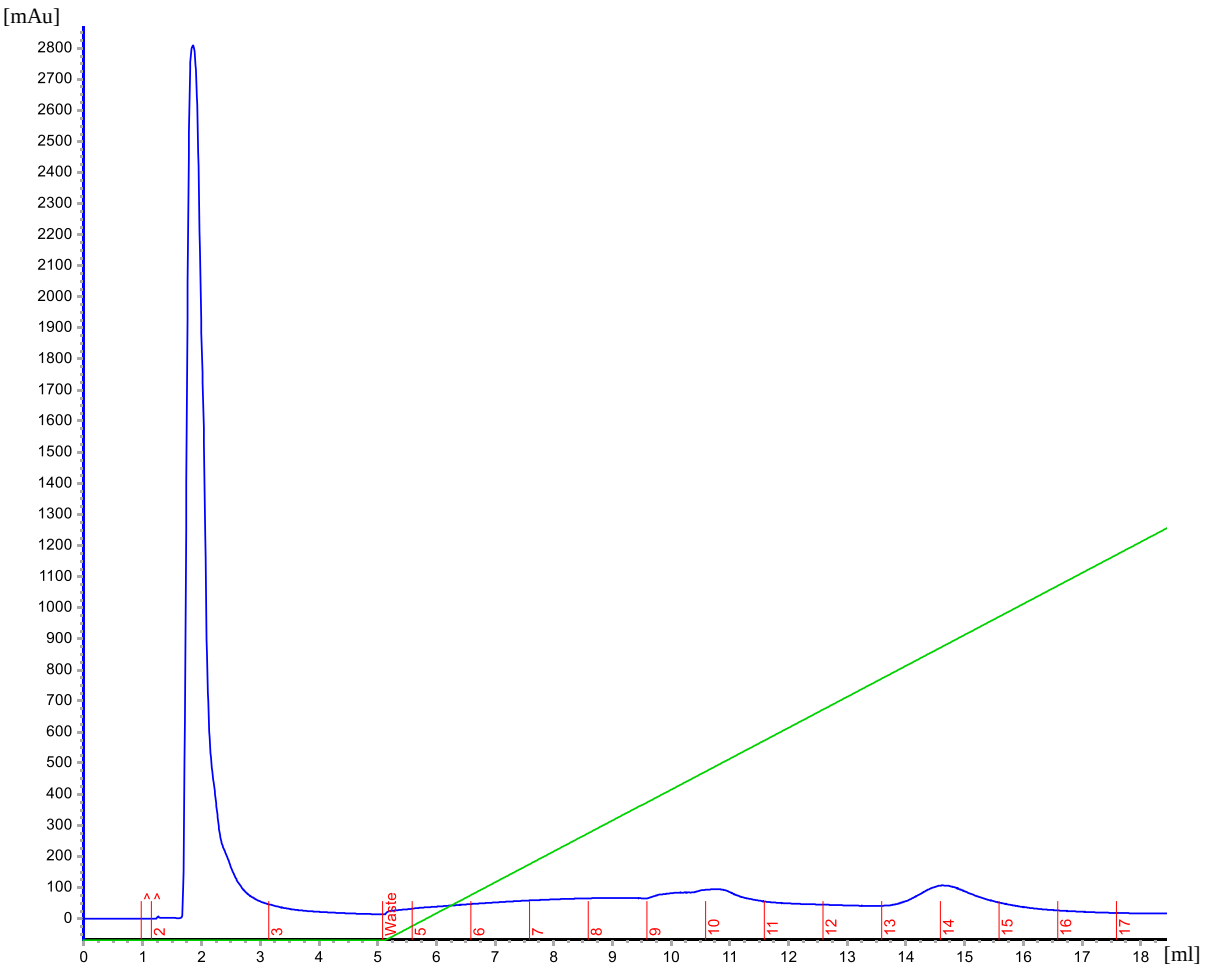

Figure 54: ***Chromatogram from hexamerin purification by IONEX on Mono Q 5/50 column****. Blue line represents the signal from UV detector, green corresponds to KCl gradient.*

5.2.10 DLS analysis of IONEX purified hexamerin

The IONEX purified hexamerin (1 mg/ml) was analysed by DLS. Two populations were found, the first of them (size 597 kDa) corresponds to hexamers of hexamerin subunits (6 × 84.2 kDa = 505 kDa), the second one to large aggregates (Figure 55).

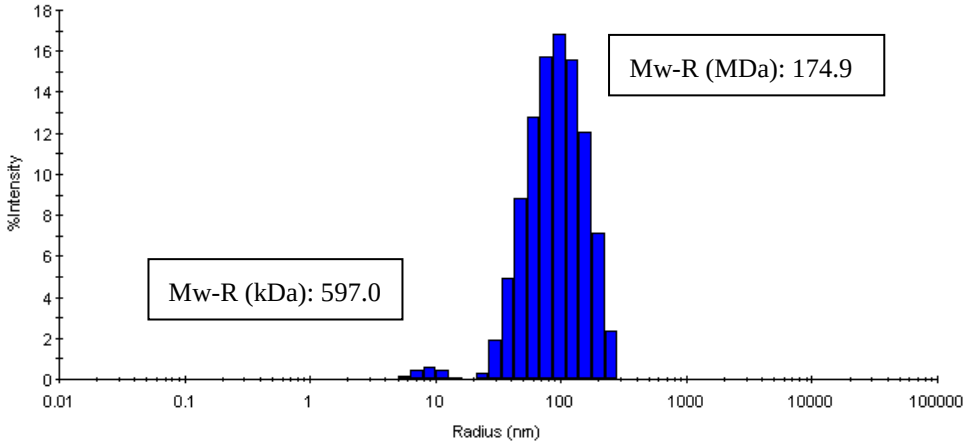

Figure 55: ***Histogram of hexamerin particle size distribution measured by DLS analysis****. Sample of hexamerin was measured at concentration 1 mg/ml in final buffer Q. Hexamerin sample contains two populations of particles, one roughly corresponds to one hexamerin composed of 6 hexamerin subunits, the second represents hexamerin aggregates.*

5.2.11 Cryo-EM of hexamerin on graphene coated grids

Particles used for cryo-EM 3D reconstruction suffered from preferred orientation in the holey carbon coated grids. This might be caused by adsorption of the particles to the air–water interface. This leads not only to preferred particle orientations but also to partial denaturation of the protein where it touches the interface [75]. This may explain the bad quality of the reconstructed map at the periphery of the hexamerin particle. To overcome this problem, we tried to immobilize and vitrify hexamerin particles on graphene coated holey carbon grids. Hexamerin adhered well to the graphene layer Figure 56; however, the vitrified sample contained very low amount of usable areas for microscopy, therefore, automatic acquisition was not possible. Further optimization of the graphene surface is needed to overcome the hydrophobicity of the graphene layer.

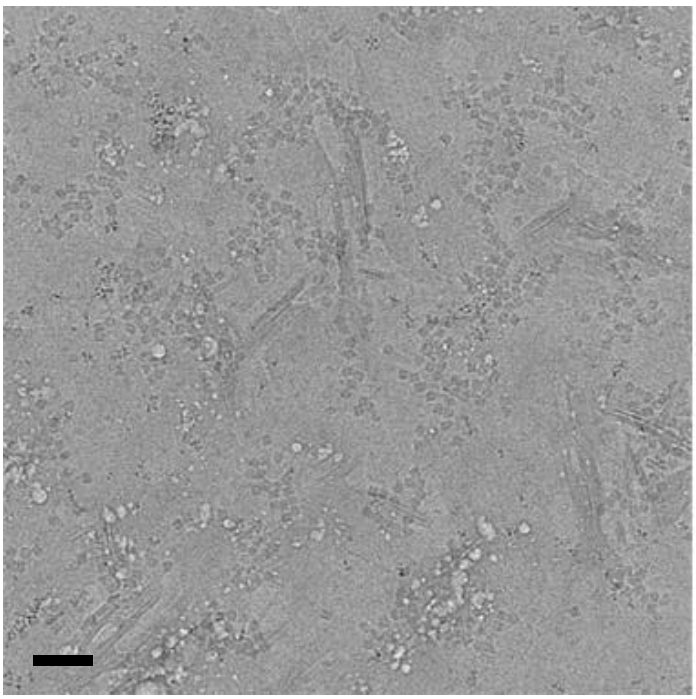

Figure 56: ***Cryo-EM micrograph of graphene coated grids with hexamerin sample****. Hexamerin concentration 0.05 mg/ml, magnification 62k, TEM Tecnai F20, scale bar corresponds to 50 nm.*

6 CONCLUSIONS

6.1 Structural studies of protein TmpH

Phage therapy is widely considered to be an alternative method to antibiotics. Before it will be possible to widely apply phage therapy in human medicine a careful research of phages is necessary. In this thesis we dealt with structural study of Tail morphogenetic protein H from *S. aureus* phage *Φ812.*

The gene of Tail morphogenetic protein H was cloned into several expression vectors and expression and purification trials were performed.

TmpH with N-terminal His_6 tag bound very weakly to a Histrap column and most of the protein remained in flow-through. The cleavage of the His tag by Ulp1-ac protease was not efficient. We speculate that the His tag might be buried in the protein and not accessible for the protease and IMAC. Non-tagged TmpH protein purification via precipitation with ammonium sulphate followed by HIC did not yield protein of desired quantity and purity for crystallization experiments.

Finally, C-terminally His_6 tagged TmpH protein was purified using NiNTA resin followed by size exclusion chromatography on Superdex 75 pg 16/600 column. The purified protein was analyzed using DLS and mass spectroscopy and found to be suitable for crystallization trials.

Using crystallization screens we found 15 suitable conditions for TmpH crystallization that were further optimized using hanging drop method.

Retention time from chromatogram from SEC suggested that TmpH exists in solution as a pentamer. This hypothesis was confirmed by DLS analysis. However, we found TmpH pentamers to be too small in size for cryo-EM studies; therefore, we will have to continue with X-ray crystallography to determine its structure.

Template-based homology model of TmpH was generated using Raptor X server, which predicted presence of two domains connected by a flexible linker. The domains consist mostly of β-sheets.

6.2 Structural studies of *T. castaneum* hexamerin

Beetle *T. castaneum* is a worldwide pest causing damage to food. The beetle became resistant to many types of insecticides. Hexamerin is the most abundant protein in haemolymph of larvae and pupae and serves as amino acid source during metamorphosis. There is evidence that hexamerin binds molecules of juvenile hormone and thus influences the beetle's development. Solving of the structure of *T. castaneum* hexamerin might shed light on the lifecycle regulation of this pest.

Purification of hexamerin from *T. castaneum* pupae lead to high purity protein suitable for crystallization and cryo-EM analyses.

Using crystallization screens, multiple crystallization conditions for *T. castaneum* hexamerin were identified. These conditions produced crystals of size and quality suitable for X-ray crystallography. Several dataset of hexamerin crystal scattering were collected on synchrotron; however, the quality of data was not suitable for further processing. Optimization of the crystallization conditions was done.

Cryo-EM analysis of hexamerin produced electron density map with the resolution of 3.2 Å which was suitable for building of molecular structure. The structure covers 87 % of hexamerin amino acid sequence. One hexamerin particle is composed of 6 protomers organized with D3 symmetry.

The structure of *T. castaneum* hexamerin was compared with those of other insects. The presence of glycosylation and juvenile hormone in the *T. castaneum* hexamerin structure cannot be confirmed at the moment.

Further, purification of hexamerin on IONEX column did not lead to sample more suitable for cryo-EM. Graphene coated grids were tested for preparation of hexamerin sample for cryo-EM, however the graphene layer was highly hydrophobic (even after plasma etching and non-covalent doping with 1-pyrenecarboxylic acid) and further optimization of graphene surface is needed.

7 LITERATURE

[1] Campbell, I. D. (2002) The march of structural biology. *Nature Reviews Molecular Cell Biology*. 3(5) 377-381.
[2] PDB. (2018) PDB Statistics: Growth of Structures from X-ray Crystallography Experiments Released per Year. Protein Data Bank.
[3] Turner, N. A., Sharma-Kuinkel, B. K., Maskarinec, S. A., Eichenberger, E. M., Shah, P. P., Carugati, M., Holland, T. L. and Fowler, V. G. (2019) Methicillin-resistant Staphylococcus aureus: an overview of basic and clinical research. *Nature Reviews Microbiology*. 17(2) 203-218.
[4] WHO. (2017) WHO publishes list of bacteria for which new antibiotics are urgently needed. *WHO priority pathogens list for R&D of new antibiotics*. World Health Organization, Geneva.
[5] Lin, D. M., Koskella, B. and Lin, H. C. (2017) Phage therapy: An alternative to antibiotics in the age of multi-drug resistance. *World J Gastrointest Pharmacol Ther*. 8(3) 162-173.
[6] Duin, D. (2017) Carbapenem-resistant Enterobacteriaceae: What we know and what we need to know. *Virulence*. 8(4) 379-382.
[7] Pantucek, R., Rosypalova, A., Doskar, J., Kailerova, J., Ruzickova, V., Borecka, P., Snopkova, S., Horvath, R., Gotz, F. and Rosypal, S. (1998) The polyvalent staphylococcal phage phi 812: Its host-range mutants and related phages. *Virology*. 246(2) 241-252.
[8] Matsuzaki, S., Uchiyama, J., Takemura-Uchiyama, I. and Daibata, M. (2014) The age of the phage. *Nature*. 509(7498) S9-S9.
[9] Susan J. Brown, T. D. S., Sherry Miller, Renata Bolognesi, Richard W. Beeman, Marcé D. Lorenzen, Gregor Bucher, Ernst A. Wimmer and Martin Klingler. (2012) The Red Flour Beetle, Tribolium castaneum (Coleoptera): A Model for Studies of Development and Pest Biology. Emerging Model Organisms. *Cold Spring Harbor Laboratory Press*, North Carolina State University.
[10] Burmester, T. (1999) Evolution and function of the insect hexamerins. *European Journal of Entomology*. 96(3) 213-225.
[11] Zhou, X. G., Tarver, M. R. and Scharf, M. E. (2007) Hexamerin-based regulation of juvenile hormone-dependent gene expression underlies phenotypic plasticity in a social insect. *Development*. 134(3) 601-610.
[12] Moore, P. B. (2017) Structural biology: Past, present, and future. *New Biotechnology*. 38 29-35.
[13] McPherson, A. (1991) A brief-history of protein crystal-growth. *Journal of Crystal Growth*. 110(1-2) 1-10.
[14] Rossmann, M. G. (1994) The beginnings of structural biology. *Protein Science*. 3(10) 1731-1733.
[15] Ruska, E. (1987) The development of the electron-microscope and of electron-microscopy. *Reviews of Modern Physics*. 59(3) 627-638.
[16] FRANK, J. (2006) *Three-Dimensional Electron Microscopy of Macromolecular Assemblies* 2 ed Oxford University Press, Inc., New York.
[17] Ward, A. B., Sali, A. and Wilson, I. A. (2013) Integrative Structural Biology. *Science*. 339(6122) 913-915.
[18] McPherson, A. and Gavira, J. A. (2013) Introduction to protein crystallization. *Acta crystallographica. Section F, Structural biology communications*. 70(Pt 1) 2-20.
[19] Milne, J. L. S., Borgnia, M. J., Bartesaghi, A., Tran, E. E. H., Earl, L. A., Schauder, D. M., Lengyel, J., Pierson, J., Patwardhan, A. and Subramaniam, S. (2013) Cryo-electron microscopy – a primer for the non-microscopist. *Febs Journal*. 280(1) 28-45.
[20] Glaeser, R. M. (1971) Low temperature electron microscopy - radiation damage in crystalline biological materials. *Journal of Microscopy-Oxford*. 12(1) 133.
[21] Frank, J. (2017) Advances in the field of single-particle cryo-electron microscopy over the last decade. *Nature Protocols*. 12(2) 209-212.

[22] Wagner, R. C. Schematic diagram of a TEM. University of Delware. www.udel.edu/Biology/Wags/b617/b617.htm.
[23] Venien-Bryan, C., Li, Z., Vuillard, L. and Boutin, J. A. (2017) Cryo-electron microscopy and X-ray crystallography: complementary approaches to structural biology and drug discovery. *Acta Crystallographica Section F-Structural Biology Communications*. 73 174-183.
[24] Baumeister, W., Fringeli, U. P., Hahn, M. and Seredynski, J. (1978) Radiation-damage to proteins. *Mikroskopie*. 34(5-6) 164-164.
[25] Dubochet, J., Adrian, M., Chang, J. J., Homo, J. C., Lepault, J., McDowall, A. W. and Schultz, P. (1988) Cryo-electron microscopy of vitrified specimens. *Quarterly Reviews of Biophysics*. 21(2) 129-228.
[26] Schenk, A. D., Castaño-Díez, D., Gipson, B., Arheit, M., Zeng, X. and Stahlberg, H. (2010) Chapter Four - 3D Reconstruction from 2D Crystal Image and Diffraction Data. In Jensen, G. J. (ed), *Methods in Enzymology*. Academic Press. 3(5) 377-381.
[27] Renault, L., Chou, H.-T., Chiu, P.-L., Hill, R. M., Zeng, X., Gipson, B., Zhang, Z. Y., Cheng, A., Unger, V. and Stahlberg, H. (2006) Milestones in electron crystallography. *Journal of computer-aided molecular design*. 20(7-8) 519-527.
[28] ZOU, X. (2006) *What is Electron Crystallography*? ISBN 978-1-4020-3920-1?
[29] Smyth, M. S. and Martin, J. H. (2000) X ray crystallography. *Molecular pathology* : MP. 53(1) 8-14.
[30] RHODES, G. (c2006) Cryst*allography made crystal clear: a guide for users of macromolecular models*. Elsevier/Academic Press, Boston. ISBN 978-0-12-587073-3.
[31] Bragg William, H. and Bragg William, L. (1913) The reflection of X-rays by crystals. *Proceedings of the Royal Society of London. Series A, Containing Papers of a Mathematical and Physical Character*. 88(605) 428-438.
[32] Spencer, R. K. and Nowick, J. S. (2015) A Newcomers Guide to Peptide Crystallography. *Israel Journal of Chemistry*. 55(6-7) 698-710.
[33] Dessau, M. A. and Modis, Y. (2011) Protein crystallization for X-ray crystallography. *Journal of visualized experiments : JoVE*(47) 2285.
[34] O'Neill, J. Review on Antimicrobial Resistance. *Antimicrobial Resistance:Tackling a crisis for the health and wealth of nations* (2014).
[35] WHO. (2013) Antibiotic resistance - a threat to global health security Worl Health Organization, Geneva, Switzerland.
[36] Matsuzaki, S., Uchiyama, J., Takemura-Uchiyama, I. and Daibata, M. (2014) Perspective: The age of the phage. *Nature*. 509 (7498) S9-S9.
[37] Kortright, K. E., Chan, B. K., Koff, J. L. and Turner, P. E. (2019) Phage Therapy: A Renewed Approach to Combat Antibiotic-Resistant Bacteria. Review. © 2019 Elsevier Inc., *Cell Host and Microbe*. 25(2) 219 – 232.
[38] Kingwell, K. (2015) Bacteriophage therapies re-enter clinical trials. *Nature Reviews Drug Discovery*. 14(8) 515-516.
[39] Kasparek, P., Pantucek, R., Kahankova, J., Ruzikova, V. and Doskar, J. (2007) Genome Rearrangements in host-range mutants of the polyvalent staphylococcal bacteriophage 812. *Folia Microbiologica*. 52(4) 331-338.
[40] SÚKL. (2018) STAFAL. Státní Ústav pro Kontrolu Léčiv.
[41] McGuinness, W. A., Malachowa, N. and DeLeo, F. R. (2017) Vancomycin Resistance in Staphylococcus aureus. *Yale Journal of Biology and Medicine*. 90(2):269-281.
[42] Zdrahal, Z., Eyer, L., Konecna, H. and Preisler, J. (2005) Characterization of bacteriophage 812 proteome. *Chemicke Listy*. 99(12) 962-966.

[43] Novacek, J., Siborova, M., Benesik, M., Pantucek, R., Doskar, J. and Plevka, P. (2016) Structure and genome release of Twort-like Myoviridae phage with a double-layered baseplate. *Proceedings of the National Academy of Sciences of the United States of America*. 113(33) 9351-9356.
[44] Botka, Benesik, Maslanova, Petras, Ruzickova, Havlickova, Varga, Zemlickova, Kolackova, Florianova, Jakubu, Karpiskova, Doskar (2018) Staphylococcus phage 812, complete genome. NCBI database.
[45] Lobocka, M. et al. (2012) Genomics of staphylococcal Twort-like phages--potential therapeutics of the post-antibiotic era. *Advances in Virus Research*. 83 143-216.
[46] Botka, T., Pantucek,R., Benesik,M., Maslanova,I., Petras,P.,, Ruzickova, V., Havlickova,P., Varga,M., Zemlickova,H., Kolackova,I., and Florianova, M., Jakubu,V., Karpiskova,R. and Doskar,J. (2018) Staphylococcus phage 812, complete genome. NCBI database.
[47] Fraser, J. S., Maxwell, K. L. and Davidson, A. R. (2007) Immunoglobulin-like domains on bacteriophage: weapons of modest damage? *Current Opinion in Microbiology*. 10(4) 382-387.
[48] Tatun, N., Vajarasathira, B., Tungjitwitayakul, J. and Sakurai, S. (2014) Inhibitory effects of plant extracts on growth, development and alpha-amylase activity in the red flour beetle Tribolium castaneum (Coleoptera: Tenebrionidae). *European Journal of Entomology*. 111(2) 181-188.
[49] Doucet, D., Cusson, M. and Retnakaran, A. (2008) Insect endocrinology and hormone-based pest control products in IPM.
[50] Bale, J. S., van Lenteren, J. C. and Bigler, F. (2008) Biological control and sustainable food production. *Philosophical Transactions of the Royal Society B-Biological Sciences*. 363(1492) 761-776.
[51] Dent, D. (2000) *Insect Pest Management* 2 ed CABI Bioscience, UK Centre, Ascot, UK.
[52] McGavin, G. C. (1994) The insects - an outline of entomology - Gullan, Cranston. *Nature*. 370(6487) 261-262.
[53] Dhadialla, T. S., Carlson, G. R. and Le, D. P. (1998) New insecticides with ecdysteroidal and juvenile hormone activity. *Annual Review of Entomology*. 43 545-569.
[54] Cusson, M. and Palli, S. R. (2000) Can juvenile hormone research help rejuvenate integrated pest management? *Canadian Entomologist*. 132(3) 263-280.
[55] Villa, I. L. and Stolt, J. (2015) Holometabolous metamorphosis: Why do insect metamorphose? Available at https://allyouneedisbiology.wordpress.com/tag/holometabolous-metamorphosis/.
[56] SOKOLOFF, A. (1974) *The biology of Tribolium with special emphasis on genetic aspects*. Oxford at the Clarendon Press, London. ISBN 978-01-985-75122.
[57] Taxonomy - Tribolium castaneum (Red flour beetle). UniProt database, https://www.uniprot.org/taxonomy/7070.
[58] Kumar, H., Panigrahi, M., Chhotaray, S., Bhanuprakash, V., Shandilya, R., Sonwane, A. and Bhushan, B. (2018) Red flour beetle (Tribolium castaneum): From population genetics to functional genomics. *Veterinary World*. 11(8) 1043-1046.
[59] Scharf, I., Wertheimer, K. O., Xin, J. L., Gilad, T., Goldenberg, I. and Subach, A. (2019) Context-dependent effects of cold stress on behavioral, physiological, and life-history traits of the red flour beetle. *Insect Science*. 26(1) 142-153.
[60] Tatun, N., Kumdi, P., Tungjitwitayakul, J. and Sakurai, S. (2018) Effects of 20-hydroxyecdysone on the development and morphology of the red flour beetle, Tribolium castaneum (Coleoptera: Tenebrionidae). *European Journal of Entomology*. 115 424-431.
[61] CABI. (2007) *Tribolium castaneum* (red flour beetle) datasheet. *Invasive Species Compendium* CAB International Publishing, Wallingford, UK.
[62] Martins, J. R., Nunes, F. M. F., Cristino, A. S., Simoes, Z. P. and Bitondi, M. M. G. (2010) The four hexamerin genes in the honey bee: structure, molecular evolution and function deduced from expression patterns in queens, workers and drones. *Bmc Molecular Biology*. 11 20.

[63] Sato, J. D. and Roberts, D. B. (1983) Synthesis of larval serum proteins 1 and 2 of Drosophila melanogaster by third instar fat body. *Insect Biochemistry*. 13(1) 1-5.
[64] Beverley Sm Fau - Wilson, A. C. and Wilson, A. C. (1982) Molecular evolution of Drosophila and higher Diptera. I. Micro-complement fixation studies of a larval hemolymph protein. *Journal of Molecular Evolution*. 18(4) 251-64.
[65] Miller, S. G. and Silhacek, D. L. (1982) The synthesis and uptake of haemolymph storage proteins by the fat body of the greater wax moth Galleria mellonella (L.). *Insect Biochemistry*. 12(3) 293-300.
[66] Telfer, W. H. and Kunkel, J. G. (1991) The function and evolution of insect storage hexamers. *Annual Review of Entomology*. 36 205 – 28.
[67] Levenbook, L. and Bauer, A. C. (1984) The fate of the larval storage protein calliphorin during adult development of calliphora-vicina. *Insect Biochemistry*. 14(1) 77.
[68] L., G. and M.G., P. (1983) Selective crosslinking of tyrosine- rich larval serum proteins and of soluble Manduca sexta cuticle proteins by nascent N-acetyldopamine-quinone and N-a-alanyl dopamine-quinone. In Scheller K. (ed): The Larval Serum Proteins of Insects: Function, Biosynthesis, Genetic. Thieme, Stuttgart, New York.
[69] Froger, A. and Hall, J. E. (2007) Transformation of plasmid DNA into E. coli using the heat shock method. *Journal of visualized experiments* : *JoVE*(6) 253-253.
[70] Howard, D. H. (1956) The preservation of bacteria by freezing in glycerol broth. *Journal of bacteriology*. 71(5) 625-625.
[71] Rosano, G. L. and Ceccarelli, E. A. (2014) Recombinant protein expression in Escherichia coli: advances and challenges. *Frontiers in microbiology*. 5 172-172.
[72] Studier, F. W. (2005) Protein production by auto-induction in high-density shaking cultures. *Protein Expression and Purification*. 41(1) 207-234.
[73] Candiano, G., Bruschi M Fau - Musante, L., Musante L Fau - Santucci, L., Santucci L Fau - Ghiggeri, G. M., Ghiggeri Gm Fau - Carnemolla, B., Carnemolla B Fau - Orecchia, P., Orecchia P Fau - Zardi, L., Zardi L Fau - Righetti, P. G. and Righetti, P. G. (2004) Blue silver: a very sensitive colloidal Coomassie G-250 staining for proteome analysis. *Electrophoresis*. 25(9) 1327-33.
[74] Wingfield, P. (2001) Protein precipitation using ammonium sulfate. *Current protocols in protein science*. Appendix 3: Appendix 3F.
[75] D'Imprima, E., Floris, D., Joppe, M., Sanchez, R., Grininger, M. and Kuhlbrandt, W. (2019) Protein denaturation at the air-water interface and how to prevent it. *eLife*. 42747.
[76] Wagner, T. et al. (2019) SPHIRE-crYOLO: A fast and accurate fully automated particle picker for cryo-EM. *bioRxiv* 356584.
[77] Zivanov, J., Nakane, T., Forsberg, B. O., Kimanius, D., Hagen, W. J. H., Lindahl, E. and Scheres, S. H. W. (2018) New tools for automated high-resolution cryo-EM structure determination in RELION-3. *eLife*. 7e42166.
[78] Emsley, P., Lohkamp B Fau - Scott, W. G., Scott Wg Fau - Cowtan, K. and Cowtan, K. (2010) Features and development of Coot. *Acta crystallographica. Section D, Biological Crystallography*. 66(Pt 4) 486-501.
[79] Vagin, A. A., Steiner, R. A., Lebedev, A. A., Potterton, L., McNicholas, S., Long, F. and Murshudov, G. N. (2004) REFMAC5 dictionary: organization of prior chemical knowledge and guidelines for its use. *Acta Crystallographica. Section D. Biological Crystallography*. 60(Pt 12 Pt 1) 2184-95.
[80] Chen, V. B., Arendall, W. B., 3rd, Headd, J. J., Keedy, D. A., Immormino, R. M., Kapral, G. J., Murray, L. W., Richardson, J. S. and Richardson, D. C. (2010) MolProbity: all-atom structure validation for macromolecular crystallography. A*cta crystallographica. Section D, Biological Crystallography.* 66(Pt 1) 12-21.

[81] Gasteiger E., H. C., Gattiker A., Duvaud S., Wilkins M.R., Appel R.D., Bairoch A. (2019) *Protein Identification and Analysis Tools on the ExPASy Server. TmpH - computed parameters*.
[82] BEINHAUEROVÁ, M. (2016) *Klonování a exprese strukturních genů polyvalentního stafylokokového bakteriofága*. Diplomová práce. Přírodovědecká fakulta. Masarykova univerzita, Brno.
[83] Held, P. (2003) *Peptide and Amino Acid Quantification Using UV Fluorescence in Synergy HT Multi-Mode Microplate Reader.* Available at https://www.biotek.com/resources/application-notes/peptide-and-amino-acid-quantification-using-uv-fluorescence-in-synergy-ht-multi-mode-microplate-reader/.
[84] Kallberg, M., Wang H Fau - Wang, S., Wang S Fau - Peng, J., Peng J Fau - Wang, Z., Wang Z Fau - Lu, H., Lu H Fau - Xu, J. and Xu, J. (2012) Template-based protein structure modeling using the RaptorX web server. *Nature Protocols*. 7(8) 1511-22.
[85] Langstroth, L. (11. 2. 2008) *Langstroth on the Hive and the Honey-Bee A Bee Keeper's Manual*. [HTML document]. Gutenberg EBook, EBook, 1857 [cit. 13. 1. 2019]. Available at http://www.gutenberg.org/ebooks/24583.
[86] Pettersen, E. F., Goddard Td Fau - Huang, C. C., Huang Cc Fau - Couch, G. S., Couch Gs Fau - Greenblatt, D. M., Greenblatt Dm Fau - Meng, E. C., Meng Ec Fau - Ferrin, T. E. and Ferrin, T. E. (2004) UCSF Chimera--a visualization system for exploratory research and analysis. *Journal of Computational Chemistry*. 25(13) 1605-12.
[87] Hou, Y., Li, J., Li, Y., Dong, Z., Xia, Q. and Yuan, Y. A. (2014) Crystal structure of Bombyx mori arylphorins reveals a 3:3 heterohexamer with multiple papain cleavage sites. *Protein Science*. 23(6) 735-746.
[88] Adams, P. D. et al. (2010) PHENIX: a comprehensive Python-based system for macromolecular structure solution. *Acta crystallographica. Section D, Biological Crystallography*. 66(Pt 2) 213-221.
[89] Vagin, A. A., Steiner Ra Fau - Lebedev, A. A., Lebedev Aa Fau - Potterton, L., Potterton L Fau - McNicholas, S., McNicholas S Fau - Long, F., Long F Fau - Murshudov, G. N. and Murshudov, G. N. (2004) REFMAC5 dictionary: organization of prior chemical knowledge and guidelines for its use. *Acta Crystallograhica. Section D, Biological crystallography*. 60(Pt 12 Pt 1) 2184-95.
[90] Ryu, K. S. et al. (2009) The presence of monoglucosylated N196-glycan is important for the structural stability of storage protein, arylphorin. *The Biochemical Journal*. 421(1) 87-96.
[91] Moreira, C. K., Capurro, M. d. L., Walter, M., Pavlova, E., Biessmann, H., James, A. A., deBianchi, A. G. and Marinotti, O. (2004) Primary characterization and basal promoter activity of two hexamerin genes of Musca domestica. *Journal of insect science*. 4 2-2.

8 LIST OF USED ABBREVIATIONS AND SYMBOLS

APS	ammonium persulfate
BIS	N, N'-methylene-bis-acrylamide
BLAST	Basic Local Alignment Search Tool
C	cytosine
cryo-EM	cryo electron microscopy
dH_2O	distilled water
ddH_2O	demineralized water
DMSO	dimethylsulphoxide
dNTPs	deoxynucleotide triphosphates
DTT	dithiothreitol
E. coli	*Escherichia coli*
EDTA	ethylenediaminetetraacetic acid
EM	electron microscopy
G	guanine
HEPES	4-(2-hydroxyethyl)-1-piperazineethanesulfonic acid
HIC	chromatography of hydrophobic interactions
Ig	immunoglobulin
IMAC	immobilized metal ion affinity chromatography
IONEX	ion exchange chromatography
IPTG	isopropyl β-D-1-thiogalactopyranoside
JH	juvenile hormone
LB	lysogeny broth
LC	liquid chromatography
LIC	ligation independent cloning
MRSA	methicillin resistant *S. aureus* strains
NMR	nuclear magnetic resonance
NTA	nitrilotriacetic acid
PCR	polymerase chain reaction
PDB	Protein Data Bank
pI	isoelectric point
S. aureus.	*Staphylococcus aureus*
SDS-PAGE	polyacrylamide gel electrophoresis with sodium dodecyl sulphate
SEC	size exclusion chromatography
SOC	super optimal broth with catabolite repression
SPA	single particle analysis
TAE	buffer containing Tris base, acetic acid and EDTA
T. castaneum	*Tribolium castaneum*
TCEP	tris(2-carboxyethyl)phosphine
TEMED	N, N, N', N'-tetramethylenediamine
TRIS	tris(hydroxymethyl)aminomethane
UV light	ultraviolet light
WHO	World Health Organization